KfK 5290
Dezember 1994

Stress Intensity Factors and Weight Functions for One-dimensional Cracks

T. Fett, D. Munz
Institut für Materialforschung

Kernforschungszentrum Karlsruhe

KERNFORSCHUNGSZENTRUM KARLSRUHE
Institut für Materialforschung

KfK 5290

Stress intensity factors and weight functions for one-dimensional cracks

T. Fett, D. Munz

Kernforschungszentrum Karlsruhe GmbH, Karlsruhe

Kernforschungszentrum Karlsruhe GmbH
Postfach 3640, 76021 Karlsruhe

ISSN 0303-4003

Stress intensity factors and weight functions for one-dimensional cracks

Abstract

Stress intensity factors and weight functions are technical tools for all scientists and engineers concerned with problems in linear-elastic fracture mechanics. Solutions for a wide field of applications are provided in a number of handbooks. In recent years the authors have developed several solutions to special fracture-mechanical problems. This report is a compilation containing mainly solutions which are not available world-wide. First methods will be described which allow to determine stress intensity factors and weight functions for one-dimensional cracks. The second part contains solutions to cracks exposed to mode-I loadings as well as to mode-II and mixed-mode loadings.

Spannungsintensitätsfaktoren und Gewichtsfunktionen für eindimensionale Risse

Kurzfassung

Spannungsintensitätsfaktoren und Gewichtsfunktionen sind wichtige bruchmechanische Größen, die die Behandlung des Versagens von Komponenten im Bereich der linear-elastischen Bruchmechanik ermöglichen. In einer Reihe von Handbüchern sind Spannungsintensitätsfaktoren für einen breiten Anwendungsbereich angegeben. In den letzten Jahren haben die Autoren zusätzlich Lösungen für Gewichtsfunktionen zu speziellen bruchmechanischen Problemen erarbeitet. Sie sind in diesem Bericht zusammengestellt. Im ersten Teil werden Methoden zur Ermittlung der Gewichtsfunktion für eindimensionale Risse beschrieben. Der zweite Teil enthält Lösungen für Mode-I, Mode-II sowie "Mixed-Mode"-Belastungen.

Contents

1. Stress intensity factors and weight functions

1.1 Stress intensity factors

In fig.1 a simple geometry, plate of width W and thickness B with an external crack of length a, is considered. Three characteristic loading modes lead to high stresses near the crack tip:

Mode I: Tensile stress perpendicular to the crack face.
Mode II: Shear stress in direction of the crack.
Mode III: Out of plane shear stress.

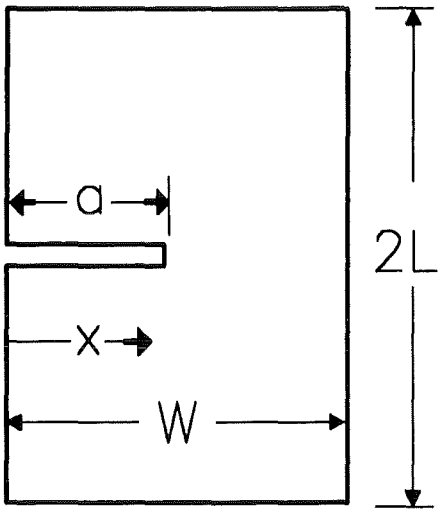

Figure 1. Plate with a through-the-thickness crack. Definition of geometric data.

The stresses near the crack tip for all loading modes can be described as

$$\sigma_{ij} = \frac{K}{\sqrt{2\pi r}} f_{ij}(\varphi) \qquad (1.1.1)$$

where r and φ are polar coordinates (see fig.2) and f is the angular function. K is the stress intensity factor. For the different loading modes the designations K_I, K_{II}, and K_{III} are used. The stress intensity factor can be written as

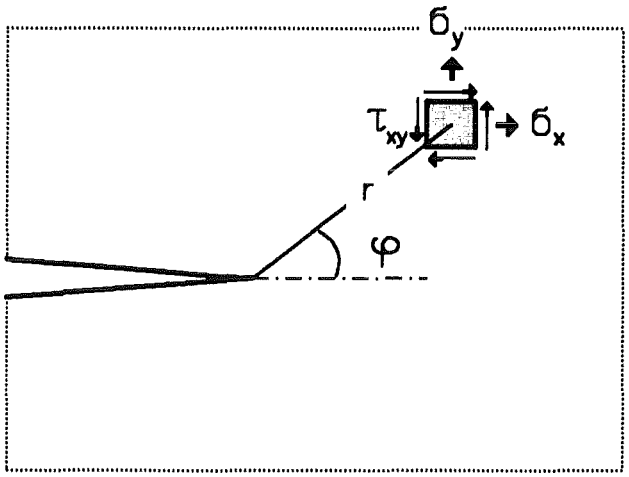

Figure 2. Stresses in front of a crack. Geometric data.

$$K_I = \sigma_y^* \sqrt{a}\, Y_I(a/W) \quad , \quad K_{II} = \tau_{xy}^* \sqrt{a}\, Y_{II}(a/W) \quad , \quad K_{III} = \tau_{xz}^* \sqrt{a}\, Y_{III}(a/W) \tag{1.1.2}$$

σ_y^*, τ_{xy}^* and τ_{xz}^* are characteristical stresses in the component, e.g. the outer fiber stress in a bending bar or the notch root stress in a notched component. Y_I, Y_{II} and Y_{III} are functions of the ratio of the crack length to the specimens width. The functions $Y(a/W)$ depend on the geometry of the component, on the geometry and location of the crack, and on the stress distribution in the uncracked component.
In some cases it is useful to apply the load F instead of a characteristic stress. Then K_I can be written as

$$K_I = \frac{F}{W^{3/2}} Y_I^*(a/W) \tag{1.1.3}$$

The crack-size dependence is fully described by the function Y^*. For through-the-thickness cracks in plates of thickness B the stress intensity factor can be written as

$$K_I = \frac{F}{B\sqrt{W}} Y^*(a/W) \tag{1.1.4}$$

In the following sections the index I for Y or Y^* and the index I for σ^* are omitted for mode-I loading.

A great number of methods have been developed for the determination of stress intensity factors:

- method of complex stress function [1],
- method of conform mapping [2],
- extrapolation of stress concentration factors of notched components to vanishing radius [3],
- method of asymptotic interpolation [4],
- integral transformation method [5],
- weight function method [6] [7],
- finite element method (FEM) [8],

- boundary element method (BEM),
- boundary collocation method (BCM) [9], [10].

This list is not complete. The weight function method will be described in detail. The references given above are in most cases the first publications of the method.

1.2 Mode-I weight functions

Most of the methods mentioned before require separate calculation of the stress intensity factor for each stress distribution and each crack length. The weight function method developed by Bueckner [6] simplifies the determination of stress intensity factors considerably. A weight function exists for any crack problem specified by the geometry of the component and a crack type. If this function is known, the stress intensity factor can be obtained by simply multiplying this function by the stress distribution and integrating it along the crack length.
In this section plane problems will be treated, with the crack size characterised by one parameter a. These problems are applicable to all components with through-the-thickness cracks.
An external crack in a component is considered. The distribution of the stress perpendicular to the crack area in the uncracked component along the location of the crack is $\sigma_y(x)$. The stress intensity factor for this stress distribution is given by

$$K_I = \int_0^a \sigma_y(x) h(x,a)\, dx \tag{1.2.1}$$

The integration has to be performed along the crack length from $x = 0$ at the surface until $x = a$. The weight function $h(x,a)$ depends only on the geometry of the component.
For internal cracks (s. Fig.3) the origin of the x-axis is located at the center of the crack. The crack length is usually specified as $2a$ and the integration has to be performed between $-a < x < a$. For an internal crack in an infinite body - in reality a small crack in a large plate - an analytical form of the weight function exists (for point A)

$$h(x,a) = \sqrt{\frac{1}{\pi a}} \left(\frac{a+x}{a-x} \right)^{1/2} \tag{1.2.2}$$

This function is shown in Fig.4. The dimension of the weight function is $(length)^{-1/2}$. Therefore, it is convenient to plot weight functions in a dimensionless form as $h\sqrt{a}$ or $h\sqrt{W}$ versus x/a. It can be seen that if x approaches the crack tip, h increases to infinity. Therefore, stresses near the crack tip strongly influence the stress intensity factor.
Rice [7] has shown that the weight function can be obtained from the crack opening displacement $v_r(x,a)$ of any arbitrarily chosen loading and the corresponding stress intensity factor $K_{Ir}(a)$ according to

$$h(x,a) = \frac{E'}{K_{Ir}(a)} \frac{\partial}{\partial a} v_r(x,a) \tag{1.2.3}$$

with $E' = E$ for plane stress and $E' = E/(1 - \nu^2)$ for plane strain. The chosen load case - the reference load case - is denoted by an index r. K_{Ir} is the stress intensity factor for the reference stress distribution $\sigma_r(x)$ and dependent on the crack length. v_r is the corresponding displacement of the crack borders in y-direction. It is convenient to use $\sigma_r = \sigma_0 = const.$ as a reference stress distribution. For the determination of the weight function according to eq.(1.2.3) it is necessary to know for one load case $K_{Ir}(a)$ and $v_r(x,a)$. In many cases $K_{Ir}(a)$ is known and $v_r(x,a)$ is unknown. In the reverse situation K_{Ir} can be obtained from crack opening displacement. Combining eqs.(1.2.1)

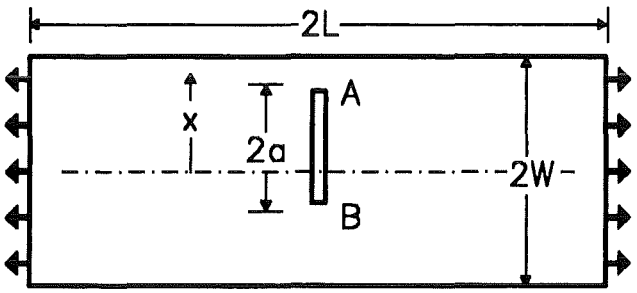

Figure 3. Internal crack in a plate under tensile loading.

and (1.2.3) and replacing the arbitrary stress distribution $\sigma(x)$ by the reference stress distribution - and therefore K_I by K_{Ir} - leads to

$$K_{Ir}^2 = E' \int_0^a \sigma_r \frac{\partial v_r(x,a)}{\partial a} dx \qquad (1.2.4)$$

For constant reference stress $\sigma_r = \sigma_0$ eq.(1.2.4) is simplified to read

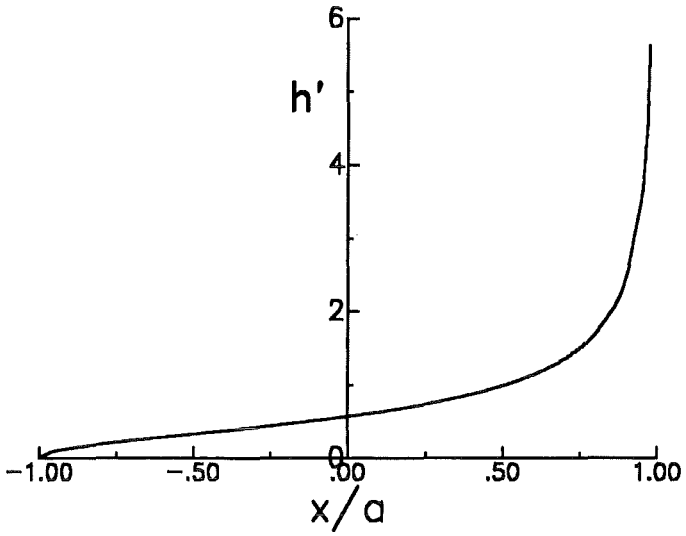

Figure 4. Weight function for an internal crack in an infinite body. $h' = h\sqrt{a}$.

$$K_{Ir}^2 = E' \sigma_0 \int_0^a \frac{\partial v_r(x,a)}{\partial a} dx \tag{1.2.5}$$

Equation (1.2.1) or (1.2.5) is only correct if the external load leading to the stress distribution $\sigma(x)$ in the uncracked component does not change due to the presence of the crack. If the total displacement of the component is restricted, the external forces applied may be reduced.
The weight function $h(x',a)$ can be interpreted as the Green's function for a stress intensity factor problem. This means that the weight function is identical to the stress intensity factor caused by a pair of normal forces with $P = 1$ acting at the point x'.
If we express the single forces P in terms of the Dirac delta function by a stress distribution (thickness of specimen $B = 1$)

$$\sigma(x) = P\,\delta(x - x') \tag{1.2.6}$$

and introduce this in eq.(1.2.1), we obtain

$$K_I = P \int_0^a h(x,a)\,\delta(x - x')\,dx = P\,h(x', a) \tag{1.2.7}$$

and for the unit force

$$K_I = h(x', a) \tag{1.2.8}$$

2. Approximate methods for the determination of weight functions for one-dimensional cracks

2.1 Approximate weight functions for a component with an external crack

2.1.1 Crack opening displacements

The determination of the reference crack opening displacement is based on a method first developed by Petroski and Achenbach [17]. The displacement is calculated from the reference stress intensity factor and several geometric conditions. The procedure is shown for the external crack in a plate of finite width.
Dimensionless quantities

$$\alpha = \frac{a}{W} \quad , \quad \rho = \frac{x}{a} \tag{2.1.1}$$

are used. The crack opening displacement near the crack tip is given by the relation [18]

$$v_N = \sqrt{8/\pi}\ \frac{\sigma_r^*}{E'}\, aY(\alpha)\sqrt{1-\rho} \tag{2.1.2}$$

The complete crack opening displacement is related to v_N and expressed as

$$\frac{v_r}{v_N} = \sum_{\nu=0}^{\infty} C_\nu (1-\rho)^\nu \tag{2.1.3}$$

or

$$v_r(x,a) = \sum_{\nu=0}^{\infty} A_\nu (1-\rho)^{\nu+1/2} = A_0 \sum_{\nu=0}^{\infty} C_\nu (1-\rho)^{\nu+1/2} \quad \text{with} \quad C_\nu = A_\nu / A_0 \tag{2.1.4}$$

and

$$A_0 = \sqrt{8/\pi}\ \frac{\sigma_r^*}{E'}\, aY_r(\alpha) \quad , \quad C_0 = 1 \tag{2.1.5}$$

2.1.2 Weight functions based on single reference loading cases

The weight function follows from eqs.(1.2.3) and (2.1.4)

$$h(x,a) = \sqrt{\frac{8}{\pi a}} \sum_{\nu=0}^{\infty} C_\nu \left[\left(1 + \frac{\alpha}{Y}\frac{dY}{d\alpha} + \frac{\alpha}{C_\nu}\frac{dC_\nu}{d\alpha} \right)(1-\rho)^{\nu+1/2} + \rho\left(\nu + \frac{1}{2}\right)(1-\rho)^{\nu-1/2} \right] \tag{2.1.6}$$

or if we replace the factors ρ by the identity $\rho = 1 - (1-\rho)$

$$h(x,a) = \sqrt{\frac{2}{\pi a}} \sum_{\nu=0}^{\infty} \left[(3-2\nu)C_{\nu-1} + (2\nu+1)C_\nu + 2\frac{\alpha}{Y}\frac{dY}{d\alpha}C_{\nu-1} + 2\alpha\frac{dC_{\nu-1}}{d\alpha} \right](1-\rho)^{\nu-1/2} \quad , \quad C_\nu = 0 \text{ for } \nu < 0 \tag{2.1.7}$$

The coefficients C_ν can be determined applying different conditions. One condition follows from the integration of eq.(1.2.4)

$$\int_0^a K_{Ir}^2\, da' = E' \int_0^a \sigma_r\, v_r(x,a)dx \tag{2.1.8}$$

This equation can be called the energy balance condition or the condition of self-consistence. Taking into account eqs.(2.1.4) and (2.1.5) leads to

$$\sum C_\nu I_\nu = \sqrt{\pi/8}\, \frac{1}{\alpha^2 Y} \int_0^\alpha \alpha' Y_r^2\, d\alpha' = Q(\alpha) \tag{2.1.9}$$

with

$$I_\nu = \frac{1}{\sigma_r^*} \int_0^1 \sigma_r(\rho)(1-\rho)^{\nu+1/2}\, d\rho \tag{2.1.10}$$

For the special case of $\sigma_r(\rho) = \sigma_0 = const.$ there is

$$I_\nu = \frac{2}{2\nu+3} \tag{2.1.11}$$

For three terms eq.(2.1.9) is

$$C_1^{(0)} + \frac{5}{7}C_2^{(0)} + \frac{5}{9}C_3^{(0)} = \frac{5}{2}Q_0(\alpha) - \frac{5}{3} \tag{2.1.12}$$

The upper index at the coefficients refers to the loading case for which the crack opening displacement field is determined.
As a second reference load a linear stress distribution may be used

$$\sigma(x) = \sigma^* \frac{x}{W} \tag{2.1.13}$$

Then

$$I_\nu = \frac{4\alpha}{(2\nu+3)(2\nu+5)} \tag{2.1.14}$$

and for three terms

$$C_1^{(1)} + \frac{5}{9} C_2^{(1)} + \frac{35}{99} C_3^{(1)} = \frac{35}{4\alpha} Q_1(\alpha) - \frac{7}{3} \tag{2.1.15}$$

where $Q_1(\alpha)$ is calculated according to eq.(2.1.9) with $Y = Y_1$.
If the linear stress distribution is caused by bending of a plate the stress distribution is

$$\sigma(x) = \sigma^* \left(1 - 2\frac{x}{W}\right) \tag{2.1.16}$$

Then

$$I_\nu = \frac{2}{2\nu+3} - 2\alpha \frac{4}{(2\nu+3)(2\nu+5)} \tag{2.1.17}$$

and for three terms

$$\frac{2}{3} - \frac{8\alpha}{15} + \left(\frac{2}{5} - \frac{8\alpha}{35}\right) C_1^{(b)} + \left(\frac{2}{7} - \frac{8\alpha}{63}\right) C_2^{(b)} + \left(\frac{2}{9} - \frac{8\alpha}{99}\right) C_3^{(b)} = Q_b(\alpha) \tag{2.1.18}$$

where $Q_b(\alpha)$ is calculated according to eq.(2.1.9) with $Y = Y_b$.
For a quadratic stress distribution

$$\sigma(x) = \sigma^* \left(\frac{x}{W}\right)^2 \tag{2.1.19}$$

there is

$$I_\nu = \frac{16\alpha^2}{(2\nu+3)(2\nu+5)(2\nu+7)} \tag{2.1.20}$$

and for three terms

$$C_1^{(2)} + \frac{5}{11} C_2^{(2)} + \frac{35}{143} C_3^{(2)} = \frac{315}{16\alpha^2} Q_2(\alpha) - 3 \tag{2.1.21}$$

For components with an external crack a further condition [19] is the vanishing curvature of the crack-opening profile at the surface:

$$\frac{d^2 v_r}{d\rho^2}\Big|_{\rho=0} = 0 \tag{2.1.22}$$

leading to

$$\sum_{\nu=0}^{\infty}(\nu+1/2)(\nu-1/2)C_\nu = 0 \tag{2.1.23}$$

For three terms there is

$$C_1 + 5C_2 + \frac{35}{3}C_3 = \frac{1}{3} \tag{2.1.24}$$

More conditions, leading to more coefficients are given in [20]. The simplest one is the requirement that also the third derivative of the crack opening profile must vanish at the surface, i.e.

$$\frac{d^3 v_r}{d\rho^3}\Big|_{\rho=0} = 0 \tag{2.1.25}$$

This relation leads to

$$\sum_{\nu=0}^{\infty}(\nu+1/2)(\nu-1/2)(\nu-3/2)C_\nu = 0 \tag{2.1.26}$$

and for three terms:

$$C_1 - 5C_2 - 35C_3 = 1 \tag{2.1.27}$$

If one available reference load case is combined with the condition leading to eq.(2.1.24), the coefficients can be obtained from the following relations:

- a) Reference load: constant stress and eq.(2.1.24).

$$C_1^{(0)} = \frac{35}{12}Q_0 - 2 \quad , \quad C_2^{(0)} = \frac{7}{15} - \frac{7}{12}Q_0 \tag{2.1.28}$$

$$\frac{dC_1^{(0)}}{d\alpha} = \frac{35}{12}\left[Q_0\left(-\frac{2}{\alpha} - \frac{Y'_0}{Y_0}\right) + \sqrt{\pi/8}\,\frac{Y_0}{\alpha}\right] \tag{2.1.29}$$

$$\frac{dC_2^{(0)}}{d\alpha} = -\frac{7}{12}\left[Q_0\left(-\frac{2}{\alpha} - \frac{Y'_0}{Y_0}\right) + \sqrt{\pi/8}\,\frac{Y_0}{\alpha}\right] \tag{2.1.30}$$

- b) Reference load: linear stress - eq.(2.1.12) - and eq.(2.1.24)

$$C_1^{(1)} = \frac{315}{32}\frac{Q_1}{\alpha} - \frac{8}{3} \quad , \quad C_2^{(1)} = -\frac{63}{32}\frac{Q_1}{\alpha} + \frac{3}{5} \tag{2.1.31}$$

$$\frac{dC_1^{(1)}}{d\alpha} = \frac{315}{32}\left[Q_1\left(-\frac{3}{\alpha^2} - \frac{Y'_1}{Y_1\alpha}\right) + \sqrt{\pi/8}\,\frac{Y_1}{\alpha^2}\right] \tag{2.1.32}$$

$$\frac{dC_2^{(1)}}{d\alpha} = -\frac{63}{32}\left[Q_1\left(-\frac{3}{\alpha^2} - \frac{Y'_1}{Y_1\alpha}\right) + \sqrt{\pi/8}\,\frac{Y_1}{\alpha^2}\right] \tag{2.1.33}$$

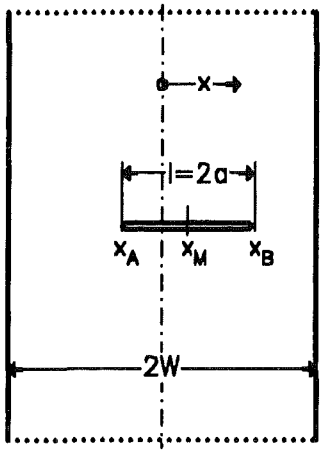

Figure 5. Geometry of a crack in a strip of finite width.

The weight function for two coefficients reads by use of eq.(2.1.7)

$$h(x,a) = \sqrt{\frac{2}{\pi a}}\left\{(1-\rho)^{-1/2} + (1-\rho)^{1/2}\left[1 + 3C_1 + 2\frac{\alpha}{Y}\frac{dY}{d\alpha}\right]\right.$$
$$+ (1-\rho)^{3/2}\left[-C_1 + 5C_2 + 2\frac{\alpha}{Y}\frac{dY}{d\alpha}C_1 + 2\alpha\frac{dC_1}{d\alpha}\right] \qquad (2.1.34)$$
$$\left. + (1-\rho)^{5/2}\left[-3C_2 + 2\frac{\alpha}{Y}\frac{dY}{d\alpha}C_2 + 2\alpha\frac{dC_2}{d\alpha}\right]\right\}$$

with coefficients $C_\nu^{(0)}$ or $C_\nu^{(1)}$ depending on the chosen reference load case. For Y the value Y_0 or Y_1 respectively has to be applied.

2.1.3 Weight functions based on multiple reference loading cases

In Section 2.1.2 the approximate weight functions were based on single reference cases and the crack opening displacement fields were determined either for tension or for other special stress distributions. It is possible to improve the procedure furthermore by simultaneous application of different reference solutions. The treatment will be explained in this section for the example of the crack opening displacement field under pure tension. In order to simplify the notation the upper index - in this section (0) - will be dropped. It will be shown how the reference stress intensity factor solutions for an arbitrary load will improve the crack opening displacement field for constant stress. The crack opening displacements for an edge crack loaded with constant stress σ_0 is given by eqs.(2.1.4)-(2.1.5) as

$$v^{(0)} = \sqrt{\frac{8}{\pi}}\frac{\sigma_0}{E'}aY_0\sum_{\nu=0}^{\infty}C_\nu\left(1-\frac{x}{a}\right)^{\nu+1/2} \qquad (2.1.35)$$

If a number of P loading cases is available eq.(1.2.3) provides the relations

$$\int_0^a \sigma_p v^{(0)} dx = \frac{1}{E'} \int_0^a K_{Ip} K_{I0} da' \quad , \quad p = 1,2,...,P \tag{2.1.36}$$

We define

$$Q_{0,p} = \sqrt{\frac{\pi}{8}} \frac{1}{\alpha^2 Y_0(\alpha)} \int_0^\alpha Y_0(\alpha') Y_p(\alpha') \alpha' d\alpha' \tag{2.1.37}$$

and

$$I_\nu^{(p)} = \frac{1}{\sigma_p^*} \int_0^1 \sigma_p(\rho)(1-\rho)^{\nu+1/2} d\rho \tag{2.1.38}$$

If we use a number of P independent reference loading cases and the two conditions for the second and third derivative we obtain $P+2$ linear equations

$$\sum_{(\nu)} C_\nu I_\nu^p = Q_{0,p} \quad , \quad p = 1,2,...,P \tag{2.1.39}$$

$$\sum_{(\nu)} (\nu + 1/2)(\nu - 1/2) C_\nu = 0 \tag{2.1.40}$$

$$\sum_{(\nu)} (\nu + 1/2)(\nu - 1/2)(\nu - 3/2) C_\nu = 0 \tag{2.1.41}$$

which allow up to $P+2$ coefficients $C_\nu = C_\nu^{(1)}$ to be determined. For the two reference cases $\sigma = \sigma_0$ and $\sigma = \sigma_0 \cdot a/x$ and the first of the geometric conditions we obtain the system of linear equations

$$C_1 + \frac{5}{7} C_2 + \frac{5}{9} C_3 = \frac{5}{2} Q_{0,0} - \frac{5}{3} \tag{2.1.42}$$

$$C_1 + \frac{5}{9} C_2 + \frac{35}{99} C_3 = \frac{35}{4\alpha} Q_{0,1} - \frac{7}{3} \tag{2.1.43}$$

$$C_1 + 5C_2 + \frac{35}{3} C_3 = \frac{1}{3} \tag{2.1.44}$$

with the solution

$$C_1 = \frac{3465}{64\alpha} Q_{0,1} - \frac{105}{8} Q_{0,0} - \frac{17}{3} \tag{2.1.45}$$

$$C_2 = -\frac{3465}{32\alpha} Q_{0,1} + \frac{63}{2} Q_{0,0} + \frac{13}{5} \tag{2.1.46}$$

$$C_3 = \frac{18711}{448\alpha} Q_{0,1} - \frac{693}{56} Q_{0,0} - \frac{99}{35} \tag{2.1.47}$$

The derivatives read

$$\frac{dC_1}{d\alpha} = -\frac{3465}{64}\left[Q_{0,1}\left(2 + \frac{1}{\alpha^2} + \frac{\alpha}{Y_1}\frac{dY_1}{d\alpha}\right) - \sqrt{\frac{\pi}{8}}\frac{Y_1}{\alpha^3}\right] + \frac{105}{8}\left[Q_{0,0}\left(2\alpha + \frac{\alpha^2}{Y_0}\frac{dY_0}{d\alpha}\right) - \sqrt{\frac{\pi}{8}}\frac{Y_0}{\alpha^2}\right] \tag{2.1.48}$$

$$\frac{dC_2}{d\alpha} = \frac{3465}{32}\left[Q_{0,1}\left(2 + \frac{1}{\alpha^2} + \frac{\alpha}{Y_1}\frac{dY_1}{d\alpha}\right) - \sqrt{\frac{\pi}{8}}\frac{Y_1}{\alpha^3}\right] - \frac{63}{2}\left[Q_{0,0}\left(2\alpha + \frac{\alpha^2}{Y_0}\frac{dY_0}{d\alpha}\right) - \sqrt{\frac{\pi}{8}}\frac{Y_0}{\alpha^2}\right] \tag{2.1.49}$$

$$\frac{dC_3}{d\alpha} = -\frac{18711}{448}\left[Q_{0,1}\left(2 + \frac{1}{\alpha^2} + \frac{\alpha}{Y_1}\frac{dY_1}{d\alpha}\right) - \sqrt{\frac{\pi}{8}}\frac{Y_1}{\alpha^3}\right] + \frac{693}{56}\left[Q_{0,0}\left(2\alpha + \frac{\alpha^2}{Y_0}\frac{dY_0}{d\alpha}\right) - \sqrt{\frac{\pi}{8}}\frac{Y_0}{\alpha^2}\right] \tag{2.1.50}$$

2.2 Approximate procedure for components with internal cracks

2.2.1 Weight functions based on single reference loading cases

The eccentric crack For the treatment of internal cracks an extension of the procedure originally developed for edge cracks is given in [15]. This procedure allows internal eccentric cracks, loaded by non-symmetric stress distributions to be treated. In case of an internal crack it is of advantage to express the weight function in terms of the total crack length $\ell = 2a$.
The stress intensity factors at the points x_A and x_B (see Fig.5) can be written as

$$K_{IA} = \int_{x_B}^{x_A} \sigma(x) h_A(x, \ell)\, dx$$
$$K_{IB} = \int_{x_A}^{x_B} \sigma(x) h_B(x, \ell)\, dx \tag{2.2.1}$$

where the subscripts A and B refer to the crack tips at the locations x_A and x_B, respectively, and $h_A(x, \ell)$, $h_B(x, \ell)$ are the weight functions which have to be determined for a given crack and specimen geometry. The formula of Rice [7] then reads

$$h_A(x,\ell) = \frac{E'}{K_{IAr}} \frac{\partial v_r(x,\ell)}{\partial \ell_A} \quad , \quad h_B(x,\ell) = \frac{E'}{K_{IBr}} \frac{\partial v_r(x,\ell)}{\partial \ell_B} \tag{2.2.2}$$

considering a virtually infinitesimal crack extension $\partial \ell_A$ whilst the crack tip at x_B remains fixed and vice versa. The crack-opening displacement field can be expressed by a power series

$$v(x,\ell) = \sum_{\nu=0}^{\infty} \left\{ \begin{array}{ll} A_\nu \left(1 - \frac{2}{\ell}(x - x_m)\right)^{\nu+1/2} & \text{for } x_M < x \le x_M + 1/2\ell \\ B_\nu \left(1 + \frac{2}{\ell}(x - x_m)\right)^{\nu+1/2} & \text{for } x_M - 1/2\ell \le x < x_M \end{array} \right\} \tag{2.2.3}$$

or

$$v(x,\ell) = \sum_{\nu=0}^{\infty} \left\{ \begin{array}{ll} A_0 C_\nu \left(1 - \frac{2}{\ell}(x - x_m)\right)^{\nu+1/2} & \text{for } x_M < x \le x_M + 1/2\ell \\ B_0 \tilde{C}_\nu \left(1 + \frac{2}{\ell}(x - x_m)\right)^{\nu+1/2} & \text{for } x_M - 1/2\ell \le x < x_M \end{array} \right\} \tag{2.2.4}$$

$$\text{with} \quad A_\nu / A_0 = C_\nu \quad \text{and} \quad B_\nu / B_0 = \tilde{C}_\nu$$

The coefficients A_ν and B_ν can be determined by application of the following conditions [15]:

- For $x \to x_A$ and $x \to x_B$, the asymptotic displacement field is known from the reference stress intensity factors, leading to

$$A_0 = \frac{2\sigma_r^* \ell}{\sqrt{\pi}\, E'} Y_{Ar} \quad \text{and} \quad B_0 = \frac{2\sigma_r^* \ell}{\sqrt{\pi}\, E'} Y_{Br} \tag{2.2.5}$$

  with the geometric functions defined by

$$\left\{ \begin{array}{l} K_{Ar} \\ K_{Br} \end{array} \right\} = \sigma_r^* \sqrt{\ell} \left\{ \begin{array}{l} Y_{Ar}(\ell/W, x_M/W) \\ Y_{Br}(\ell/W, x_M/W) \end{array} \right\} \tag{2.2.6}$$

- Energy relations between a number of γ different reference solutions available can be obtained [15]. If only one reference load-case is available, the condition - equivalent to eq.(2.1.9) - reads

$$\int_{x_A}^{x_B} \sigma_r(x) v(x)\, dx = \frac{1}{E'} \int_0^{\ell} K_{Ar}^2(\ell')\, d\ell' \tag{2.2.7}$$

  Introducing the abbreviations

$$L_\nu = \frac{1}{\sigma_r^*} \int_0^1 \sigma_r(\eta)\, (1-\eta)^{\nu+1/2}\, d\eta \qquad M_\nu = \frac{1}{\sigma_r^*} \int_{-1}^0 \sigma_r(\eta)\, (1+\eta)^{\nu+1/2}\, d\eta \tag{2.2.8}$$

$$\eta = 2\,\frac{x - x_M}{\ell}$$

and

$$Q = 2\frac{\sigma_r^*}{\ell E'}\int_0^{\ell} Y_{Ar}^2 \ell'\, d\ell' \quad , \quad Q^* = \frac{Q}{A_0} = \frac{\sqrt{\pi}}{Y_{Ar}(\ell/W)^2}\int_0^{\ell/W} Y_{Ar}^2\, \ell'/W\, d\ell'/W \tag{2.2.9}$$

the final result

$$\sum_{\nu=0}^{\infty} L_\nu A_\nu + \sum_{\nu=0}^{\infty} M_\nu B_\nu = Q \tag{2.2.10}$$

$$\sum_{\nu=0}^{\infty} L_\nu C_\nu + \sum_{\nu=0}^{\infty} M_\nu \tilde{C}_\nu \frac{Y_{Ar}}{Y_{Br}} = Q^* \tag{2.2.11}$$

is obtained. The reduced coefficients for eq.(2.2.11) are

$$C_\nu = A_\nu/A_0 \ , \ \tilde{C}_\nu = B_\nu/B_0 \tag{2.2.12}$$

For a reference load with $\sigma_0 = \text{const.}$

$$L_\nu = M_\nu = \frac{2}{2\nu+3} \tag{2.2.13}$$

for a linear stress $\sigma = \sigma_0 \bullet \eta$

$$L_\nu = \frac{4}{4\nu^2 + 16\nu + 15} = -M_\nu \tag{2.2.14}$$

for a quadratic stress $\sigma = \sigma_0 \bullet \eta^2$

$$L_\nu = M_\nu = \frac{16}{8\nu^3 + 60\nu^2 + 142\nu + 105} \tag{2.2.15}$$

- The condition for continuity of the displacements and their derivatives at the point $x = x_M$ provide the relations

$$\sum_{\nu=0}^{\infty} (A_\nu - B_\nu) = 0$$

$$\sum_{\nu=0}^{\infty} (\nu+1/2)(A_\nu + B_\nu) = 0 \tag{2.2.16}$$

$$\sum_{\nu=0}^{\infty} (\nu+1/2)(\nu-1/2)(A_\nu - B_\nu) = 0$$

In order to obtain an inhomogeneous system of linear equations with a unique solution, it is sufficient to use the stress intensity factor solution for one reference loading case. For the reference solution ($\sigma = const$) and three relations of eq.(2.2.16) one obtains

$$A_1 + A_2 - B_1 - B_2 = B_0 - A_0 \tag{2.2.17}$$

$$3A_1 + 5A_2 + 3B_1 + 5B_2 = -B_0 - A_0 \tag{2.2.18}$$

$$3A_1 + 15A_2 - 3B_1 - 15B_2 = -B_0 + A_0 \tag{2.2.19}$$

$$\frac{2}{5}A_1 + \frac{2}{7}A_2 + \frac{2}{5}B_1 + \frac{2}{7}B_2 = Q_0 - \frac{2}{3}A_0 - \frac{2}{3}B_0 \tag{2.2.20}$$

The solution of these equations is

$$A_1 = \frac{35}{16}Q_0 - 2A_0 - \frac{2}{3}B_0 \tag{2.2.21}$$

$$A_2 = -\frac{21}{16}Q_0 + \frac{13}{15}A_0 + \frac{8}{15}B_0 \tag{2.2.22}$$

$$B_1 = \frac{35}{16}Q_0 - \frac{2}{3}A_0 - 2B_0 \tag{2.2.23}$$

$$B_2 = -\frac{21}{16}Q_0 + \frac{8}{15}A_0 + \frac{13}{15}B_0 \tag{2.2.24}$$

or

$$C_1 = \frac{35}{16}Q_0^* - 2 - \frac{2}{3}(Y_{Br}/Y_{Ar}) \quad , \quad C_2 = -\frac{21}{16}Q_0^* + \frac{13}{15} + \frac{8}{15}(Y_{Br}/Y_{Ar}) \tag{2.2.25}$$

$$\tilde{C}_1 = \frac{35}{16}Q_0^*\frac{Y_{Ar}}{Y_{Br}} - \frac{2}{3}\frac{Y_{Ar}}{Y_{Br}} - 2 \quad , \quad \tilde{C}_2 = -\frac{21}{16}Q_0^*\frac{Y_{Ar}}{Y_{Br}} + \frac{8}{15}\frac{Y_{Ar}}{Y_{Br}} + \frac{13}{15} \tag{2.2.26}$$

The weight function results as

$$h_A^{(+)} = \frac{2}{\sqrt{\pi\ell}}\sum_{\nu=0}^{N}\left\{\frac{\partial(C_\nu \ell\, Y_{Ar})}{Y_{Ar}\,\partial\ell} + (\nu+1/2)C_\nu\frac{1+\eta}{1-\eta}\right\}\left[1-\eta\right]^{\nu+1/2} \tag{2.2.27}$$

for $x - x_M > 0$ ($\eta > 0$) and

$$h_A^{(-)} = \frac{2}{\sqrt{\pi\ell}}\sum_{\nu=0}^{N}\left\{\frac{\partial(\tilde{C}_\nu \ell Y_B)}{Y_{Ar}\,\partial\ell} - (\nu+1/2)\tilde{C}_\nu Y_B/Y_A\right\}\left[1+\eta\right]^{\nu+1/2} \tag{2.2.28}$$

for $x - x_M \leq 0$, i.e. $\eta < 0$. The expression for h_B can be simply obtained from eqs.(2.2.27) and (2.2.28) by changing the subscripts A and B and replacing $x - x_M$ by $x_M - x$. Note that $C_\nu = A_\nu/A_0$ and $\tilde{C}_\nu = B_\nu/B_0$.

The central crack As a special case of the previous analysis a central crack in a symmetric structure is considered. In this case it holds for pure tension as reference load ($\sigma_r^* = \sigma_0$)

$$x_M = 0 \quad , \quad A_\nu = B_\nu \quad , \quad C_\nu = \tilde{C}_\nu \quad , \quad Y_{Ar} = Y_{Br} \quad , \quad h_A = h_B \tag{2.2.29}$$

From reasons of symmetry it is more convenient to use $a = \ell/2$ and the redefined geometric function

$$K = \sigma_0 \sqrt{a}\, Y(a/W) \quad , \quad Y(a/W) = \sqrt{2}\, Y(\ell/W) \tag{2.2.30}$$

with $Y(\ell/W)$ defined by eq.(2.2.6). Equations (2.2.5) and (2.2.21)-(2.2.24) reduce to

$$A_0 = \sqrt{\frac{8}{\pi}}\, \frac{\sigma_0}{E'}\, aY(a/W) \tag{2.2.31}$$

$$A_1 = \frac{35}{16} Q_0 - \frac{8}{3} A_0 \tag{2.2.32}$$

$$A_2 = -\frac{21}{16} Q_0 + \frac{7}{5} A_0 \tag{2.2.33}$$

with

$$Q_0 = \frac{2\sigma_0}{aE'} \int_0^a Y^2(a'/W)\, a'\, da' \tag{2.2.34}$$

The weight function then reads

$$h_A^{(+)} = \sqrt{\frac{2}{\pi a}} \sum_{\nu=0}^{N} \left\{ \frac{\partial (C_\nu a\, Y_{Ar})}{A_{Ar}\, \partial a} + (\nu + 1/2) C_\nu \frac{1+\rho}{1-\rho} \right\} \left(1-\rho\right)^{\nu+1/2} \qquad \rho > 0 \tag{2.2.35}$$

$$h_A^{(-)} = \sqrt{\frac{2}{\pi a}} \sum_{\nu=0}^{N} \left\{ \frac{\partial (C_\nu a\, Y_{Ar})}{Y_{Ar}\, \partial a} - (\nu + 1/2) C_\nu \right\} \left(1+\rho\right)^{\nu+1/2} \qquad \rho \le 0 \tag{2.2.36}$$

2.2.2 Weight functions based on multiple reference loading cases

2.2.2.1 The eccentric crack

The application of more than one reference solution - described in Section 2.1.3 for edge-cracked components - can also be used for internal cracks. The procedure is illustrated by an example. For three reference solutions ($\sigma = \sigma_0 = const$, $\sigma = \sigma_0 \bullet \eta$ and $\sigma = \sigma_0 \bullet \eta^2$ with $\eta = (x - x_M)/a$) and the first three relations of eq.(2.2.16) one obtains

$$A_1 + A_2 - B_1 - B_2 = B_0 - A_0 \tag{2.2.37}$$

$$3A_1 + 5A_2 + 3B_1 + 5B_2 = -B_0 - A_0 \tag{2.2.38}$$

$$3A_1 + 15A_2 - 3B_1 - 15B_2 = -B_0 + A_0 \tag{2.2.39}$$

$$\frac{2}{5}A_1 + \frac{2}{7}A_2 + \frac{2}{5}B_1 + \frac{2}{7}B_2 = Q_{0,0} - \frac{2}{3}A_0 - \frac{2}{3}B_0 \tag{2.2.40}$$

$$\frac{4}{35}A_1 + \frac{4}{63}A_2 - \frac{4}{35}B_1 - \frac{4}{63}B_2 = Q_{0,1} - \frac{4}{15}A_0 + \frac{4}{15}B_0 \tag{2.2.41}$$

$$\frac{16}{315}A_1 + \frac{16}{693}A_2 + \frac{16}{315}B_1 + \frac{16}{693}B_2 = Q_{0,2} - \frac{16}{105}A_0 - \frac{16}{105}B_0 \tag{2.2.42}$$

with

$$Q_{0,p} = 2\frac{\sigma_0}{\ell E'}\int_0^{\ell} Y_0(\ell')\, Y_p(\ell')\, \ell'\, d\ell' \tag{2.2.43}$$

For a total number of 4 conditions the solution of these equations is:

- 3 conditions of continuity (2.2.17)-(2.2.19) and one reference load case (2.2.20)

$$A_1 = \frac{35}{16}Q_{0,0} - 2A_0 - \frac{2}{3}B_0 \tag{2.2.44}$$

$$A_2 = -\frac{21}{16}Q_{0,0} + \frac{13}{15}A_0 + \frac{8}{15}B_0 \tag{2.2.45}$$

$$B_1 = \frac{35}{16}Q_{0,0} - \frac{2}{3}A_0 - 2B_0 \tag{2.2.46}$$

$$B_2 = -\frac{21}{16}Q_{0,0} + \frac{8}{15}A_0 + \frac{13}{15}B_0 \tag{2.2.47}$$

- 2 conditions of continuity (2.2.17),(2.2.18) and two reference load cases (2.2.20) and (2.2.41)

$$A_1 = \frac{315}{32}Q_{0,1} + \frac{35}{16}Q_{0,0} - \frac{10}{3}A_0 + \frac{2}{3}B_0 \tag{2.2.48}$$

$$A_2 = -\frac{315}{32}Q_{0,1} - \frac{21}{16}Q_{0,0} + \frac{11}{5}A_0 - \frac{4}{5}B_0 \tag{2.2.49}$$

$$B_1 = -\frac{315}{32}Q_{0,1} + \frac{35}{16}Q_{0,0} + \frac{2}{3}A_0 - \frac{10}{3}B_0 \tag{2.2.50}$$

$$B_2 = \frac{315}{32}Q_{0,1} - \frac{21}{16}Q_{0,0} - \frac{4}{5}A_0 + \frac{11}{5}B_0 \tag{2.2.51}$$

- 1 condition of continuity (2.2.17), and three reference load cases (2.2.20)-(2.2.42)

$$A_1 = \frac{3465}{128}Q_{0,2} + \frac{315}{32}Q_{0,1} - \frac{35}{16}Q_{0,0} - \frac{14}{3}A_0 - \frac{2}{3}B_0 \tag{2.2.52}$$

$$A_2 = -\frac{4851}{128} Q_{0,2} - \frac{315}{32} Q_{0,1} + \frac{77}{16} Q_{0,0} + \frac{61}{15} A_0 + \frac{16}{15} B_0 \tag{2.2.53}$$

$$B_1 = -\frac{3465}{128} Q_{0,2} - \frac{315}{32} Q_{0,1} - \frac{35}{16} Q_{0,0} - \frac{2}{3} A_0 - \frac{14}{3} B_0 \tag{2.2.54}$$

$$B_2 = -\frac{4851}{128} Q_{0,2} + \frac{315}{32} Q_{0,1} + \frac{77}{16} Q_{0,0} + \frac{16}{15} A_0 + \frac{61}{15} B_0 \tag{2.2.55}$$

2.2.2.2 The central crack

In case of a central crack ($x_M = 0, \eta = \rho$) it holds for the integrals $Q_{0,p}$

$$Q_{0,p} = 0 \tag{2.2.56}$$

if the stress distribution is antisymmetric, i.e. if

$$\sigma(x) = -\sigma(-x) \tag{2.2.57}$$

This is for instance the case for all stresses of type

$$\sigma(x) \propto x^{2n+1} \tag{2.2.58}$$

especially for

$$\sigma(x) \propto x \quad , \quad \rightarrow \quad , \quad Q_{0,1} = 0 \tag{2.2.59}$$

Taking into consideration $A_0 = B_0$ and $Q_{0,1} = 0$ reduces the relations eqs.(2.2.52)-(2.2.55):

- remaining condition of continuity and reference load case $\sigma = \sigma_0 \rightarrow$ eqs.(2.2.32) and (2.2.33).
- reference load cases $\sigma = \sigma_0$ and $\sigma = \sigma_0 \cdot (\rho)^2$

$$A_1 = \frac{3465}{128} Q_{0,2} - \frac{35}{16} Q_{0,0} - \frac{16}{3} A_0 \tag{2.2.60}$$

$$A_2 = -\frac{4851}{128} Q_{0,2} + \frac{77}{16} Q_{0,0} + \frac{77}{15} A_0 \tag{2.2.61}$$

2.3 Modification of the extended Petroski-Achenbach procedure

In all examples of sections 2.1 and 2.2 the energy balance condition - the fundamental idea of Petroski and Achenbach [17] - has been applied for the determination of unknown coefficients of the crack opening displacement relation. Unfortunately, in some special applications this condition cannot be used. This is the case for instance for compact tension (CT) specimens. The evaluation of the integral $Q(\alpha)$ needs the geometric function Y for the whole range $0 \leq \alpha' \leq \alpha$. But stress intensity factor solutions are only available for $\alpha > 0.2$. On the other hand also the stress distribution along the crack line - necessary for the determination of the integrals I_v - is not sufficiently known.
Fortunately, for fracture mechanics standard test specimens displacements at certain locations are known. This allows the determination of the needed number of coefficients. This modified

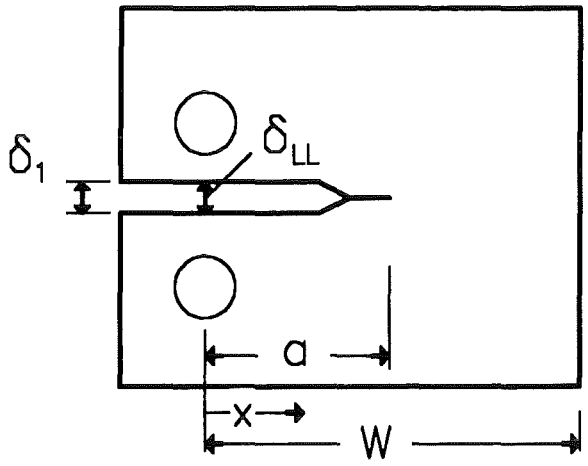

Figure 6. CT-specimen. Geometric data of a Compact-Tension specimen.

procedure has been applied in [23] to the Round-CT-specimen. Here the general procedure will be illustrated for the normal CT-specimen which is shown in fig.6. The information of the reference stress intensity factor solution and some crack opening conditions allow a number of coefficients in eq.(2.1.4) to be determined. As an example the following conditions may be used:

1. The crack-tip field is related to the stress intensity factor by eq.(2.1.2).
2. In addition we may use for instance the condition of vanishing curvature at $x = x_1$.
3. At the same location we demand that the crack opening displacement set-up must yield the known displacement δ_1.
4. In the load line the displacement should equal δ_{LL}.

One obtains a set of linear equations

$$\begin{aligned} 3C_1(1-x_1/a) + 15C_2(1-x_1/a)^2 + 35C_3(1-x_1/a)^3 &= 1 \\ C_1 + C_2 + C_3 &= R_1 \\ C_1(1-x_1/a)^{3/2} + C_2(1-x_1/a)^{5/2} + C_3(1-x_1/a)^{7/2} &= R_2 \end{aligned} \tag{2.2.62}$$

with

$$R_1 = \frac{\delta_{LL}}{2A_0} - 1 \quad , \qquad R_2 = \frac{\delta_1}{2A_0} - (1-x_1/a)^{1/2} \tag{2.3.1}$$

from which the coefficients C_1 to C_3 can be found as

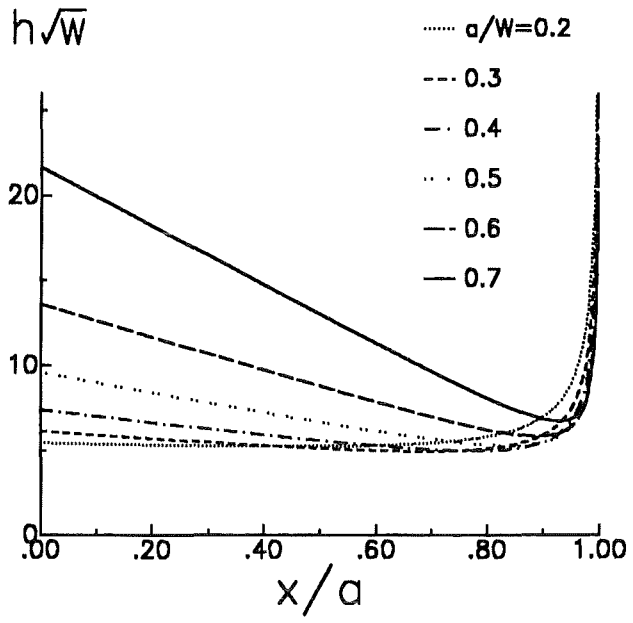

Figure 7. Weight function for a Compact-Tension specimen.

$$C_1 = \frac{20R_1U^{11/2} + 15R_2U^2 + U^{7/2} - U^{5/2} - 35R_2U^3}{20U^{11/2} - 32U^{9/2} + 12U^{7/2}}$$

$$C_2 = \frac{-32U^{9/2} - U^{7/2} - 35R_2U^3 + U^{3/2} - 3R_1U}{20U^{11/2} - 32U^{9/2} + 12U^{7/2}} \qquad (2.3.2)$$

$$C_3 = R_1 - C_1 - C_2$$

$$U = 1 - x_1/a$$

In case of the standard specimen (ASTM Standard E-399-72) it holds $x_1 = -W/4$ and the geometric function and displacements are ([14])

$$K_I = \sigma_0\sqrt{W}\,F_I\ , \quad \sigma_0 = \frac{P}{Wt}\ , \quad F_I = \frac{(2+\alpha)(0.886 + 4.64\alpha - 13.32\alpha^2 + 14.72\alpha^3 - 5.6\alpha^4)}{(1-\alpha)^{3/2}} \qquad (2.3.3)$$

(B = thickness, P = load applied).

$$\delta_{LL} = \frac{P}{E'B}\,V_{LL}(\alpha)$$

$$V_{LL}(\alpha) = \left(\frac{1+\alpha}{1-\alpha}\right)^2\left(2.163 + 12.219\alpha - 20.065\alpha^2 - 0.9925\alpha^3 + 20.609\alpha^4 - 9.9314\alpha^5\right) \qquad (2.3.4)$$

$$\delta_1 = \frac{P}{E'B}\,V_1(\alpha)$$

$$V_1(\alpha) = \left(1 + \frac{0.25}{\alpha}\right)\left(\frac{1+\alpha}{1-\alpha}\right)^2\left(1.6137 + 12.678\alpha - 14.231\alpha^2 - 16.61\alpha^3 + 35.05\alpha^4 - 14.494\alpha^5\right) \qquad (2.3.5)$$

The resulting weight function is shown in fig.7. A description by a fitting formula will be given in section 3.1.7.

2.4 Extension of approximate weight functions to rotationally-symmetric problems

2.4.1 The internal crack

Due to the rotational symmetry, tube problems with circumferential cracks - in principle two-dimensional cracks - can be treated in the same way as shown before for the merely pure one-dimensional cracks. The general approach will be explained for a tube of inside radius r and outside radius R containing an inner circumferential crack of depth a. Figure 8 illustrates the situation.
In contrast to eq.(1.2.3), the weight function is given by

$$h = \frac{E'}{K_{Ir}} \frac{r+x}{r+a} \frac{\partial v_r}{\partial a} \tag{2.4.1}$$

In the special case of a thin-walled tube ($r \ll R$) eq.(2.4.1) becomes identical with (1.2.3). The crack opening displacement field is also described by a power series, and the unknown coefficients C_0, C_1, C_2 result from the near-tip displacement field and the curvature at the free surface in the same manner as outlined for the edge-cracks. Only the energy condition has to be modified which results in

$$\int_0^a K_{Ir}^2(r+a')da' = E' \int_0^a \sigma_r(x) v_r(r+x)dx \tag{2.4.2}$$

For $\sigma = \sigma_r^* = const$ the condition for the coefficients follows as

$$\sum \frac{C_\nu}{\nu+3/2}\left(1+\frac{a}{r}\frac{1}{\nu+5/2}\right) = \frac{\sigma_r^*}{E' A_0 a}\int_0^a Y_r^2 a'(1+\frac{a'}{r})da' = Q_0 \tag{2.4.3}$$

(A_0 from eq.(2.1.5)). The first three coefficients are

$$C_0 = 1 \quad , \quad C_1 = \frac{1}{3} - 5C_2 \quad , \quad C_2 = \frac{\frac{4}{5} + \frac{32}{105}\frac{a}{r} - Q_0}{\frac{12}{7} + \frac{32}{63}\frac{a}{r}} \tag{2.4.4}$$

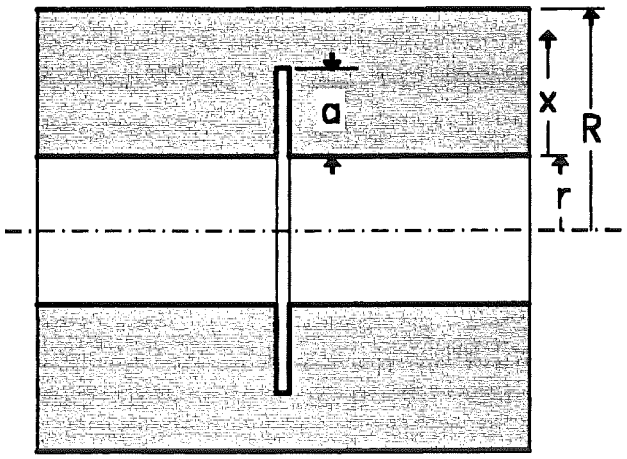

Figure 8. Geometry of a circumferential crack in a tube

2.4.2 The external crack

For the external crack the weight function is given by

$$h = \frac{E'}{K_{Ir}} \frac{R-x}{R-a} \frac{\partial v_r}{\partial a} \tag{2.4.5}$$

where now the origin of the x-coordinate has the origin at the outer surface. The energy condition reads

$$\int_0^a K_{Ir}^2 (R-a')da' = E'\,\sigma_r^* \int_0^a v_r (R-x)dx \tag{2.4.6}$$

and the condition for the coefficients are

$$\sum \frac{C_\nu}{\nu+3/2}\left(1-\frac{a}{R}\frac{1}{\nu+5/2}\right) = \frac{\sigma_0}{E'\,A_0 a}\int_0^a Y_r^2 a'(1-\frac{a'}{R})da' = Q_0 \tag{2.4.7}$$

yielding

$$C_0 = 1 \quad , \quad C_1 = \frac{1}{3} - 5C_2 \quad , \quad C_2 = \frac{\frac{4}{5} - \frac{32}{105}\frac{a}{R} - Q}{\frac{12}{7} - \frac{32}{63}\frac{a}{R}} \tag{2.4.8}$$

2.5 Direct adjustment of the weight function to reference stress intensity factors and geometric conditions

2.5.1 General relations

A disadvantage of the usual procedure treated before is that numerical integrations are necessary to evaluate the right-hand integrals in eq.(2.1.9), eq.(2.2.9) and eq.(2.4.3). A more direct determination of the weight function is possible that does not require the complete COD-field but only the near-tip crack opening displacement field to be known [24], [25]. As becomes obvious from introducing eq.(2.1.4) in eq.(1.2.3), a set-up for the weight function is given by

$$h(x,a) = \sqrt{\frac{2}{\pi a}}\left[\frac{\rho}{\sqrt{1-\rho}} + \sum_{\nu=0}^{\infty} D_\nu (1-\rho)^{\nu+1/2}\right] \quad , \quad \rho = x/a \tag{2.5.1}$$

or if we replace the factor ρ again by the identity $\rho = 1-(1-\rho)$

$$h(x,a) = \sqrt{\frac{2}{\pi a}}\left[\frac{1}{\sqrt{1-\rho}} + \sum_{\nu=0}^{\infty} \tilde{D}_\nu (1-\rho)^{\nu+1/2}\right] \tag{2.5.2}$$

where $\tilde{D}_0 = D_0 - 1$ and $\tilde{D}_\nu = D_\nu$ for $\nu \geq 1$. The tilde is dropped in the following sections. The coefficients D_ν are different from those used in eq.(2.1.4), which represent the crack opening displacements.
A number of conditions can be derived for the determination of the coefficients D_ν. If a number of μ reference loading cases are known, the weight function must fulfill a number of μ conditions

$$\int_0^a h(x,a)\sigma_{r,i}(x)\,dx = \sigma^*_{r,i}\sqrt{a}\,Y_{r,i} \quad , \quad i = 1...\mu \tag{2.5.3}$$

The integrals on the left-hand side of eq.(2.5.3) can be determined easily, especially for power-shaped and thus polynomial stress distributions. For constant stress (tension loading, $Y = Y_0$)

$$\int_0^a h(x,a)\,dx = \sqrt{a}\,Y_0 \tag{2.5.4}$$

$$\sum_{\nu=0}^{\infty} D_\nu \frac{2}{2\nu+3} = \sqrt{\frac{\pi}{2}}\,Y_0 - \frac{4}{3} \tag{2.5.5}$$

For four terms this leads to

$$D_0 + \frac{3}{5}D_1 + \frac{3}{7}D_2 + \frac{1}{3}D_3 = R_0 \tag{2.5.6}$$

with

$$R_0 = \frac{3}{2}\sqrt{\frac{\pi}{2}}\,Y_0 - 2 \tag{2.5.7}$$

For linear stress distribution ($Y = Y_1$)

$$\sigma = \sigma^* \frac{x}{W} \tag{2.5.8}$$

$$\int_0^a h(x,a)\,\frac{x}{W}\,dx = \sqrt{a}\,Y_1 \tag{2.5.9}$$

or

$$\sum D_\nu \frac{1}{(2\nu+3)(2\nu+5)} = \frac{1}{4\alpha}\sqrt{\frac{\pi}{2}}\,Y_1 - \frac{4}{15} \tag{2.5.10}$$

For four terms this leads to

$$D_0 + \frac{3}{7}D_1 + \frac{5}{21}D_2 + \frac{5}{33}D_3 = R_1 \tag{2.5.11}$$

with

$$R_1 = \frac{15}{4\alpha}\sqrt{\frac{\pi}{2}}\,Y_1 - 4 \tag{2.5.12}$$

If the linear stress distribution is caused by bending of a plate ($Y = Y_b$)

$$\sigma = \sigma^*\left(1 - \frac{2x}{W}\right)$$

$$\sum D_\nu\left(\frac{1}{2\nu+3} - \frac{4\alpha}{(2\nu+3)(2\nu+5)}\right) = \frac{16}{15}\alpha - \frac{2}{3} + \frac{1}{2}\sqrt{\frac{\pi}{2}}\,Y_b \tag{2.5.13}$$

where Y_b is the geometric function for bending. For four terms this leads to

$$\begin{aligned} &D_0\left(\frac{1}{3} - \frac{4}{15}\alpha\right) + D_1\left(\frac{1}{5} - \frac{4}{35}\alpha\right) + D_2\left(\frac{1}{7} - \frac{4}{63}\alpha\right) + \\ &D_3\left(\frac{1}{9} - \frac{4}{99}\alpha\right) = \frac{16}{15}\alpha - \frac{2}{3} + \frac{1}{2}\sqrt{\frac{\pi}{2}}\,Y_b \end{aligned} \tag{2.5.14}$$

If the stress intensity factors for tension and bending loading are known then eq.(2.5.11) can be applied with

$$R_1 = \frac{15}{8\alpha}\sqrt{\frac{\pi}{2}}\,(Y_0 - Y_b) - 4 \tag{2.5.15}$$

For quadratic stress distribution

$$\sigma = \sigma^*\left(\frac{x}{W}\right)^2 \tag{2.5.16}$$

$$\int_0^a h(x,a)\left(\frac{x}{W}\right)^2 dx = \sqrt{a}\,Y_2 \tag{2.5.17}$$

$$\sum D_\nu \frac{1}{(2\nu+3)(2\nu+5)(2\nu+7)} = -\frac{6}{105} + \frac{1}{16\alpha^2}\sqrt{\frac{\pi}{2}}\,Y_2 \tag{2.5.18}$$

For four terms this leads to

$$D_0 + \frac{1}{3}D_1 + \frac{5}{33}D_2 + \frac{35}{429}D_3 = R_2 \tag{2.5.19}$$

with

$$R_2 = -6 + \frac{105}{16\alpha^2}\sqrt{\frac{\pi}{2}}\,Y_2 \tag{2.5.20}$$

Since for edge-cracks normal to the component surface the conditions (2.1.22) and (2.1.25) must hold, one obtains due to

$$\frac{\partial^2 h}{\partial x^2} = \frac{E'}{K_{Ir}}\frac{\partial}{\partial a}\frac{\partial^2 v_r}{\partial x^2} \quad , \quad \frac{\partial^3 h}{\partial x^3} = \frac{E'}{K_{Ir}}\frac{\partial}{\partial a}\frac{\partial^3 v_r}{\partial x^3}$$

the conditions

$$\frac{\partial^2 h}{\partial x^2}\Big|_{x=0} = 0 \quad \text{i.e.} \quad \frac{\partial^2 h}{\partial \rho^2}\Big|_{\rho=0} = 0 \tag{2.5.21}$$

and

$$\frac{\partial^3 h}{\partial x^3}\Big|_{x=0} = 0 \quad \text{i.e.} \quad \frac{\partial^3 h}{\partial \rho^3}\Big|_{\rho=0} = 0 \tag{2.5.22}$$

Equation (2.5.21) leads to

$$\sum_{\nu=0}^{\infty} D_\nu(\nu+1/2)(\nu-1/2) = -1 \tag{2.5.23}$$

and for four terms

$$D_0 - 3D_1 - 15D_2 - 35D_3 = 4 \tag{2.5.24}$$

Equation (2.5.22) leads to

$$\sum_{\nu=0}^{\infty} D_\nu(\nu+1/2)(\nu-1/2)(\nu-3/2) = \frac{9}{4} \tag{2.5.25}$$

and for four terms

$$D_0 - D_1 + 5D_2 + 35D_3 = 6 \tag{2.5.26}$$

If μ equations of type (2.5.3) and k geometric conditions are used, the resulting $(\mu+k)x(\mu+k)$ system of linear equations allows $(\mu+k)$ coefficients to be determined. In this procedure the same conditions are applied as for approximating the crack opening displacement field. Therefore, the same accuracy can be expected from both methods.

2.5.2 Calculation of weight functions

The different relations for the coefficients D are summarised:

constant stress:

$$D_0+\frac{3}{5}D_1+\frac{3}{7}D_2+\frac{1}{3}D_3=R_0 \qquad (I)$$

linear stress distribution:

$$D_0+\frac{3}{7}D_1+\frac{5}{21}D_2+\frac{5}{33}D_3=R_1 \qquad (II)$$

quadratic stress distribution:

$$D_0+\frac{1}{3}D_1+\frac{5}{33}D_2+\frac{35}{429}D_3=R_2 \qquad (III)$$

second derivative:

$$D_0-3D_1-15D_2-35D_3=4 \qquad (IV)$$

third derivative:

$$D_0-D_1+5D_2+35D_3=6 \qquad (V)$$

Weight functions with two three or four coefficients can be obtained from these relations. If only one reference load case is available equation I, II or III should be combined with equation IV. Using in addition eq.V and thus obtaining three coefficients leads to a larger deviation from the correct weight function than using only eq.IV and then only two coefficients.
The coefficients are:

a. Constant stress

$$D_0=\frac{2}{3}+\frac{5}{6}R_0=-1+\frac{5}{4}\sqrt{\frac{\pi}{2}}Y_0$$

$$D_1=-\frac{10}{9}+\frac{5}{18}R_0=-\frac{5}{3}+\frac{5}{12}\sqrt{\frac{\pi}{2}}Y_0$$

b. Linear stress distribution

$$D_0=\frac{1}{2}+\frac{7}{8}R_1$$

$$D_1=-\frac{7}{6}+\frac{7}{24}R_1$$

c. Quadratic stress distribution

$$\sigma = \sigma^*(x/W)^2$$

$$D_0 = \frac{2}{5} + \frac{9}{10} R_2 = -5 + \frac{189}{32\alpha^2} \sqrt{\frac{\pi}{2}} Y_2$$

$$D_1 = -\frac{6}{5} + \frac{3}{10} R_2 = -3 + \frac{63}{32\alpha^2} \sqrt{\frac{\pi}{2}} Y_2$$

If two reference load cases are avaliable these can be combined with eq.IV leading to three coefficients or with eqs.IV and V leading to four coefficients.

a. Constant and linear stress distribution and eq.IV:

$$D_0 = -\frac{35}{12} R_0 + \frac{63}{16} R_1 - \frac{1}{12}$$

$$D_1 = \frac{70}{9} R_0 - \frac{63}{8} R_1 + \frac{7}{18}$$

$$D_2 = -\frac{35}{20} R_0 + \frac{147}{80} R_1 - \frac{7}{20}$$

b. Constant and quadratic stress distribution and eq.IV:

$$D_0 = -\frac{1}{15} - \frac{35}{24} R_0 + \frac{99}{40} R_2$$

$$D_1 = \frac{16}{45} + \frac{175}{36} R_0 - \frac{99}{20} R_2$$

$$D_2 = -\frac{77}{225} - \frac{77}{72} R_0 + \frac{231}{200} R_2$$

c. Constant and linear stress distribution and eqs.IV and V:

$$D_0 = -\frac{19}{80} - \frac{105}{32} R_0 + \frac{693}{160} R_1$$

$$D_1 = \frac{101}{80} + \frac{315}{32} R_0 - \frac{1617}{160} R_1$$

$$D_2 = -\frac{621}{400} - \frac{147}{32} R_0 + \frac{3927}{800} R_1$$

$$D_3 = \frac{1221}{2800} + \frac{33}{32} R_0 - \frac{891}{800} R_1$$

If the boundary condition $h'' = 0$ and $h''' = 0$ are not applicable (thus will be the case if the crack is not perpendicular to the contour of the component) two coefficients can be obtained from reference solutions for constant and linear stress:

$$D_0 = -\frac{5}{2} R_0 + \frac{7}{2} R_1$$

$$D_1 = \frac{35}{6}(R_0 - R_1)$$

In these relations R_0 is obtained from eq.(2.5.22), R_2 from eq.(2.5.18) and R_1 from eq.(2.5.12) or eq.(2.5.15).

2.5.3 Adjusting of coefficients to COD-results

The COD-data reported in the literature for specific fracture mechanics test specimens can, in principle, also be used for the direct adjusting of weight functions to stress intensity factor solutions. Starting from eq.(1.2.3) we can compute the displacement at any location x of the crack as

$$\delta(x) = \frac{1}{E'}\int_x^a K_I(a')\, h(x,a')\, da' \tag{2.5.27}$$

Using the set-up for the weight function

$$h = \sqrt{\frac{2}{\pi a}} \sum_{\nu=0}^{N} D_\nu (1 - x/a)^{\nu - 1/2} \quad , \quad D_0 = 1 \tag{2.5.28}$$

eq.(2.5.28) can be written

$$\delta(x) = \frac{\sigma^*}{E'}\sqrt{\frac{2}{\pi a}} \sum_{\nu=0}^{N} D_\nu\, I_\nu(x,a) \tag{2.5.29}$$

with

$$I_\nu(x,a) = \int_x^a Y_I(a')\sqrt{a'}\,(1 - x/a')^{\nu - 1/2}\, da' \tag{2.5.30}$$

Equation (2.5.29) allows an additional coefficient D_ν to be determined. This should be recommended for special problems where the geometric function Y_I is independent of the crack size, e.g. cracks in infinite and semi-infinite bodies. In this case eq.(2.5.30) can be integrated analytically. If Y depends on the crack length the integration has to be performed numerically. Therefore, the main advantage of the direct adjustment method, i.e. the purely analytical treatment, may be lost.

2.5.4 Stress intensity factor for power-shaped stress distributions

Very often it is possible to describe the stress-distribution in the uncracked component by

$$\sigma(x) = \sum_{n=0}^{N} \sigma_n \left(\frac{x}{W}\right)^n \tag{2.5.31}$$

The stress intensity factor of each term can be obtained by applying the weight function in the form of eq.(2.5.1). Then the integration leads to

$$K = \sum_{n=0}^{N} \sigma_n \sqrt{a}\, Y_n \tag{2.5.32}$$

with

$$Y_n = \sqrt{\frac{2}{\pi}}\, \alpha^n \left[\frac{(n+1)!\sqrt{\pi}}{\Gamma(n+5/2)} + \sum_{\nu=0}^{N} D_\nu \frac{n!\Gamma(\nu+3/2)}{\Gamma(\nu+n+5/2)} \right] \tag{2.5.33}$$

2.6 Direct adjustment procedure for internal cracks

2.6.1 Basic relations

The method described in the previous section for edge cracks can also be applied for internal cracks. As suggested by eqs.(2.2.27) and (2.2.28) we will make a set-up for the most general case

$$h_A^{(+)}(x,a) = \sqrt{\frac{2}{\pi a}} \sum_{\nu=0}^{\infty} D_\nu (1-\eta)^{\nu-1/2} \quad , \quad \eta = (x - x_M)/a \quad \text{for } \eta > 0 \tag{2.6.1}$$

$$h_A^{(-)}(x,a) = \sqrt{\frac{2}{\pi a}} \sum_{\nu=0}^{\infty} \tilde{D}_\nu (1+\eta)^{\nu+1/2} \qquad \text{for } \eta < 0 \tag{2.6.2}$$

with

$$D_0 = 1 \quad , \quad \tilde{D}_0 = \frac{1}{2}\frac{Y_B}{Y_A} + a\frac{\partial}{\partial a}\left(\frac{Y_B}{Y_A}\right) \tag{2.6.3}$$

The unknown coefficients D_1, D_2 and $\tilde{D}_1$, $\tilde{D}_2$ can be determined from reference solutions and conditions of continuity at $\eta = 0$. If we restrict the series to N terms the unknown coefficients may be obtained for instance by a number of $N - \gamma$ conditions of continuity

$$h_A^{(-)} = h_A^{(+)} \quad , \quad \frac{\partial}{\partial \eta} h_A^{(-)} = \frac{\partial}{\partial \eta} h_A^{(+)} \quad , \quad \frac{\partial^2}{\partial \eta^2} h_A^{(-)} = \frac{\partial^2}{\partial \eta^2} h_A^{(+)} \quad \text{etc.} \tag{2.6.4}$$

and the conditions for γ reference stress intensity factors

$$\int_{-a}^{0} h_A^{(-)} \sigma_r(x)\, dx + \int_{0}^{a} h_A^{(+)} \sigma_r(x)\, dx = \sigma_0 Y_A \sqrt{a} \tag{2.6.5}$$

This leads for the three first conditions of continuity $h^{(+)}(0) = h^{(-)}(0)$, $dh^{(+)}/d\eta(0) = dh^{(-)}/d\eta(0)$, $d^2h^{(+)}/d\eta^2(0) = d^2h^{(-)}/d\eta^2(0)$ and the three loading cases $\sigma = \sigma_0$, $\sigma = \sigma_0 \bullet \eta$ and $\sigma = \sigma_0 \bullet \eta^2$ to the linear system of equations

$$D_1 + D_2 + D_3 - \tilde{D}_1 - \tilde{D}_2 - \tilde{D}_3 = \tilde{D}_0 - 1 \tag{2.6.6}$$

$$D_1 + 3D_2 + 5D_3 + 3\tilde{D}_1 + 5\tilde{D}_2 + 7\tilde{D}_3 = -\tilde{D}_0 + 1 \tag{2.6.7}$$

$$D_1 - 3D_2 - 15D_3 + 3\tilde{D}_1 + 15\tilde{D}_2 + 35\tilde{D}_3 = \tilde{D}_0 + 3 \tag{2.6.8}$$

$$D_1 + \frac{3}{5}D_2 + \frac{3}{7}D_3 + \frac{3}{5}\tilde{D}_1 + \frac{3}{7}\tilde{D}_2 + \frac{3}{9}\tilde{D}_3 = \frac{3}{2}\sqrt{\frac{\pi}{2}}Y_0 - \tilde{D}_0 - 3 \tag{2.6.9}$$

$$D_1 + \frac{3}{7}D_2 + \frac{5}{21}D_3 - \frac{3}{7}\tilde{D}_1 - \frac{5}{21}\tilde{D}_2 - \frac{5}{33}\tilde{D}_3 = \frac{15}{4}\sqrt{\frac{\pi}{2}}Y_1 + \tilde{D}_0 - 5 \tag{2.6.10}$$

$$D_1 + \frac{1}{3}D_2 + \frac{5}{33}D_3 + \frac{1}{3}\tilde{D}_1 + \frac{5}{33}\tilde{D}_2 + \frac{35}{429}\tilde{D}_3 = \frac{105}{16}\sqrt{\frac{\pi}{2}}Y_2 - \tilde{D}_0 - 7 \tag{2.6.11}$$

For practical use knowledge of a reduced number of coefficients may be sufficient. If we restrict the series expansion for the weight function to $v \leq N = 2$ we obtain by use of:

- three conditions of continuity (in increasing order) and the constant stress $\sigma_r = \sigma_0$ as reference solution

$$D_1 = \frac{315}{208}\sqrt{\frac{\pi}{2}}Y_0 - \frac{8}{13}\tilde{D}_0 - \frac{42}{13} \tag{2.6.12}$$

$$D_2 = -\frac{175}{208}\sqrt{\frac{\pi}{2}}Y_0 + \frac{22}{39}\tilde{D}_0 + \frac{19}{13} \tag{2.6.13}$$

$$\tilde{D}_1 = \frac{245}{208}\sqrt{\frac{\pi}{2}}Y_0 - \frac{62}{39}\tilde{D}_0 - \frac{24}{13} \tag{2.6.14}$$

$$\tilde{D}_2 = -\frac{105}{208}\sqrt{\frac{\pi}{2}}Y_0 + \frac{7}{13}\tilde{D}_0 + \frac{14}{13} \tag{2.6.15}$$

- two conditions of continuity (in increasing order) combined with constant stress reference case $\sigma = \sigma_0$ and the linear stress $\sigma_r = \sigma_0 \bullet \eta$ as a second reference solution

$$D_1 = \frac{105}{176}\sqrt{\frac{\pi}{2}}Y_0 + \frac{1575}{352}\sqrt{\frac{\pi}{2}}Y_1 + \frac{4}{11}\tilde{D}_0 - \frac{74}{11} \tag{2.6.16}$$

$$D_2 = \frac{35}{176}\sqrt{\frac{\pi}{2}}Y_0 - \frac{1785}{352}\sqrt{\frac{\pi}{2}}Y_1 - \frac{6}{11}\tilde{D}_0 + \frac{179}{33} \tag{2.6.17}$$

$$\tilde{D}_1 = \frac{455}{176}\sqrt{\frac{\pi}{2}}Y_0 - \frac{2415}{352}\sqrt{\frac{\pi}{2}}Y_1 - \frac{34}{11}\tilde{D}_0 + \frac{116}{33} \tag{2.6.18}$$

$$\tilde{D}_2 = -\frac{315}{176}\sqrt{\frac{\pi}{2}}Y_0 + \frac{2205}{352}\sqrt{\frac{\pi}{2}}Y_1 + \frac{21}{11}\tilde{D}_0 - \frac{42}{11} \tag{2.6.19}$$

- and finally for one conditions of continuity combined with constant stress reference case $\sigma = \sigma_0$, the linear stress $\sigma_r = \sigma_0 \bullet \eta$ and a quadratic stress distribution $\sigma_r = \sigma_0 \bullet \eta^2$

$$D_1 = -\frac{1155}{976}\sqrt{\frac{\pi}{2}}\,Y_0 + \frac{4725}{1952}\sqrt{\frac{\pi}{2}}\,Y_1 + \frac{72765}{7808}\sqrt{\frac{\pi}{2}}\,Y_2 - \frac{16}{61}\tilde{D}_0 - \frac{642}{61} \tag{2.6.20}$$

$$D_2 = \frac{3255}{976}\sqrt{\frac{\pi}{2}}\,Y_0 - \frac{2835}{1952}\sqrt{\frac{\pi}{2}}\,Y_1 - \frac{128205}{7808}\sqrt{\frac{\pi}{2}}\,Y_2 + \frac{34}{61}\tilde{D}_0 + \frac{739}{61} \tag{2.6.21}$$

$$\tilde{D}_1 = -\frac{1365}{976}\sqrt{\frac{\pi}{2}}\,Y_0 - \frac{22365}{1952}\sqrt{\frac{\pi}{2}}\,Y_1 + \frac{162855}{7808}\sqrt{\frac{\pi}{2}}\,Y_2 - \frac{274}{61}\tilde{D}_0 - \frac{304}{61} \tag{2.6.22}$$

$$\tilde{D}_2 = \frac{3465}{976}\sqrt{\frac{\pi}{2}}\,Y_0 + \frac{24255}{1952}\sqrt{\frac{\pi}{2}}\,Y_1 - \frac{218295}{7808}\sqrt{\frac{\pi}{2}}\,Y_2 + \frac{231}{61}\tilde{D}_0 + \frac{462}{61} \tag{2.6.23}$$

In case of the central crack it holds in accordance to eq.(2.2.29) $D_\nu = \tilde{D}_\nu$ and $\tilde{D}_0 = 1/2$.

2.6.2 Internal crack in an infinite body

The internal crack in an infinite body ($\eta = \rho$), the so-called Griffith-crack, is analytically solved. The weight function, here noted as h_{exact}, is given by

$$h_{exact} = \frac{1}{\sqrt{\pi a}}\sqrt{\frac{a-x}{a+x}} \tag{2.6.24}$$

and therefrom a number of reference stress intensity factors can be derived. For $\sigma = \sigma_0$ we obtain

$$Y_0 = \sqrt{\pi} \tag{2.6.25}$$

for the linear stress $\sigma = \sigma_0 \bullet \eta$

$$Y_1 = \frac{1}{2}\sqrt{\pi} \tag{2.6.26}$$

and for the quadratic stress $\sigma = \sigma_0 \bullet \eta^2$

$$Y_2 = \frac{1}{2}\sqrt{\pi} \tag{2.6.27}$$

The approximate weight function resulting from eqs.(2.6.6)-(2.6.11) has been calculated and is compared with the exact solution in fig.9. In this representation the relative deviations from the exact solution are plotted. It can be seen that the maximum deviations are less than 0.4%. A more detailed analysis with respect to convergence and accuracy will be given in 2.8.

2.7 Approximative procedure for weight functions in mode-II loading

The method of determining stress intensity factors using an approximative crack-opening displacement field, well-known for mode-I loaded cracks, can be extended to include mode-II loaded cracks.

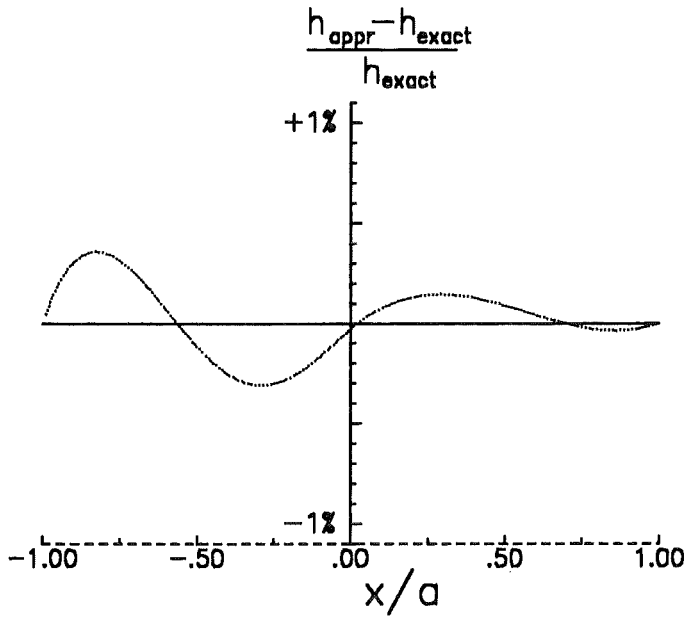

Figure 9. Weight function for an internal crack in an infinite body. Deviations between an approximation based on 6 coefficients and the exact weight function.

The weight function method for the determination of stress intensity factors for complicated stress distributions is applicable to mode-II loadings, too. For any given shear-stress distribution $\tau(x)$ in the uncracked component the stress intensity factor K_{II} results as

$$K_{II} = \int_0^a h_{II}(x,a)\tau(x)\,dx \tag{2.7.1}$$

where h_{II} is the mode-II weight function. According to the mode-I case, the weight function can be derived from crack opening displacements u (in x-direction, see fig.10) of a reference load case (subscript r) and the related reference stress intensity factor

$$h_{II}(x,a) = \frac{E'}{K_{IIr}} \frac{\partial}{\partial a} u_r(x,a) \tag{2.7.2}$$

The crack-opening displacements can be expressed again by power-series representations [31], [32]

$$u_r = \sum_{\nu=0}^{\infty} D_\nu \left(1 - \frac{x}{a}\right)^{\nu+1/2} \tag{2.7.3}$$

with the coefficients D_n dependent on the relative crack length a/W.
A number of conditions can be applied to determine the unknown coefficients of eq.(2.7.3):

1. The crack-tip field is related to the stress intensity factor by [17]

$$u_r(x \to a) = \left(\frac{8}{\pi}\right)^{1/2} \frac{K_{IIr}}{E'} \sqrt{a - x} \tag{2.7.4}$$

2. The energy balance condition requires

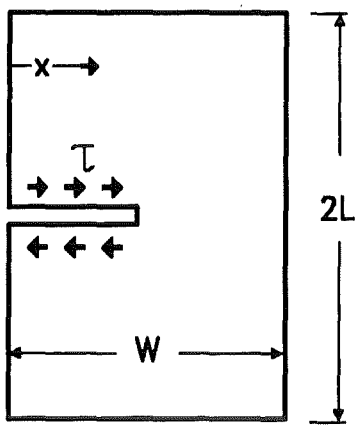

Figure 10. The edge crack in a plate under shear stresses

$$\int_0^a K_{IIr}^2 da' = E' \int_0^a \tau_r(x) u_r(x,a) dx \tag{2.7.5}$$

If stress intensity factors for a number of p loading cases (subscript p) are known, eq.(2.7.5) provides p relations

3. For symmetrically loaded central internal cracks it follows from the condition of symmetry that odd derivatives must vanish

$$u^{(2i+1)} = 0 \qquad (i = 0,1,2,..) \quad \text{for } x = 0 \tag{2.7.6}$$

4. As has been shown in [31] for mode-II loadings for an edge crack, the second derivative must vanish:

$$\frac{\partial^2 v}{\partial x^2} = 0 \quad , \quad \frac{\partial^2 u}{\partial x^2} = 0 \tag{2.7.7}$$

5. and also the third derivatives must disappear at the crack mouth

$$\frac{\partial^3 v}{\partial x^3} = 0 \quad , \quad \frac{\partial^3 u}{\partial x^3} = 0 \tag{2.7.8}$$

as has been proved in [32].

6. For simple crack/component geometries (e.g. an edge crack in a rectangular plate or a disc) relations of equilibrium can be derived ([32]).

The further procedure to determine approximative weight functions is identical with the mode-I case outlined in detail before.

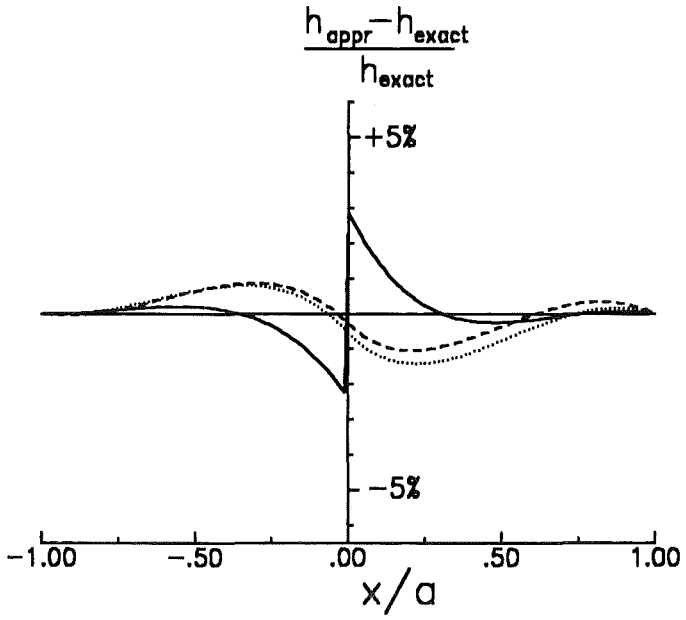

Figure 11. Internal crack in an infinite body. Approximate weight functions based on the improved Petroski-Achenbach procedure compared with the exact weight function; solid curve: computed for a single reference stress intensity factor solution ($\sigma = \sigma_0$), dashed curve: computed for two simultaneously applied reference solutions ($\sigma = \sigma_0$ and $\sigma = \sigma_0 \cdot (x/a)^2$).

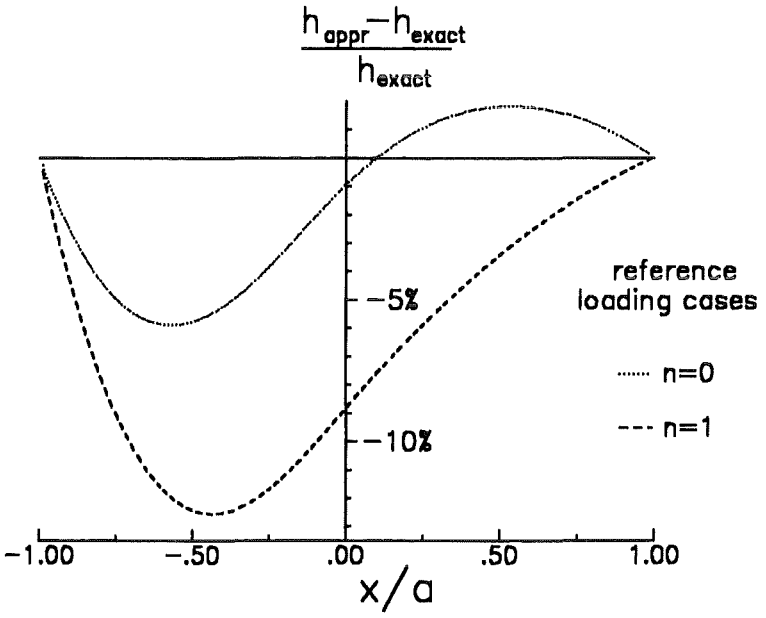

Figure 12. Internal crack in an infinite body. Direct adjusting method; relative deviations between approximate and exact weight function; solid curve: single reference case $\sigma = \sigma_0$, dashed curve: single reference case $\sigma = \sigma_0 \cdot x/a$.

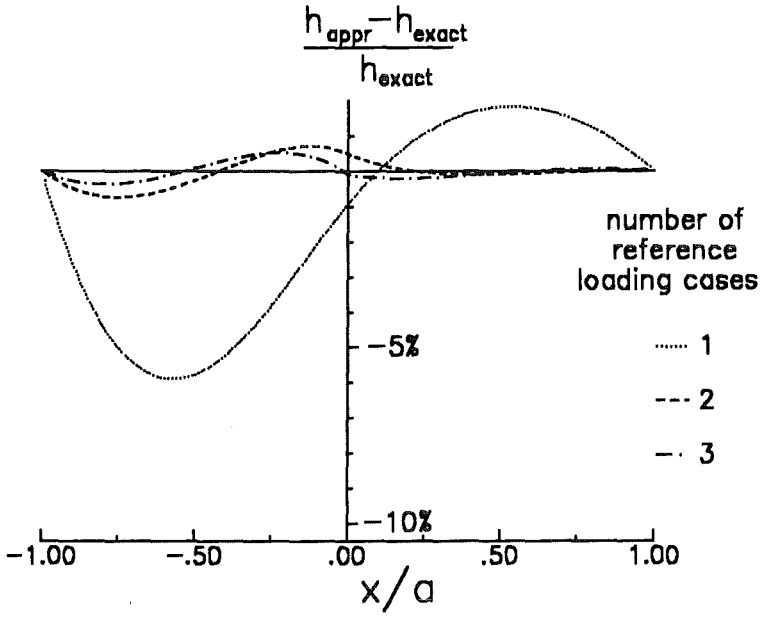

Figure 13. Internal crack in an infinite body. Direct adjusting method; relative deviations between approximate and exact weight function; dotted curve: 3 conditions of continuity and $\sigma = \sigma_0$ as reference load case; dashed curve: 2 conditions of continuity, $\sigma = \sigma_0$ and $\sigma = \sigma_0 \cdot x/a$ as reference cases; dash-dotted curve: 1 condition of continuity, $\sigma = \sigma_0$, $\sigma = \sigma_0 \cdot x/a$ and $\sigma = \sigma_0 \cdot (x/a)^2$ as reference cases; solid line: eq.(2.6.24).

2.8 Convergence and accuracy of approximate procedures

In order to allow the quality of the previously described procedures to be judged it is necessary to use exact reference solutions for the stress intensity factors. Exact stress intensity factor solutions were determined for internal cracks in infinite bodies (see e.q. [12]) and for edge-cracked discs [33]. A weight function of high accuracy can be derived for the edge-cracked semi-infinite body on the basis of crack opening displacement calculations given by Wigglesworth [34]. This solution is of very high quality but not exact. The accuracy of the results can be checked in cases where exact analytical solutions of the weight function are available. Such a solution is known for internal cracks in infinite bodies.

2.8.1 The internal crack in an infinite body

Improved Petroski-Achenbach procedure

The integrals $Q_{0,0}$ and $Q_{0,2}$ necessary for the determination of approximate weight functions by eqs.(2.2.32), (2.2.33), (2.2.60) and (2.2.61) are

$$Q_{0,0} = \frac{\sigma_0}{E'}\pi a \quad , \quad Q_{0,2} = \frac{1}{4}\frac{\sigma_0}{E'}\pi a \tag{2.8.1}$$

leading to

$$C_1 = \frac{35}{32}\frac{\pi}{\sqrt{2}} - \frac{8}{3} \quad , \quad C_2 = -\frac{21}{64}\frac{\pi}{\sqrt{2}} + \frac{7}{5} \tag{2.8.2}$$

for constant stress as the single reference load, and

$$C_1 = \frac{35}{32}\frac{\pi}{\sqrt{2}} - \frac{8}{3} \quad , \quad C_2 = -\frac{3619}{512}\frac{\pi}{\sqrt{2}} + \frac{77}{15} \tag{2.8.3}$$

for combined linear and quadratic stresses. It should be mentioned, that the first and the third of the conditions of displacement continuity are automatically fulfilled for central crack and therefore, in reality, only one geometric condition provides information on the needed coefficients.
The approximate weight functions computed with the coefficients of Section 2.2.2.2 are represented in fig.11. From the constant stress load case, eqs.(2.2.32) and (2.2.33), the dashed curve results and from the combination of constant and linear stress, eqs.(2.2.60) and (2.2.61), one obtains the solid curve. I can be seen that already for one single reference load case ($\sigma = \sigma_0$) the maximum deviations from the exact solution are at most 1.05%.

procedure	total number of conditions	$n=0$	$n=1$	$n=2$	maximum deviation
improved Petroski-Achenbach	4	x			1.05%
	4			x	1.42%
	4	x		x	2.85%
direct adjustment	4	x			5.8%
	4	x	x		0.76%
	4	x	x	x	0.50%
	6	x	x	x	0.35%

Table 1. Accuracy of approximate weight functions. Internal crack in an infinite body; reference cases: $\sigma = \sigma_0(x/a)^n$.

Direct adjustment procedure
First the influence of the choice of the single reference loading case is shown. The 3 first conditions of continuity, eqs.(2.6.6)-(2.6.8), were combined with the reference case of constant stress, eq.(2.6.9). The resulting weight function is entered in fig.12 as the solid curve. Considering the linear stress as the reference case, i.e. replacing eq.(2.6.9) by eq.(2.6.10), leads to the dashed curve and finally if we consider the quadratic stress distribution as the reference case, eq.(2.6.10), the dotted curve is obtained. From fig.12 we can conclude that the approximation becomes more and more poor if the reference stress distribution is concentrated more and more at the crack tips. This has to be expected since for stresses strongly concentrated at $x = a$ the stress intensity factor is only governed by the first term in the series expansion $1/\sqrt{1 - x/a}$ and a decreasing amount of information on the other series terms is the consequence.
The approximate weight functions computed with an increasing number of reference loading cases (and consequently reduced number of conditions of continuity) are shown in fig.13. The approximation computed with only one reference stress intensity factor shows small deviations from the exact solution whilst the deviations of the higher approximations can hardly be identified. Therefore, the relative deviations from the correct solution are plotted in fig.13.

2.8.2 The edge crack in a semi-infinite body

Weight function and stress intensity factors

A high-accurate asymptotic expansion for the crack opening displacement field for an edge-cracked semi-infinite body was determined by Wigglesworth [34]

$$v = \sqrt{8/\pi}\ a\ 1.1215\frac{\sigma_r}{H}\sum_{\nu=0}^{12} C_\nu\left(1-\frac{x}{a}\right)^{\nu+1/2} \tag{2.8.4}$$

with the coefficients

$$\begin{aligned} &C_0 = 1.00000 \quad C_1 = -0.143719 \quad C_2 = 0.019965 \\ &C_3 = 0.019665 \quad C_4 = 0.011856 \quad C_5 = 0.006254 \\ &C_6 = 0.002993 \quad C_7 = 0.001256 \quad C_8 = 0.000390 \\ &C_9 = -0.00001 \quad C_{10} = -0.000172 \quad C_{11} = -0.000213 \\ &C_{12} = -0.000212 \end{aligned} \tag{2.8.5}$$

Based on these displacements we can compute the a high-accurate weight function according to eq.(2.1.7)

$$h(x,a) = \sqrt{\frac{2}{\pi a}}\sum_{\nu=1}^{13}\overline{C}_\nu(1-x/a)^{\nu-1/2} \tag{2.8.6}$$

with the coefficients

$$\begin{aligned} \overline{C}_0 &= 1 \\ \overline{C}_\nu &= -(2\nu-3)C_{\nu-1} + (2\nu+1)C_\nu \quad , \quad \text{for } 0<\nu\le 12 \\ \overline{C}_{13} &= -23C_{12} \end{aligned} \tag{2.8.7}$$

If we select for the reference cases

$$\sigma = \sigma_0 \bullet \rho^n \tag{2.8.8}$$

we obtain the high-accurate geometric functions

$$Y_n = \sqrt{\frac{2}{\pi}}\sum_{\nu=0}^{13}\overline{C}_\nu\frac{n!\,\Gamma(\nu+1/2)}{\Gamma(n+\nu+3/2)} \tag{2.8.9}$$

This relation is not restricted to integer exponents n. The first values are

$$\begin{aligned} &Y_0 = 1.1216\sqrt{\pi} \quad , \quad Y_1 = 0.6829\sqrt{\pi} \quad , \quad Y_2 = 0.5255\sqrt{\pi} \\ &Y_3 = 0.4410\sqrt{\pi} \quad , \quad Y_4 = 0.3868\sqrt{\pi} \quad , \quad Y_5 = 0.3485\sqrt{\pi} \end{aligned} \tag{2.8.10}$$

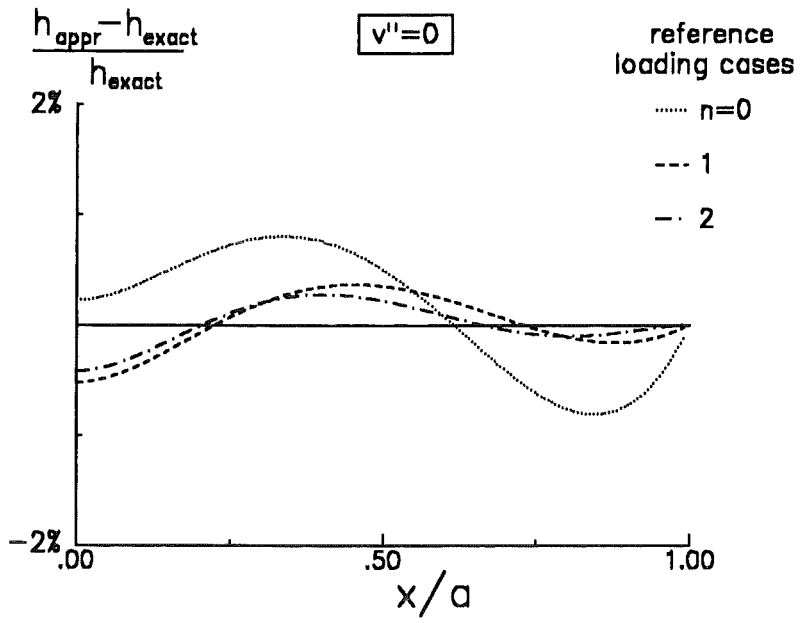

Figure 14. Edge crack in a semi-infinite body. Approximate weight functions computed with the improved Petroski-Achenbach procedure; dotted curve: $h'' = 0$ and $\sigma = \sigma_0$; dashed curve: $h'' = 0$, $\sigma = \sigma_0$ and $\sigma = \sigma_0 \cdot x/a$; dash-dotted curve: $h'' = 0$, $\sigma = \sigma_0$, $\sigma = \sigma_0 \cdot x/a$ and $\sigma = \sigma_0 \cdot (x/a)^2$.

and consequently

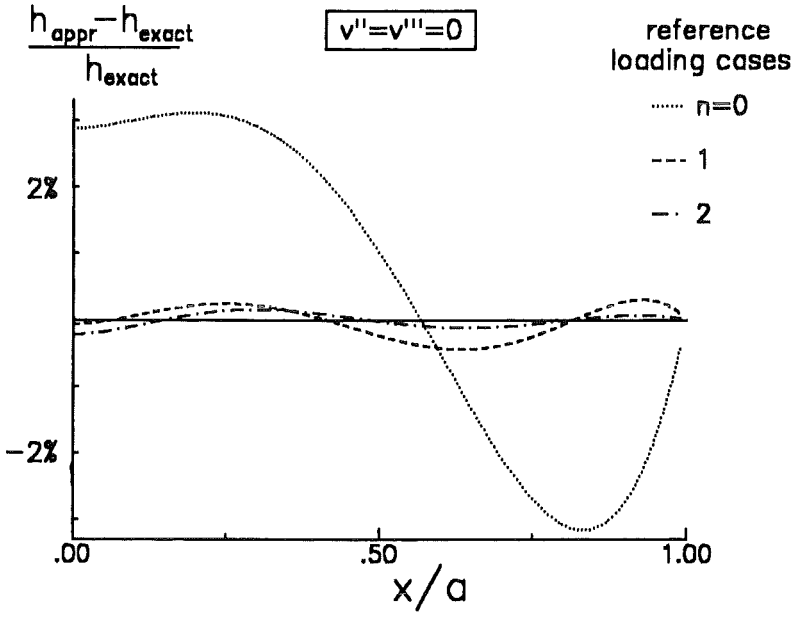

Figure 15. Edge crack in a semi-infinite body. Approximate weight functions computed with the improved Petroski-Achenbach procedure; dotted curve: $h'' = 0$, $h''' = 0$ and $\sigma = \sigma_0$; dashed curve: $h'' = 0$, $h''' = 0$, $\sigma = \sigma_0$ and $\sigma = \sigma_0 \cdot x/a$; dash-dotted curve: $h'' = 0$, $h''' = 0$, $\sigma = \sigma_0$, $\sigma = \sigma_0 \cdot x/a$ and $\sigma = \sigma_0 \cdot (x/a)^2$.

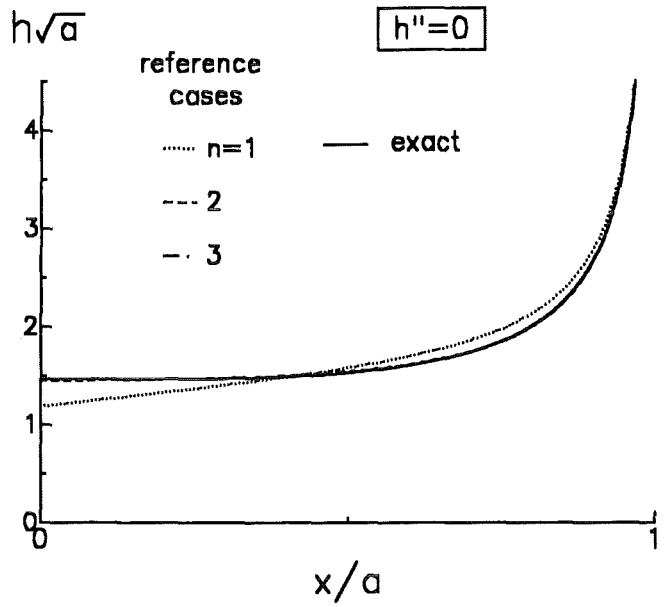

Figure 16. Edge crack in a semi-infinite body. Approximate weight functions computed with the direct adjusting method; dotted curve: $h'' = 0$ and $\sigma = \sigma_0$; dashed curve: $h'' = 0$, $\sigma = \sigma_0$ and $\sigma = \sigma_0 \cdot x/a$; dash-dotted curve: $h'' = 0$, $\sigma = \sigma_0$, $\sigma = \sigma_0 \cdot x/a$ and $\sigma = \sigma_0 \cdot (x/a)^2$.

$$Q_{0,p} = \sqrt{\frac{\pi}{8}}\,\frac{1}{a^2}\int_0^a Y_p(a')\,a'\,da' = \sqrt{\frac{\pi}{8}}\,\frac{1}{a^2}\,Y_p(a)\int_0^a (a'/a)^p\,a'\,da' \tag{2.8.11}$$

$$= \sqrt{\frac{\pi}{8}}\,\frac{Y_p}{p+2}$$

Improved Petroski-Achenbach procedure

From the considerations of Section 2.1.3 we can derive a system of linear equations which is based on the two vanishing derivatives and the first three reference loading cases $\sigma = \sigma_0$, $\sigma = \sigma_0 \cdot a/x$ and $\sigma = \sigma_0 \cdot (a/x)^2$

$$C_1 + 5C_2 + \frac{35}{3}C_3 + 21C_4 + 33C_5 = \frac{1}{3} \tag{2.8.12}$$

$$C_1 - 5C_2 - 35C_3 - 105C_4 - 231C_5 = 1 \tag{2.8.13}$$

$$C_1 + \frac{5}{7}C_2 + \frac{5}{9}C_3 + \frac{5}{11}C_4 + \frac{5}{13}C_5 = \frac{5}{2}Q_{0,0} - \frac{5}{3} \tag{2.8.14}$$

$$C_1 + \frac{5}{9}C_2 + \frac{35}{99}C_3 + \frac{35}{143}C_4 + \frac{35}{195}C_5 = \frac{35}{4\alpha}Q_{0,1} - \frac{7}{3} \tag{2.8.15}$$

$$C_1 + \frac{5}{7}C_2 + \frac{35}{143}C_3 + \frac{21}{143}C_4 + \frac{21}{221}C_5 = \frac{315}{16\alpha^2}Q_{0,2} - 3 \tag{2.8.16}$$

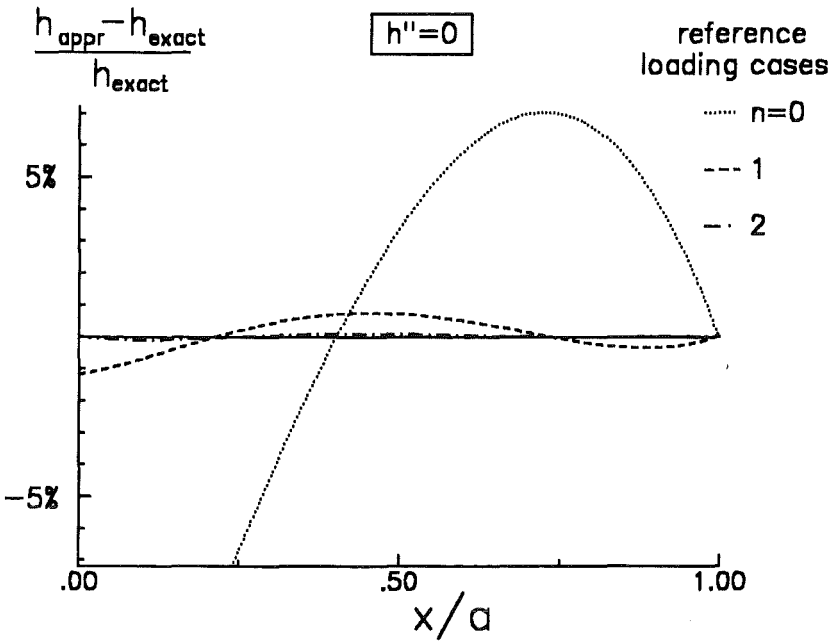

Figure 17. Edge crack in a semi-infinite body. Approximate weight functions computed with the direct adjusting method; deviations from the weight function given by eq.(2.8.6), notation as in fig.16.

with the integrals $Q_{0,\rho}$, identical to those of eq.(2.8.6). Different combinations of these relations were used to calculate approximate weight functions. As an example in fig.14 the influence of the number of reference loading cases is represented for the condition $v''=0$. Figure 15 shows the results for the two conditions $v'' = v''' = 0$.
Also for the edge crack the tendency of an increased accuracy with increased number of reference cases becomes obvious. In Table 2 the maximum deviations from eq.(2.8.6) are entered.

Direct adjusting procedure
The direct adjusting precedure was also applied to the edge-cracked semi-infinite body. The coefficients for the weight function can be determined from the system if linear equations

$$D_0 + \frac{3}{5} D_1 + \frac{3}{7} D_2 + \frac{1}{3} D_3 + \frac{3}{11} D_4 = R_0$$

$$D_0 + \frac{3}{7} D_1 + \frac{5}{21} D_2 + \frac{5}{33} D_3 + \frac{15}{143} D_4 = R_1$$

$$D_0 + \frac{1}{3} D_1 + \frac{5}{33} D_2 + \frac{35}{429} D_3 + \frac{7}{143} D_4 = R_2$$

$$D_0 - 3D_1 - 15D_2 - 35D_3 - 63D_4 = 4$$

$$D_0 - D_1 + 5D_2 + 35D_3 + 105D_4 = 6$$

The results obtained are shown in fig.16 for use of the condition $h'' = 0$. The maximum deviations from eq.(2.8.6) are entered in Table 2.

procedure	$v''=0$	$v'''=0$	$n=0$	$n=1$	$n=2$	maximum deviation
improved Petroski - Achenbach			x			3.0%
	x		x			0.81%
	x		x	x		0.52%
	x		x	x	x	0.42%
	x	x	x			3.16%
	x	x	x	x		0.45%
	x	x	x	x	x	0.225%
direct adjustment			x			5.3%
	x		x			19.0%
	x		x	x		1.2%
	x		x	x	x	0.12%
	x	x	x			36%
	x	x	x	x		3.2%
	x	x	x	x	x	0.53%

Table 2. Accuracy of approximate weight functions. Edge crack in a semi-infinite body; reference cases: $\sigma = \sigma_0 \rho^n$.

2.8.3 Edge crack in a disc

The edge crack in a circular disc was chosen to demonstrate the direct adjustment procedure in case of a crack in a finite body. In case of the edge-cracked circular disc no exact weight function is available. For this problem exact stress intensity factors were determined by Gregory [33] for constant and quadratically distributed crack surface loadings. The geometrical data are defined in fig.37 (Section 3.7). For constant surface loading we can fit the data given in [33] by

$$Y_0 = \frac{1.1216\sqrt{\pi}}{(1-\alpha)^{3/2}} \tag{2.8.17}$$

and for a quadratic stress distribution

$$\sigma(x) = \sigma_0\left(1 - \frac{2x}{D}\right)^2 \tag{2.8.18}$$

the results provided by Gregory [33] are fitted as

$$Y_2 = \frac{1.1216\sqrt{\pi}}{(1-\alpha)^{3/2}}\left(1 - 2.4431\alpha + 3.2427\alpha^2 - 1.8106\alpha^3 + 0.34404\alpha^4\right) \tag{2.8.19}$$

The coefficients for the weight function are given by the system of linear equations

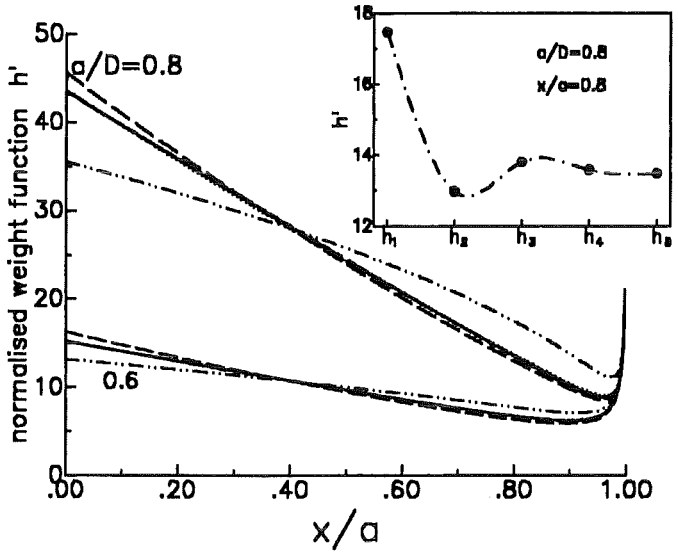

Figure 18. Approximate weight functions for an edge crack in a circular disc. Normalized weight function $h' = h\sqrt{D}$; dash-dotted: h_1, wide dashed: h_2, dotted: h_3, solid: h_4, narrow dashed: h_5.

$$
\begin{aligned}
D_0 - 3D_1 - 15D_2 - 35D_3 &= 4 \\
D_0 - D_1 + 5D_2 + 35D_3 &= 6 \\
\frac{2}{3}D_0 + \frac{2}{5}D_1 + \frac{2}{7}D_2 + \frac{2}{9}D_3 &= R_1 \\
C^{(0)}D_0 + C^{(1)}D_1 + C^{(2)}D_2 + C^{(3)}D_3 &= R_2
\end{aligned}
\qquad (2.8.20)
$$

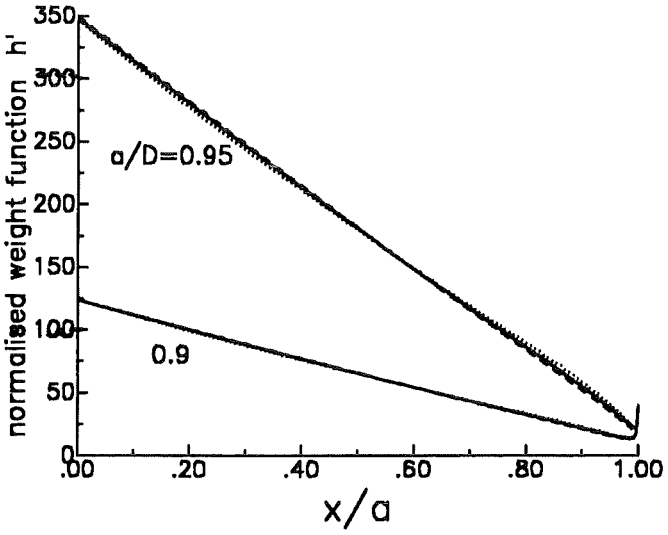

Figure 19. Approximate weight functions for the edge-crack in a circular disc. Application of the direct adjustment procedure for $a/D = 0.9$ and 0.95, (dotted: h_3, solid: h_4, dashed: h_5).

with

$$C^{(0)} = \frac{2}{3} - \frac{16}{15}\alpha + \frac{64}{105}\alpha^2$$

$$C^{(1)} = \frac{2}{5} - \frac{16}{35}\alpha + \frac{64}{315}\alpha^2$$

$$C^{(2)} = \frac{2}{7} - \frac{16}{63}\alpha + \frac{64}{693}\alpha^2 \qquad (2.8.21)$$

$$C^{(3)} = \frac{2}{9} - \frac{16}{99}\alpha + \frac{64}{1287}\alpha^2$$

and

$$R_1 = Y_0\sqrt{\pi/2} - \frac{4}{3}$$

$$R_2 = Y_2\sqrt{\pi/2} - \left(\frac{4}{3} - \frac{64}{15}\alpha + \frac{384}{105}\alpha^2\right) \qquad (2.8.22)$$

The approximate weight function has been calculated for an increasing number of conditions in the following way:

1. h_1: only one reference loading case ($\sigma = const.$) used.
2. h_2: use of reference loading case ($\sigma = const.$) and geometrical condition $h''|_{x=0} = 0$.
3. h_3: use of reference loading case ($\sigma = const.$) and reference loading case $\sigma \propto (1 - 2x/D)^2$.
4. h_4: use of reference loading case ($\sigma = const.$), reference loading case $\sigma \propto (1 - 2x/D)^2$ and geometrical condition $h''|_{x=0} = 0$.
5. h_5: conditions used for h_4 and $h'''|_{x=0} = 0$.

In fig.18 the weight functions $h_1 - h_5$ are plotted for relative crack depths of $a/D = 0.6$ and 0.8. As can be seen, only the very roughly approximated weight function h_1 deviates by more than 10% from the higher order solutions. The weight functions h_3, h_4 and h_5 can hardly be distinguished. The insert in fig.18 illustrates the convergence for a fixed value of $x/a = 0.8$.
Figure 19 illustrates the weight functions $h_3 - h_5$ for $a/D = 0.9$ and $a/D = 0.95$. Especially for $a/D = 0.95$, the solutions differ little more, but above all the solutions h_4 and h_5 agree also for this extremely high value of relative crack depth with maximum deviations of less than 3%.

2.9 Weight function for remote tractions

In most cases of practical interest the crack-surface weight function considered in the sections before is applied. But the weight-function method is not restricted to crack-surface loadings. In its more general formulation the procedure can be applied also to tractions which act at any given contour in the body (fig.20). Such weight functions are of special interest in computation of R-curves in ceramics when phase transformations occur in the crack-tip region [35]. In this more general case one can write

$$K_I = \int h(s,a)T(s)\,ds \qquad (2.9.1)$$

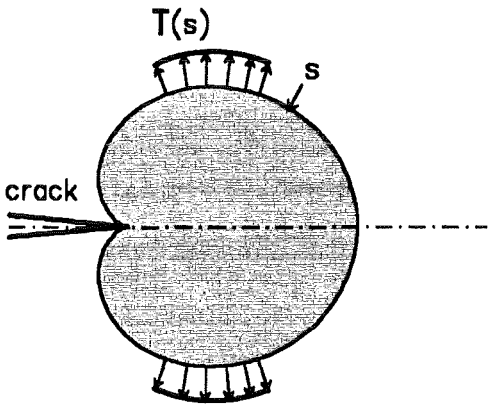

Figure 20. . Tractions along a surface at the crack tip.

where $T(s)$ are tractions over a surface s. As shown by Rice [7][12], the weight function can be related to the displacements u_r^T of a reference loading case (subscript r) which act in the direction of the tractions $T(s)$ in the actual loading case:

$$h(s,a) = \frac{E'}{K_{Ir}} \frac{\partial}{\partial a} u_r^T(s,a) \tag{2.9.2}$$

Obviously, eq.(2.9.2) covers also the crack-face weight function when the surface s is chosen to be the crack surface. In order to determine the weight function for a crack/component configuration, we have to determine the displacement field of the reference load case as well as the related stress intensity factor. The weight functions can be calculated by determination of the displacements around the crack tip, which is fully known if we succeed in the determination of the Airy stress-function Φ.
The stress components in a cracked body can be represented in polar coordinates - with the pole in the crack tip (fig.21) - as

$$\sigma_r = \frac{1}{r}\frac{\partial \Phi}{\partial r} + \frac{1}{r^2}\frac{\partial^2 \Phi}{\partial \varphi^2} \qquad \sigma_\varphi = \frac{\partial^2 \Phi}{\partial r^2} \qquad \tau_{r\varphi} = \frac{1}{r^2}\frac{\partial \Phi}{\partial \varphi} - \frac{1}{r}\frac{\partial^2 \Phi}{\partial r \partial \varphi} \tag{2.9.3}$$

The Airy stress-function results as a solution of the bipotential equation

$$\Delta\Delta\Phi = 0 \tag{2.9.4}$$

Due to the linearity of eq.(2.9.4), the stress function Φ can be divided into a fraction Φ_s which is symmetric with respect to $\varphi = 0$, and an antisymmetric fraction Φ_a.

$$\Phi = \Phi_s + \Phi_a \tag{2.9.5}$$

The general treatment of the crack problem will be explained here in more detail by the example of the symmetric fraction of the stress function.
The solution of eq.(2.9.4) has been given by Williams [59] as

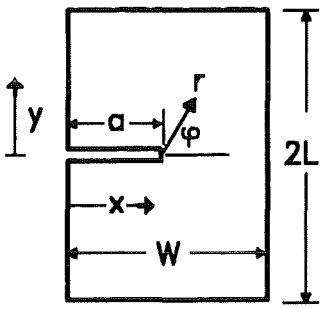

Figure 21. Edge-crack in a plate. Geometric data.

$$\Phi_s = \sum_{n=0}^{\infty} r^{n+3/2} A_n \left[\cos(n+3/2)\varphi - \frac{n+3/2}{n-1/2} \cos(n-1/2)\varphi \right]$$

$$+ \sum_{n=0}^{\infty} r^{n+2} A_n^* [\cos(n+2)\varphi - \cos n\varphi] \qquad (2.9.6)$$

The displacements u and v (u=radial and v=angular component) can be calculated from the radial strains ε_r and tangential strains ε_φ. The following relation holds:

$$\varepsilon_r = \frac{\partial u}{\partial r} \quad , \quad \varepsilon_\varphi = \frac{u}{r} + \frac{1}{r} \frac{\partial v}{\partial \varphi} \qquad (2.9.7)$$

From the Hook law in plane strain

$$\varepsilon_r = \frac{1}{E'} \sigma_r - \frac{\nu}{E'(1-\nu)} \sigma_\varphi \qquad (2.9.8)$$

$$\varepsilon_\varphi = \frac{1}{E'} \sigma_\varphi - \frac{\nu}{E'(1-\nu)} \sigma_r \qquad (2.9.9)$$

and the stress components given by eq.(2.9.3) we obtain the following system of equations describing the displacements

$$E' \frac{\partial u}{\partial r} = \frac{1}{r} \frac{\partial \Phi}{\partial r} + \frac{1}{r^2} \frac{\partial^2 \Phi}{\partial \varphi^2} - \frac{\nu}{1-\nu} \frac{\partial^2 \Phi}{\partial r^2} \qquad (2.9.10)$$

$$E'\left(\frac{u}{r}+\frac{1}{r}\frac{\partial v}{\partial \varphi}\right)=\frac{\partial^2\Phi}{\partial r^2}-\frac{\nu}{1-\nu}\left(\frac{1}{r}\frac{\partial\Phi}{\partial r}+\frac{1}{r^2}\frac{\partial^2\Phi}{\partial\varphi^2}\right) \tag{2.9.11}$$

After introducing the stress function, the integration of this system of differential equations leads to

$$u=\frac{1+\nu}{E}\sum_{n=0}^{\infty}A_n r^{n+1/2}\frac{n+3/2}{n-1/2}[(n+4\nu-5/2)\cos(n-1/2)\varphi-(n-1/2)\cos(n+3/2)\varphi]$$
$$+\frac{1+\nu}{E}\sum_{n=0}^{\infty}A_n^* r^{n+1}[(n+4\nu-2)\cos n\varphi-(n+2)\cos(n+2)\varphi] \tag{2.9.12}$$

$$v=\frac{1+\nu}{E}\sum_{n=0}^{\infty}A_n r^{n+1/2}\frac{n+3/2}{n-1/2}[(n-1/2)\sin(n+3/2)\varphi-(n-4\nu+3/2)\sin(n-1/2)\varphi]$$
$$+\frac{1+\nu}{E}\sum_{n=0}^{\infty}A_n^* r^{n+1}[(n+2)\sin(n+2)\varphi-(n-4\nu+4)\sin n\varphi] \tag{2.9.13}$$

The Cartesian components of the displacements are

$$u_x=u\cos\varphi-v\sin\varphi\quad,\quad u_y=u\sin\varphi+v\cos\varphi \tag{2.9.14}$$

and the components of the weight function result as

$$h_x=\frac{E'}{K_r}\frac{\partial u_x}{\partial a}\quad,\quad h_y=\frac{E'}{K_r}\frac{\partial u_y}{\partial a} \tag{2.9.15}$$

The weight function is, in principle, known provided that a set of coefficients A_n, A_n^* is known, too. One possibility to obtain these coefficients is the application of the Boundary Collocation Method (BCM) [9], [48].

3. Mode-I stress intensity factors and weight functions for one-dimensional cracks

In this chapter the stress intensity factors for simple load cases such as constant stress, linear stress distributions or in some cases parabolic distributions are given for different components with one-dimensional cracks. From these results the weight functions can be obtained applying the relations given in the previous chapter. For some cases the weight functions are presented in form of equations, tables or figures. As in the previous chapter the notation $\alpha = a/W$ and $\rho = x/a$ are used.

3.1 The edge-cracked plate

3.1.1 Loading conditions

A plate (or a bar) of width W, thickness B and length $2L$, containing a crack of depth a, is considered (see fig.22). In fig.22a no restrictions on free deformation are made. Due to the homogeneous stresses at the specimen ends bending of the cracked specimen is possible. In the arrangement of fig.22b bending is completely prevented. Besides the externally applied tensile stresses, the reaction of the roller bearing has to be taken into account. If the cracked plate with an edge crack is an element of a larger structure, the real loading conditions will be between the two limit cases illustrated in fig.22.

3.1.2 Crack in a ~~semi~~-infinite body

A crack in a semi-infinite body is equivalent to a crack with small a/W in a finite component. In this case the weight function can be easily obtained. A high-accurate asymptotic expansion for the crack opening displacement field for an edge-cracked semi-infinite body under tension loading by σ_0 was determined by Wigglesworth [34]

$$v = \sqrt{8/\pi}\; a\, Y_0 \frac{\sigma_0}{E'} \sum_{\nu=0}^{12} C_\nu \left(1-\rho\right)^{n+1/2} \tag{3.1.1}$$

with the coefficients

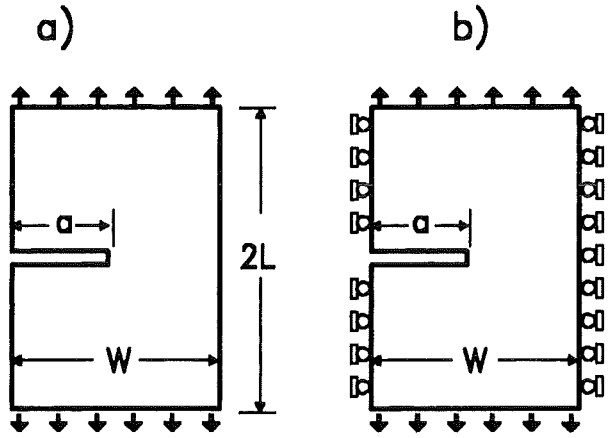

Figure 22. Geometric data and loading conditions for a plate. a) freely deformable, b) plate prevented from bending.

$$\begin{aligned} C_0 &= 1.00000 \quad C_1 = -0.143719 \quad C_2 = 0.019965 \\ C_3 &= 0.019665 \quad C_4 = 0.011856 \quad C_5 = 0.006254 \\ C_6 &= 0.002993 \quad C_7 = 0.001256 \quad C_8 = 0.000390 \\ C_9 &= -0.00001 \quad C_{10} = -0.000172 \quad C_{11} = -0.000213 \\ C_{12} &= -0.000212 \end{aligned} \tag{3.1.2}$$

Based on these displacements we can compute the a high-accurate weight function according to eq.(2.1.7)

$$h(x,a) = \sqrt{\frac{2}{\pi a}} \sum_{\nu=1}^{13} \bar{C}_\nu (1-\rho)^{\nu - 1/2} \tag{3.1.3}$$

with the coefficients

$$\begin{aligned} \bar{C}_0 &= 1 \\ \bar{C}_\nu &= -(2\nu-3)C_{\nu-1} + (2\nu+1)C_\nu \quad , \quad \text{for } 0 < \nu \leq 12 \\ \bar{C}_{13} &= -23C_{12} \end{aligned} \tag{3.1.4}$$

For power-shaped stresses

$$\sigma = \sigma_0 \cdot (x/a)^n \tag{3.1.5}$$

one obtains high-accurate geometric functions

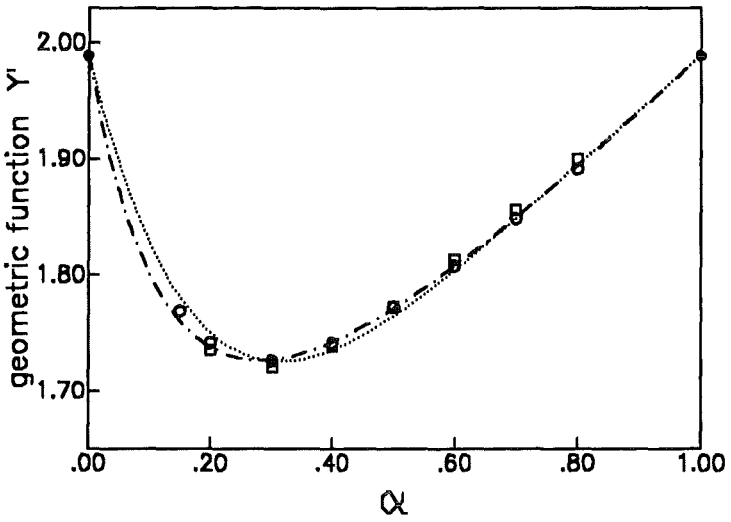

Figure 23. Comparison of the BCM-results with literature data. Dash-dotted line: eq.(3.1.9); dotted line: eq.(3.1.10); circles: Boundary Collocation Method [27]; squares: Table in [14]; $Y' = Y(1-\alpha)^{3/2}$.

$$Y_n = \sqrt{\frac{2}{\pi}} \sum_{\nu=0}^{13} \bar{C}_\nu \frac{n!\,\Gamma(\nu+1/2)}{\Gamma(n+\nu+3/2)} \tag{3.1.6}$$

for integer exponents n. For real exponents $n!$ has to be replaced by $\Gamma(n+1)$

$$Y_n = \sqrt{\frac{2}{\pi}} \sum_{\nu=0}^{13} \bar{C}_\nu \frac{\Gamma(n+1)\,\Gamma(\nu+1/2)}{\Gamma(n+\nu+3/2)} \tag{3.1.7}$$

We repeated Wigglesworth's analysis and extended the series expansion up to $N = 20$ with the following coefficients

$$\begin{array}{lll} C_0 = 1.00000 & C_1 = -0.1437181 & C_2 = 0.0199656 \\ C_3 = 0.0196651 & C_4 = 0.0118558 & C_5 = 0.0062537 \\ C_6 = 0.0029935 & C_7 = 0.0012562 & C_8 = 0.0003899 \\ C_9 = -0.0000097 & C_{10} = -0.0001718 & C_{11} = -0.0002189 \\ C_{12} = -0.0002149 & C_{13} = -0.0001909 & C_{14} = -0.0001618 \\ C_{15} = -0.0001338 & C_{16} = -0.0001095 & C_{17} = -0.0000893 \\ C_{18} = -0.0000728 & C_{19} = -0.0000595 & C_{20} = -0.0000487 \end{array} \tag{3.1.8}$$

This solution gives the possibility to check the condition $v'' = 0$ for $x = 0$ for the special case of an edge crack in a semi-infinite body. In fig.24 the second derivative is plotted as a function of the number of coefficients used in eq.(3.1.1). It can be seen that the second derivative of the displacements tends asymptotically to $v''(x=0) \to 0$ for $N \to \infty$.

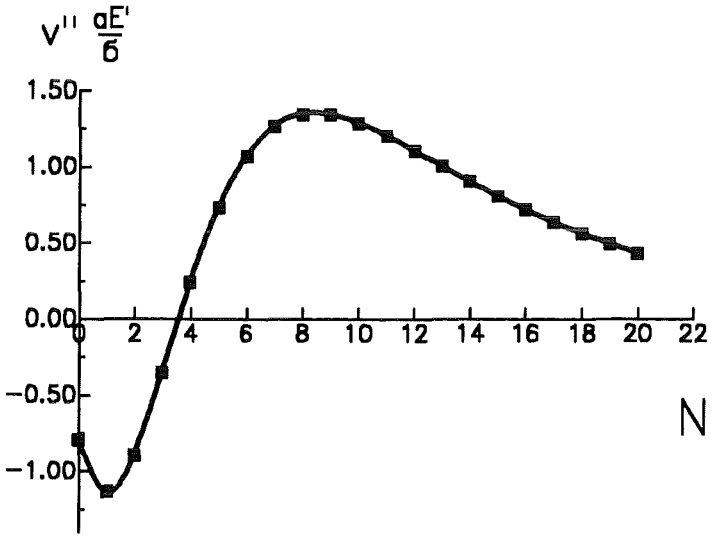

Figure 24. Second derivative for an edge crack in a semi-infinite body. Influence of the number of terms used in eq.(3.1.1) with coefficients given by eq.(3.1.8).

3.1.3 The plate under tensile loading

First the special case of a totally freely deformable plate is treated. The geometric function obtained with the Boundary Collocation Method (BCM) is given in Table 3 for several L/W-ratios [27]. Other values can be obtained by parabolic interpolation. For $L/W \geq 1$ the geometric function is independent of L/W and can be represented by the relation

$$Y = 1.988 \frac{0.026778\,(0.427103 + \alpha)^{-2.73895} + 0.26514\,\alpha + 0.72475}{(1-\alpha)^{3/2}} \tag{3.1.9}$$

The results are plotted in fig.23 together with results from the literature [12], [14]. The squares represent the geometric function tabulated in [14]. A relation given by Tada [12]

$$Y = 0.470(1-\alpha)^4 + \frac{1.519 + 0.470\alpha}{(1-\alpha)^{3/2}} \tag{3.1.10}$$

is entered as dotted line. Equation (3.1.10) does not exhibit the correct derivative at $a/W = 0$.

L/W	$\alpha = 0.20$	0.30	0.40	0.50	0.60	0.70
0.350	3.089	4.013	5.055	6.347	8.215	11.836
0.500	2.636	3.275	4.119	5.333	7.354	11.331
0.750	2.448	2.978	3.781	5.036	7.161	11.264
1.000	2.432	2.946	3.745	5.007	7.148	11.262
1.250	2.428	2.946	3.745	5.007	7.148	11.262
1.500	2.428	2.946	3.743	5.007	7.148	11.262
2.000	2.428	2.948	3.743	5.007	7.148	11.262

Table 3. Geometric function for the edge-cracked plate under tension. Influence of the length L of the plate on the geometric function for tensile loading, $Y' = Y(1-\alpha)^{3/2}$.

The geometric function of an edge-cracked plate loaded with a bolt at the ends is described by Brown and Srawley [36] for $\alpha < 0.6$ as

$$Y = 1.99 - 0.41\alpha + 18.70\alpha^2 - 38.48\alpha^3 + 53.85\alpha^4 \tag{3.1.11}$$

It has to be expected from Saint Venant's principle, that a comparison between eqs.(3.1.9) and (3.1.11) must yield similar values.
The edge-cracked plate prevented from bending is described by the geometric function

$$Y = \frac{5\sqrt{\pi}}{[20 - 13\alpha - 7\alpha^2]^{1/2}} \tag{3.1.12}$$

3.1.4 The plate in bending

The characteristic stress is the stress at the tensile surface which is related to the bending moment by $\sigma^* = 6M/(BW^2)$. In case of pure bending Nisitani und Mori [37] (quoted in [14]) obtained with the "Body Force Doublet Method"

$$Y = 1.989 - 1.987\alpha + 6.629\alpha^2 + 6.865\alpha^3 - 33.765\alpha^4 + 39.97\alpha^5 \tag{3.1.13}$$

with an error margin of $\pm 1\%$ for $\alpha \leq 0.7$. This solution is by about 2% higher than the result in [14] based on calculations of Gross und Srawley ([10]), but in excellent agreement with BCM-calculations ([27]).
For $0 < \alpha < 1$ Srawley and Gross [38] proposed

$$Y = \frac{1}{(1-\alpha)^{3/2}}\left[1.9887 - 1.326\alpha - \frac{\alpha(1-\alpha)}{(1+\alpha)^2}\left(3.49 - 0.68\alpha + 1.35\alpha^2\right)\right] \tag{3.1.14}$$

Equations (3.1.13) and (3.1.14) are only valid for the case of "pure bending" which results when a bending moment is applied at the ends of the bar (fig.25a). If bending is caused by single forces (fig.25b), deviations have to be expected. In the special case of a 4-point-bending test with an inner roller distance d also pure bending is asymptotically reached for $d/W \to \infty$. For shorter roller distances the stress intensity factor can be written as

$$K_I = K_I|_{d/W \to \infty} \cdot f(a/W, d/W, L/W) \tag{3.1.15}$$

where $K_I|_{d/W \to \infty}$ is to be computed according to eq.(3.1.13) or (3.1.14). In [14] and [37] results of the function $f(a/W, d/W, L/W)$ are published.

3.1.5 Three-point bending

The case of a three-point bending arrangement is covered by fig.25b with $d = 0$. If the reference stress for 3-point bending is written

$$\sigma^* = \frac{3}{2}\frac{FL}{W^2 B} \tag{3.1.16}$$

the geometric function derived in [27] reads for $L/W > 2$

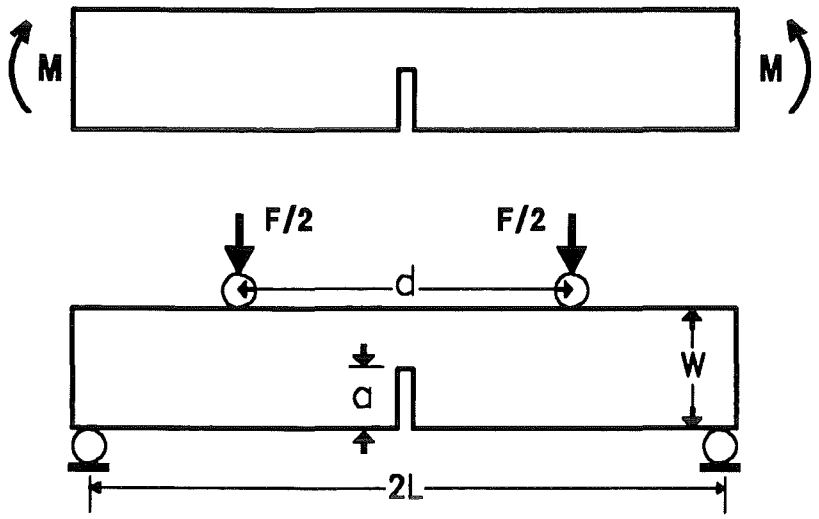

Figure 25. Geometrical data and loading of bending bars. a) upper figure: pure bending, b) lower figure: 4-point bending

$$Y = \frac{\sqrt{\pi}}{(1-\alpha)^{3/2}} \left[0.3738\alpha + (1-\alpha) \sum_{\mu,\nu=0}^{4} A_{\mu\nu} \alpha^{\mu} (W/L)^{\nu} \right] \quad , \quad \alpha = a/W \tag{3.1.17}$$

The coefficients are given as:

	$A_{\mu 0}$	$A_{\mu 1}$	$A_{\mu 2}$	$A_{\mu 3}$	$A_{\mu 4}$
$\mu=0$	1.1200	-0.2387	0.4317	-1.7351	2.4145
$\mu=1$	-1.8288	-0.2573	-4.9847	16.9047	-18.2883
$\mu=2$	2.9741	0.2706	18.6767	-60.4912	59.9239
$\mu=3$	-2.4280	0.5627	-27.3447	87.7078	-85.2405
$\mu=4$	0.6712	-0.5184	13.5837	-43.5421	42.3503

Table 4. Coefficients. $A_{\mu\nu}$, eq.(3.1.17).

3.1.6 The weight function for a plate with L/W ≥1

Based on boundary collocation computations a weight function was derived [27] that can be expressed for $0 \leq \alpha < 0.85$ by a fit relation

$$h = \sqrt{\frac{2}{\pi a}} \frac{1}{\sqrt{1-x/a}} \left[1 + \sum_{(\nu,\mu)} \frac{A_{\nu\mu} \alpha^{\mu}}{(1-\alpha)^{3/2}} (1-x/a)^{\nu+1} \right] \tag{3.1.18}$$

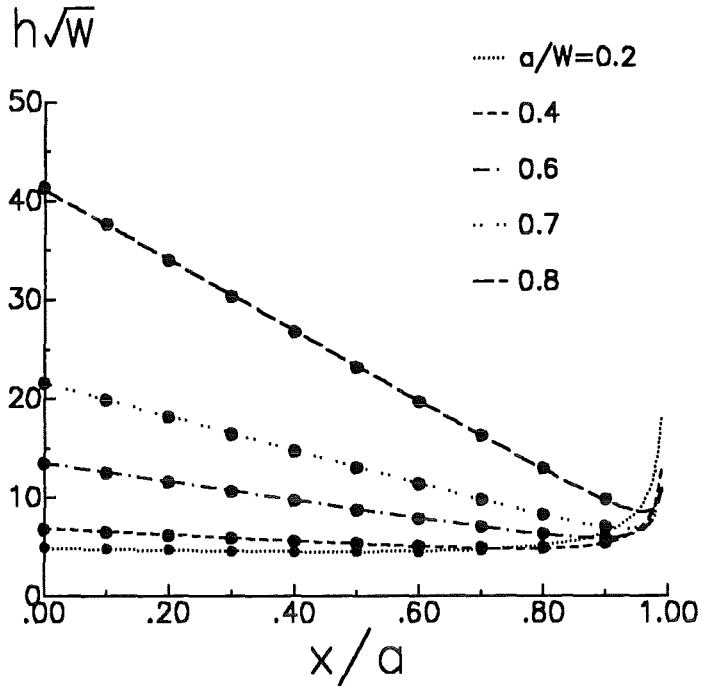

Figure 26. Weight function for an edge crack in a rectangular plate. Comparison of approximative weight function obtained by direct adjusting to the tension and the bending reference loading cases with $h'' = 0$ at $x = 0$ as the geometric condition with results from a Boundary Collocation analysis (circles) represented by eq.(3.1.18).

with the coefficients

ν	$\mu=0$	1	2	3	4
0	0.4980	2.4463	0.0700	1.3187	-3.067
1	0.5416	-5.0806	24.3447	-32.7208	18.1214
2	-0.19277	2.55863	-12.6415	19.7630	-10.986

Table 5. Coefficients for the weight function. Eq.(3.1.18)

With this weight function the approximative weight function resulting by application of the direct adjusting method were compared. Using pure tension, eq.(3.1.9), and bending, eq.(3.1.14), as the reference loading case and $h'' = 0$ at $x = 0$ as the geometric condition one obtains the weight function entered in fig.26 as lines. The weight function computed with eq.(3.1.18) is given by the circles. A good agreement between approximative weight function and results of the Boundary Collocation analysis can be concluded.

3.1.7 Compact tension specimen

The weight function for the CT-specimen is plotted in fig.7. These results were fitted according to eq.(3.1.18) with the coefficients

ν	$\mu=0$	1	2	3	4
0	2.673	-8.604	20.621	-14.635	0.477
1	-3.557	24.9726	-53.398	50.707	-11.837
2	1.230	-8.411	16.957	-12.157	-0.940
3	-0.157	0.954	-1.284	-0.393	1.655

Table 6. Coefficients for the weight function (CT specimen). Eq.(3.1.18)

3.2 Double edge-cracked plate

3.2.1 Geometric function

Geometric functions for the double edge-cracked plate (or the double edge-cracked bar) - fig.27 - were derived by Bentham and Koiter [4] using the so-called asymptotic interpolation procedure. In a representation modified by Tada [12] the relation reads:

- for tension

$$Y = \frac{1.989 - 0.994\alpha - 0.363\alpha^2 + 0.835\alpha^3 - 0.337\alpha^4}{\sqrt{1-\alpha}} \tag{3.2.1}$$

- for bending [4]

$$Y = \frac{0.7523 + 0.3761\beta + 0.2821\beta^2 + 0.2351\beta^3 - 0.833\beta^4 + 1.175\beta^5}{\beta^{3/2}} \tag{3.2.2}$$

$$\text{with} \quad \beta = 1 - \alpha$$

The stress intensity factor for the crack at the tension side is given by eq.(3.2.2), the stress intensity factor for the opposite crack is negative. Since a negative stress intensity factor does not exist, eq.(3.2.2) in case of bending is only applicable when tension is superimposed so that the total stress intensity factor at the compression side of the bar remains positive.

3.2.2 Weight function

If there is an arbitrary stress distribution in the plate, this distribution has to be divided into a symmetric part $\sigma^{(s)}(x)$ and an antisymmetric part $\sigma^{(a)}(x)$ according to:

$$\sigma(x) = \sigma^{(s)}(x) + \sigma^{(a)}(x) \tag{3.2.3}$$

The symmetric part is given by

$$\sigma^{(s)}(x) = \frac{1}{2}\left[\sigma(x' = x) + \sigma(x' = 2W - x)\right] \tag{3.2.4}$$

and the antisymmetric part results as

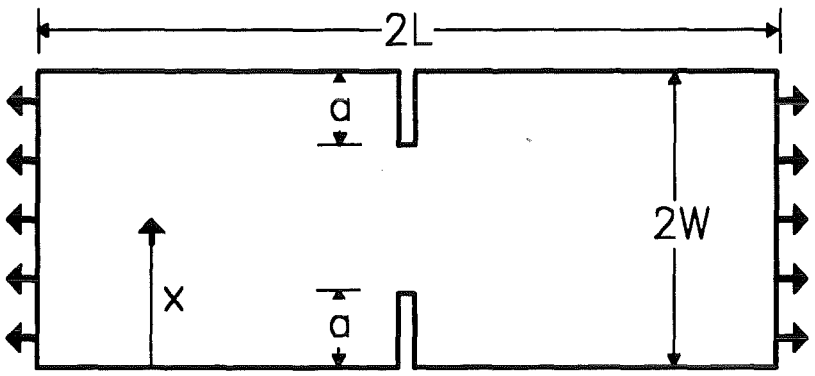

Figure 27. Double edge-cracked plate. Geometrical data and loading situation

$$\sigma^{(a)}(x) = \frac{1}{2}\left[\sigma(x' = x) - \sigma(x' = 2W - x)\right] \tag{3.2.5}$$

For the lower crack in fig.27 the stress intensity factor results

$$K_l = \int_0^a \sigma^{(s)}(x) h_l^{(s)}(x,a)\, dx + \int_0^a \sigma^{(a)}(x) h_l^{(a)}(x,a)\, dx \tag{3.2.6}$$

and for the upper crack one obtains

$$K_u = \int_{2W-a}^{2W} \sigma^{(s)}(x) h_u^{(s)}(x,a)\, dx + \int_{2W-a}^{2W} \sigma^{(a)}(x) h_u^{(a)}(x,a)\, dx \tag{3.2.7}$$

Because of the symmetry relations

$$h_l^{(s)}(x,a) = h_u^{(s)}(2W - x, a) \quad , \quad h_l^{(a)}(x,a) = h_u^{(a)}(2W - x, a) \tag{3.2.8}$$

the knowledge of one weight function, i.e. for the lower crack is sufficient. Therefore, the subscript will be dropped.
From the relations given in section 2.1.2 the weight functions for symmetric loading are listed in Table 7 for discrete values of a/W and x/a in the normalised representation

$$h^{(s)} = \sqrt{\frac{2}{\pi a}}\, \frac{g(x/a, \alpha)}{\sqrt{1 - x/a}\,\sqrt{1 - \alpha}} \tag{3.2.9}$$

α	x/a=0.	0.20	0.40	0.60	0.80	0.90	1.00
0.0	1.838	1.626	1.440	1.276	1.131	1.064	1.000
0.2	1.635	1.459	1.292	1.139	1.005	0.946	0.894
0.4	1.470	1.314	1.163	1.019	0.889	0.829	0.775
0.6	1.360	1.219	1.075	0.928	0.780	0.706	0.633
0.8	1.336	1.196	1.045	0.877	0.684	0.573	0.447
0.9	1.360	1.217	1.057	0.872	0.643	0.499	0.316
1.0	1.414	1.265	1.095	0.894	0.632	0.447	0.000

Table 7. Normalised weight function for the double edge-cracked plate. Function g(x,a) for symmetric load, eq.(3.2.9).

The weight function for **antisymmetric loadings** is described by the normalised representation

$$h^{(a)} = \sqrt{\frac{2}{\pi a}}\,\frac{g(x/a,\,\alpha)}{\sqrt{1-x/a}\,(1-\alpha)^{3/2}} \tag{3.2.10}$$

and given in Table 8.

α	x/a=0.	0.20	0.40	0.60	0.80	0.90	1.00
0.0	1.838	1.626	1.440	1.276	1.131	1.064	1.000
0.2	1.629	1.425	1.222	1.030	0.858	0.782	0.715
0.4	1.838	1.527	1.228	0.948	0.692	0.575	0.465
0.6	2.208	1.744	1.312	0.917	0.562	0.401	0.253
0.8	2.532	1.902	1.333	0.834	0.414	0.239	0.0894

Table 8. Normalised weight function for the double edge-cracked plate. Function g(x,a) for antisymmetric load, eq.(3.2.10).

In [39] approximate analytical relations for $h^{(s)}$ and $h^{(a)}$ are given.

3.3 Internal through-the-thickness crack in a plate

3.3.1 Central internal crack

Figure 28 illustrates the geometry of a finite plate with a central internal crack. In case of tensile loading the geometric function is given by [4], [12]

$$Y_{tension} = \sqrt{\pi}\,\frac{1-0.5\alpha+0.37\alpha^2-0.044\alpha^3}{\sqrt{1-\alpha}} \tag{3.3.1}$$

For pure bending with an applied bending moment M the stress intensity factor can be written in the form

$$K_{bend} = \sigma^* \sqrt{a}\, Y_{bend} \tag{3.3.2}$$

with the outer fibre bending stress σ^*

$$\sigma^* = \frac{3M}{2W^2B} \tag{3.3.3}$$

and the related geometric function [4]

$$Y_{bend} = \alpha \frac{\sqrt{1-\alpha}}{1-\alpha^3} \frac{\sqrt{\pi}}{2} \left(1 + 0.5\alpha + 3/8\alpha^2 - 11/16\alpha^3 + 0.464\alpha^4\right) \tag{3.3.4}$$

For internal cracks under bending load it should also be mentioned that the solution eq.(3.3.4) is only applicable if it is ensured by a superimposed tensile loading that no crack closure occurs at the compression side.

3.3.2 The eccentric internal crack

For fracture mechanical test specimens the central crack is often used. He represents an ideal case. In real tests - i.e. fatigue tests - it is possible that the crack will propagate at its two ends differently and, therefore, eccentricities may result. Figure 29 shows the geometric data. The solution proposed by Isida [40] reads

$$K_A = \sigma\sqrt{a}\, Y_A(\varepsilon, \lambda) \quad , \quad K_B = \sigma\sqrt{a}\, Y_B(\varepsilon, \lambda) \tag{3.3.5}$$

with

$$\varepsilon = (x_M - W)/W \quad , \quad \lambda = a/(W - x_M) \tag{3.3.6}$$

and

$$Y_A(\varepsilon, \lambda) = \sqrt{\pi}\left(1 + \sum_{n=2}^{19} C_n \lambda^n\right) \quad , \quad Y_B(\varepsilon, \lambda) = \sqrt{\pi}\left(1 + \sum_{n=2}^{19} (-1)^n C_n \lambda^n\right) \tag{3.3.7}$$

with the coefficients C_n listed in Table 9.

ε	C_2	C_3	C_4	C_5	C_6	C_7	C_8	C_9	C_{10}
0	0.5948	0	0.4812	0	0.3963	0	0.3367	0	0.2972
0.02	0.5726	0.0339	0.4462	0.0315	0.3548	0.0433	0.2917	0.0464	0.2498
0.04	0.5535	0.0639	0.4173	0.0574	0.3234	0.0759	0.2608	0.0788	0.2208
0.06	0.5371	0.0903	0.3936	0.0785	0.2998	0.1003	0.2400	0.1014	0.2035
0.08	0.5231	0.1134	0.3743	0.0958	0.2823	0.1185	0.2263	0.1172	0.1939
0.10	0.5112	0.1335	0.3585	0.1099	0.2694	0.1319	0.2175	0.1281	0.1890
0.20	0.4761	0.1975	0.3155	0.1485	0.2428	0.1576	0.2073	0.1467	0.1904
0.30	0.4635	0.2179	0.3016	0.1571	0.2374	0.1538	0.2083	0.1428	0.1936
0.40	0.4555	0.2126	0.2922	0.1507	0.2292	0.1405	0.2012	0.1310	0.1860
0.50	0.4404	0.1939	0.2754	0.1364	0.2113	0.1236	0.1832	0.1154	0.1677
0.60	0.4123	0.1707	0.2473	0.1192	0.1841	0.1061	0.1574	0.0989	0.1429

0.70	0.3704	0.1495	0.2108	0.1029	0.1529	0.0905	0.1298	0.0841	0.1175
0.80	0.3197	0.1341	0.1735	0.0899	0.1246	0.0783	0.1063	0.0727	0.0969
0.90	0.2729	0.1264	0.1449	0.0814	0.1051	0.0706	0.0910	0.0656	0.0837
1	0.25	0.125	0.1328	0.0781	0.0967	0.0671	0.0836	0.0618	0.0766

ε	C_{11}	C_{12}	C_{13}	C_{14}	C_{15}	C_{16}	C_{17}	C_{18}	C_{19}
0	0	0.2713	0	0.2535	0	0.2404	0	0.2300	0
0.02	0.0533	0.2219	0.0576	0.2021	0.0627	0.1873	0.0669	0.1756	0.0711
0.04	0.0878	0.1948	0.0920	0.1774	0.0974	0.1650	0.1011	0.1558	0.1048
0.06	0.1099	0.1810	0.1127	0.1668	0.1167	0.1575	0.1189	0.1512	0.1212
0.08	0.1241	0.1749	0.1251	0.1638	0.1275	0.1570	0.1284	0.1528	0.1294
0.10	0.1331	0.1731	0.1325	0.1644	0.1336	0.1594	0.1334	0.1567	0.1337
0.20	0.1447	0.1817	0.1413	0.1772	0.1396	0.1748	0.1383	0.1735	0.1376
0.30	0.1387	0.1854	0.1355	0.1806	0.1336	0.1776	0.1324	0.1757	0.1318
0.40	0.1266	0.1771	0.1236	0.1715	0.1218	0.1679	0.1205	0.1654	0.1197
0.50	0.1111	0.1585	0.1082	0.1526	0.1063	0.1487	0.1049	0.1459	0.1040
0.60	0.0949	0.1343	0.0921	0.1289	0.0902	0.1252	0.0888	0.1225	0.0877
0.70	0.0804	0.1104	0.0779	0.1060	0.0761	0.1030	0.0747	0.1007	0.0736
0.80	0.0694	0.0915	0.0672	0.0881	0.0655	0.0858	0.0643	0.0840	0.0632
0.90	0.0626	0.0796	0.0606	0.0770	0.0591	0.0752	0.0579	0.0737	0.0570
1	0.0585	0.0724	0.0562	0.0697	0.0544	0.0678	0.0529	0.0662	0.0517

Table 9. . Coefficients for eq.(3.3.7).

In case of the slight eccentric crack under tension the geometric function can be calculated for $a/W \leq 0.8$ as proposed in [15]. With the relative eccentricity x_M/W (see fig.29) it holds ($\eta = x - x_M$)

$$Y_A \simeq Y_A|_{x_M/W=0} + \frac{\partial Y_A}{\partial(x_M/W)} x_M/W \tag{3.3.8}$$

and

$$Y_B \simeq Y_B|_{x_M/W=0} + \frac{\partial Y_B}{\partial(x_M/W)} x_M/W \tag{3.3.9}$$

with

$$\frac{1}{Y_A}\frac{\partial Y_A}{\partial(x_M/W)} = -\frac{1}{Y_B}\frac{\partial Y_B}{\partial(x_M/W)} \simeq 2.8\left[\frac{1}{(1-\alpha^3)^{2/3}} - 1\right] \tag{3.3.10}$$

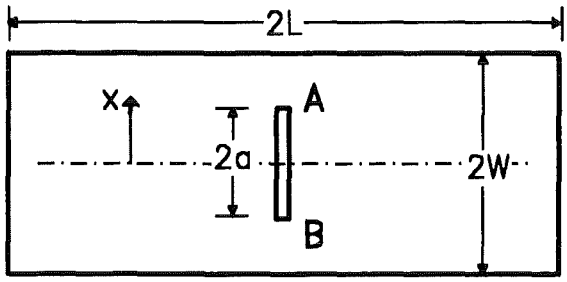

Figure 28. Geometric data of a plate with a central internal through-the-thickness crack

3.3.3 Weight function for the central internal crack

In section 2.2 the general case of an eccentric internal through-the-thickness crack has been considered. Approximate weight functions were determined by use of continuity conditions for the crack opening displacement field. In the special case of a central crack with $x_m = 0$ exposed to a symmetric load, the crack opening displacement field must be symmetric with respect to the center-line, too. Therefore, all conditions of continuity can be satisfied already by a properly chosen set-up for the displacements. This fact suggests a series expansion of type:

$$v_r = \sum_{\nu=0}^{\infty} A_\nu (a^2 - x^2)^{\nu+1/2} \tag{3.3.11}$$

Introducing eq.(3.3.11) into (2.2.2) one finds that the weight function corresponding to the crack tip A of fig.28 has the form

$$h_A = \sum_{\nu=0}^{\infty} \left(\frac{B_\nu}{a-x} + D_\nu \right) (a^2 - x^2)^{\nu+1/2} \quad , \quad B_0 = \frac{1}{\sqrt{\pi a}} \tag{3.3.12}$$

At point B it holds

$$h_B = \sum_{\nu=0}^{\infty} \left(\frac{B_\nu}{a+x} + D_\nu \right) (a^2 - x^2)^{\nu+1/2} \tag{3.3.13}$$

The first unknown coefficients can be determined by an adjustment of eqs.(3.3.12) and (3.3.13) to known reference stress intensity factor solutions. Appropriate reference solutions are given by eq.(3.3.1) for tension and by eq.(3.3.2) for bending.
The conditions yielding the coefficients then read:

$$\int_{-a}^{a} h_A(x,a)dx = \sqrt{a}\, Y_{tension} \tag{3.3.14}$$

and

$$\int_{-a}^{a} h_A(x,a)\, \frac{x}{a}\, dx = \sqrt{a}\, Y_{bend} \tag{3.3.15}$$

The two conditions allow the coefficients B_1, D_0 of the expansion (3.3.12), (3.3.13) to be determined.
In this context, it should be mentioned once more that in the representation of the crack opening displacement field according to (3.3.11) - only appropriate for central cracks - the geometric conditions have already been introduced and will therefore not provide additional coefficients. A solution of high accuracy has to be expected with only a few coefficients known.
Introducing eq.(3.3.12) and (3.3.13) into eq.(3.3.14) and eq.(3.3.15) yields, after analytical integration, the two coefficients

$$B_1 = \frac{4}{a^{5/2}}\left(\frac{2}{\pi} Y_{bend} - \frac{1}{\sqrt{\pi}}\right) \tag{3.3.16}$$

$$D_0 = \frac{2}{a^{3/2}}\left(\frac{1}{\pi} Y_{tension} - \frac{4}{\pi} Y_{bend} + \frac{1}{\sqrt{\pi}}\right) \tag{3.3.17}$$

The weight function for an internal crack in an infinite body is

$$h(x,a) = \frac{1}{\sqrt{\pi a}}\left(\frac{a+x}{a-x}\right)^{1/2} \tag{3.3.18}$$

The weight function for an internal crack in an infinite body under symmetric load is ([12])

$$h(x,a) = \frac{1}{\sqrt{\pi a}}\left[\left(\frac{a+x}{a-x}\right)^{1/2} + \left(\frac{a-x}{a+x}\right)^{1/2}\right] = \frac{2}{\sqrt{\pi a}}\frac{a}{\sqrt{a^2-x^2}} \tag{3.3.19}$$

3.3.4 Weight function for the plate with eccentric internal crack

For eccentric cracks under tension Isida [40] provided the stress intensity factors at the points A and B. Taking these solutions as the reference case the weight function can be determined by direct adjustment [25]. In order to fulfill a priori the well-known limit case of an internal crack in an infinite body, a set-up is suggested that reads for the right-hand crack tip

$$h_r = \frac{1}{\sqrt{\pi a}}\left[\left(\frac{1+\eta/a}{1-\eta/a}\right)^{1/2} + A_r\sqrt{(1-\eta/a)(1+\eta/a)}\right] \tag{3.3.20}$$

and for the left-hand crack tip

$$h_\ell = \frac{1}{\sqrt{\pi a}}\left[\left(\frac{1-\eta/a}{1+\eta/a}\right)^{1/2} + A_\ell\sqrt{(1-\eta/a)(1+\eta/a)}\right] \tag{3.3.21}$$

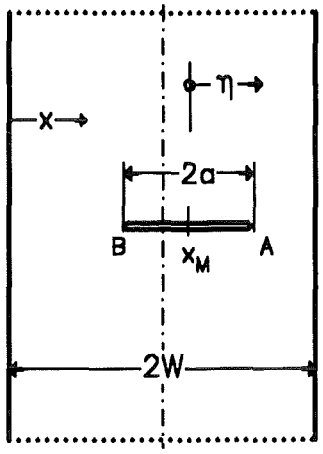

Figure 29. Eccentric crack in a plate. Geometric data

The relations for the determination of the coefficients then read

$$K_{Ir} = \sigma_0\sqrt{\pi a}\, F_r = \sigma_0 \int_{\eta=-a}^{\eta=a} h_r \, d\eta = \sqrt{\pi a}\,(1 + A_r/2) \tag{3.3.22}$$

$$K_{I\ell} = \sigma_0\sqrt{\pi a}\, F_\ell = \sigma_0 \int_{\eta=-a}^{\eta=a} h_\ell \, d\eta = \sqrt{\pi a}\,(1 + A_\ell/2) \tag{3.3.23}$$

and the coefficients result as

$$A_r = 2(F_r - 1) \quad , \qquad A_\ell = 2(F_\ell - 1) \tag{3.3.24}$$

Finally, the weight function is represented by

$$h_r = \sqrt{\frac{1+\eta/a}{\pi a}} \left[\frac{1}{\sqrt{1-\eta/a}} + (F_r - 1)\sqrt{1-\eta/a} \right] \tag{3.3.25}$$

$$h_\ell = \sqrt{\frac{1-\eta/a}{\pi a}} \left[\frac{1}{\sqrt{1+\eta/a}} + (F_\ell - 1)\sqrt{1+\eta/a} \right] \tag{3.3.26}$$

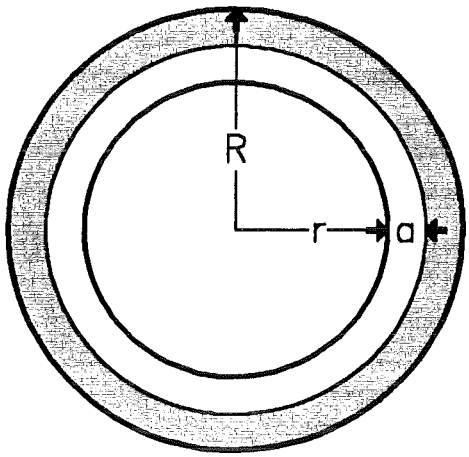

Figure 30. Geometric data of a tube with internal circumferential crack.

3.4 Tube with an internal circumferential crack

Stress intensity factors for a tube with a circumferential crack (fig.30) are given graphically in [12] for axial tension. These data are based on calculations performed by Erdogan [41]. For application of the weight-function method to arbitrary axis-symmetric stress distributions knowledge of an analytical expression for the weight function is advantageous. If we fit the curves given in [12] with respect to the relative crack depth α as well as to the ratio of the inner and outer radii r/R, we find for the ranges $0 \leq \alpha \leq 1$ and $0.1 \leq r/R \leq 0.9$ the representation

$$K_I = \frac{P}{\pi(R^2 - r^2)} \sqrt{a}\, Y(\beta, \alpha) \quad , \quad \alpha = \frac{a}{R - r} \tag{3.4.1}$$

with

$$Y = \frac{1}{\sqrt{1-\alpha}} \left[\frac{\alpha\sqrt{\pi}}{\sqrt{\pi^2 - 4}} (1 + \beta) + 1.989(1 - \alpha) + \alpha(1 - \alpha) \sum_{\nu=0}^{3} \sum_{\mu=0}^{4} A_{\mu\nu} \alpha^{\mu} \beta^{\nu} \right] \tag{3.4.2}$$

$$\beta = r/R \tag{3.4.3}$$

The coefficients $A_{\mu\nu}$ are

	$A_{\mu 0}$	$A_{\mu 1}$	$A_{\mu 2}$	$A_{\mu 3}$
$\mu = 0$	-13.779	56.546	-83.814	41.688
$\mu = 1$	79.931	-397.34	656.81	-339.45
$\mu = 2$	-211.20	1112.23	-1927.36	1047.50

$\mu=3$	247.79	-1325.67	2322.80	-1267.64
$\mu=4$	-105.96	565.64	-990.34	537.86

Table 10. . Coefficients for eq.(3.4.2).

The weight function has been computed with this reference solution according to eq.(2.4.1).

$$h = \frac{E'}{K_{Ir}} \frac{r+x}{r+a} \frac{\partial v_r}{\partial a}$$

The results for the range $0.5<\beta\leq 0.9$ are represented in the form

$$h(x,a) = \sqrt{\frac{2}{\pi a}} \frac{1}{\sqrt{1-x/a}} \left(1 + \sum_{l,n=0}^{2} \sum_{m=0}^{3} C_{lmn}\, \alpha^l \beta^m \left(\frac{x}{a}\right)^n \right) \tag{3.4.4}$$

where the coefficients C_{lmn} were determined with a fitting procedure. The coefficients have been entered in Table 11.

l	m	n=0	1	2
0	0	0.80137	-1.1649	0.33825
0	1	-0.11389	1.44533	-1.29982
0	2	0.84485	-3.3088	2.38357
0	3	-0.77471	2.11490	-1.29124
1	0	-8.85424	11.9009	-3.11618
1	1	23.9875	-42.8237	18.2163
1	2	-30.5091	58.3554	-26.2457
1	3	18.3067	-30.3985	11.1994
2	0	8.67902	-8.27454	-0.39735
2	1	-22.1279	39.9879	-16.0307
2	2	25.6029	-46.4916	16.8626
2	3	-3.67007	2.11845	3.67886

Table 11. . Coefficients for eq.(3.4.4).

In fig.31 the weight function eq.(3.4.4) is compared with data scarcely available in the literature. Labbens et al. [43] reported a weight function especially for $r/R = 5/6$ and 10/11. FE-calculations were performed by Mattheck et al. [42]. These data have been entered as circles in fig.31. Good agreement between all data has been found.

For rough estimations a much simpler weight function can be provided using the direct adjusting method (section 2.5) taking into consideration the reference loading case for tension (eq.(3.6.2)) and the surface condition for the second derivative. It results from eqs.(2.5.5) and (2.5.21)

$$h = \sqrt{\frac{2}{\pi a}} \left[\frac{\rho}{\sqrt{1-\rho}} + \left(\frac{5}{4}\sqrt{\pi/2}\, Y - 1 \right) \sqrt{1-\rho} + \left(\frac{5}{12}\sqrt{\pi/2}\, Y - \frac{5}{3} \right) (1-\rho)^{3/2} \right] \tag{3.4.5}$$

with Y taken from eq.(3.4.2).

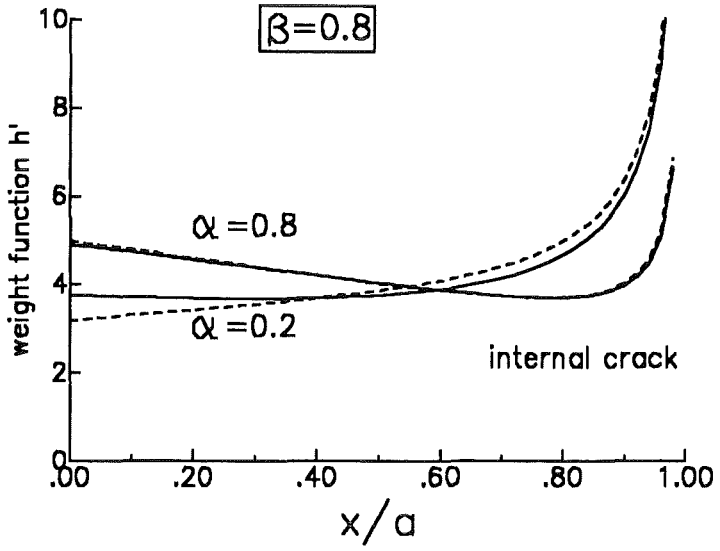

Figure 32. Weight function for the circumferential internal crack. Solid lines: weight functions according to eq.(3.4.4), dashed lines: weight functions computed with eq.(3.4.5).

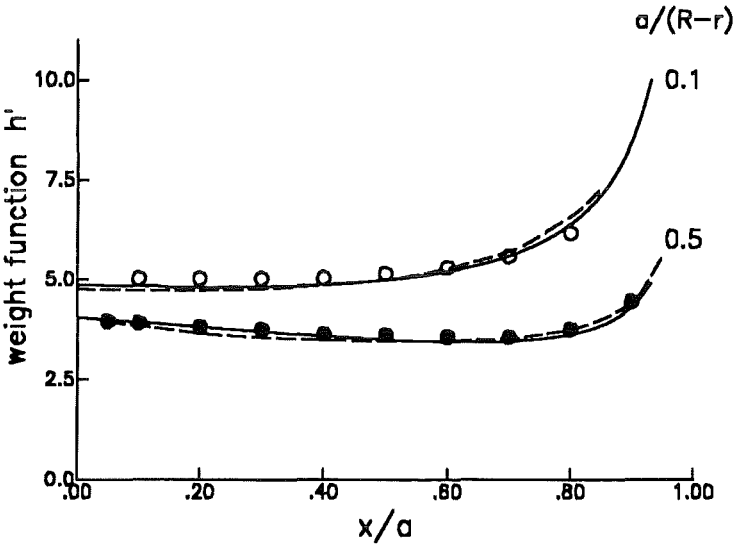

Figure 31. Weight function for the circumferential internal crack. $h' = h\sqrt{R-r}$, $r/R = 5/6$; solid line: eq.(3.4.4), dashed line: Labbens et al. [43], circles: Mattheck et al. [42].

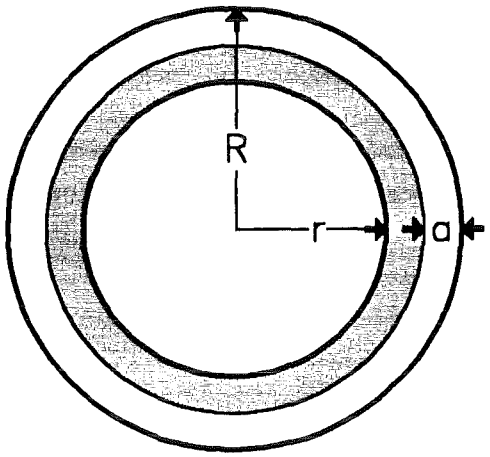

Figure 33. Geometric data of the tube with an external circumferential crack

3.5 Tube with an external circumferential crack

By fitting the stress intensity factors computed by Erdogan [41] for tension - represented graphically in [12] - one obtains, as in case of the internal circumferential crack, the geometric function for the ranges $0 \leq \alpha \leq 1$ and $0.1 \leq \beta \leq 0.9$ ($\beta = r/R$)

$$Y = \frac{1 + 1/\beta}{\sqrt{1-\alpha}} \left[\frac{1.989}{1 + 1/\beta}(1-\alpha) + \frac{\alpha\sqrt{\pi}}{\sqrt{\pi^2 - 4}} + \alpha(1-\alpha) \sum_{\nu=0}^{3} \sum_{\mu=0}^{4} A_{\mu\nu} \alpha^{\mu} \beta^{\nu} \right] \qquad (3.5.1)$$

The coefficients $A_{\mu\nu}$ are

	$A_{\mu 0}$	$A_{\mu 1}$	$A_{\mu 2}$	$A_{\mu 3}$
$\mu = 0$	-1.1186	3.2374	-4.6826	2.8760
$\mu = 1$	5.1738	-23.471	46.896	-30.835
$\mu = 2$	-27.767	130.08	-255.84	179.32
$\mu = 3$	47.959	-233.06	455.44	-316.32
$\mu = 4$	-31.866	162.15	-317.09	216.91

Table 12. . Coefficients for eq.(3.5.1).

The weight function has been computed with eq.(2.4.6)

$$h = \frac{E'}{K_{Ir}} \frac{R - x}{R - a} \frac{\partial v_r}{\partial a}$$

The results are given for $0.5 < \beta \leq 0.9$ in the form

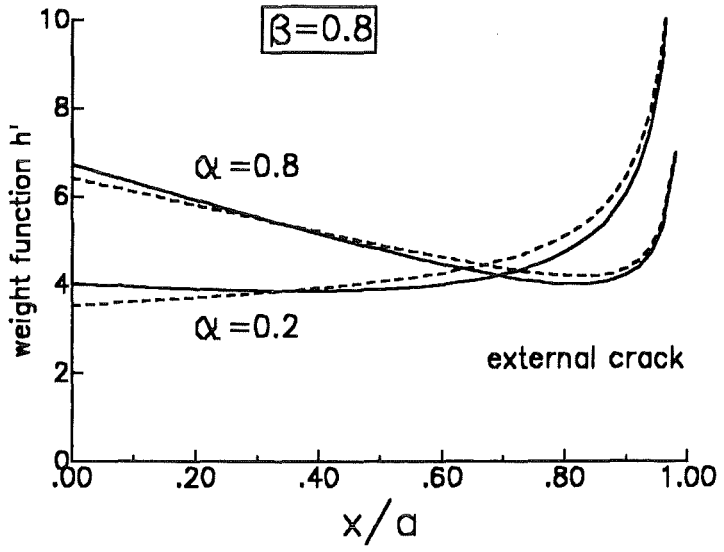

Figure 34. Weight function for the circumferential external crack. Solid lines: weight functions according to eq.(3.5.2), dashed lines: weight functions computed with eq.(3.5.3).

$$h(x,a) = \sqrt{\frac{2}{\pi a}}\,\frac{1}{\sqrt{1-x/a}}\left(1+\sum_{l,n=0}^{2}\sum_{m=0}^{3} B_{lmn}\,\alpha^{l}\beta^{m}\left(\frac{x}{a}\right)^{n}\right) \qquad (3.5.2)$$

where the coefficients B_{lmn} were determined with a fitting procedure. The coefficients are entered in Table 13.

l	m	n=0	1	2
0	0	1.2865	-1.7366	0.4050
0	1	-1.0099	2.1553	-1.0953
0	2	0.7656	-2.2599	1.4614
0	3	-0.1689	0.7548	-0.5844
1	0	-8.8095	12.2236	-2.9570
1	1	22.3252	-44.2390	20.6794
1	2	-15.1687	45.4140	-29.4765
1	3	1.6107	-12.1872	10.6199
2	0	26.6098	-33.6693	6.2652
2	1	-50.1784	88.0529	-35.8013
2	2	21.2610	-72.4823	50.4406
2	3	16.7369	-2.7446	-14.5721

Table 13. . Coefficients for eq.(3.5.2).

A simpler weight function results from direct adjusting method (section 2.5)

$$h = \sqrt{\frac{2}{\pi a}}\left[\frac{\rho}{\sqrt{1-\rho}} + \left(\frac{5}{4}\sqrt{\pi/2}\,Y - 1\right)\sqrt{1-\rho} + \left(\frac{5}{12}\sqrt{\pi/2}\,Y - \frac{5}{3}\right)(1-\rho)^{3/2}\right] \quad (3.5.3)$$

with Y taken from eq.(3.5.1).

3.6 Tube with an axial crack

3.6.1 Tube with an internal axial crack

Geometric functions for the axial internal crack in tubes exposed to power-shaped stress distributions were reported by Andrasic und Parker [44] for R/r≥1.25. In order to include also thin-walled tubes, the stress intensity factor solutions for the flat plate - constituting the limit case r/R →1 - were additionally taken into consideration and, together with the data from [44] plotted in fig.36. It holds

$$K_I = \sigma_n\sqrt{a}\; Y_n(r/R, \alpha) \quad , \quad \sigma(x) = \sigma_n\left(\frac{x}{R-r}\right)^n \quad , \quad \alpha = \frac{a}{R-r} \quad (3.6.1)$$

The geometric function in the ranges $0 \le \alpha \le 0.6$ and $1 \le R/r \le 1.75$ can be described by

$$Y_n = \frac{1}{(1-\alpha)^{3/2}} \sum A_{\mu\nu}\alpha^{\mu+n}(r/R)^\nu \quad (3.6.2)$$

with the coefficients given in Table 14 to Table 17.

	$A_{\mu 0}$	$A_{\mu 1}$	$A_{\mu 2}$	$A_{\mu 3}$	$A_{\mu 4}$
$\mu=0$	2.2069	16.933	-126.67	293.43	-123.665
$\mu=1$	-0.4700	-38.366	276.042	-604.97	239.28
$\mu=2$	0.3293	24.729	-184.51	389.60	-142.3
$\mu=3$	-0.0765	-5.431	40.716	-83.399	28.584

Table 14. Tube with internal axial crack. Coefficients for eq.(3.6.2), (n=0).

	$A_{\mu 0}$	$A_{\mu 1}$	$A_{\mu 2}$	$A_{\mu 3}$	$A_{\mu 4}$
$\mu=0$	1.1902	8.7853	-65.067	145.041	-70.304
$\mu=1$	0.0426	-20.829	140.291	-299.00	138.24
$\mu=2$	-0.0296	13.643	-93.90	193.80	-84.69
$\mu=3$	0.0065	-3.0148	20.716	-41.575	17.312

Table 15. Tube with internal axial crack. Coefficients for eq.(3.6.2), (n=1).

	$A_{\mu 0}$	$A_{\mu 1}$	$A_{\mu 2}$	$A_{\mu 3}$	$A_{\mu 4}$
$\mu=0$	0.8513	6.0221	-45.145	99.645	-52.883
$\mu=1$	0.1672	-14.70	96.872	-206.284	106.042

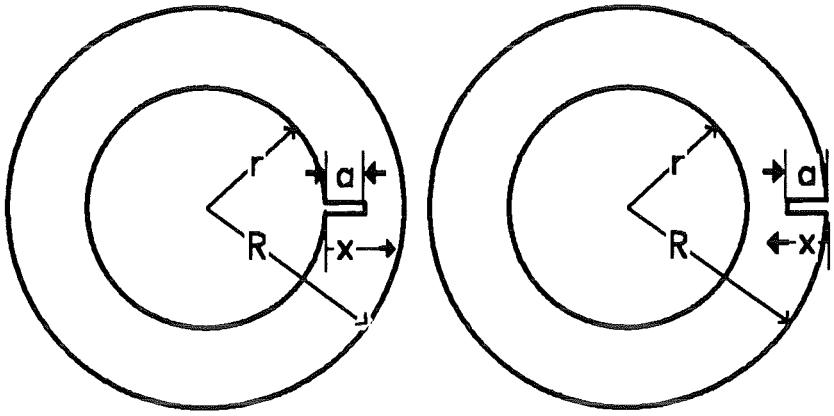

Figure 35. Geometric data of tubes with internal and external axial cracks.

$\mu=2$	-0.1142	9.6891	-65.079	135.261	-67.146
$\mu=3$	0.0256	-2.1446	14.410	-29.335	14.164

Table 16. Tube with internal axial crack. Coefficients for eq.(3.6.2), (n=2).

	$A_{\mu 0}$	$A_{\mu 1}$	$A_{\mu 2}$	$A_{\mu 3}$	$A_{\mu 4}$
$\mu=0$	0.7118	4.0775	-32.106	71.523	-39.756
$\mu=1$	0.1442	-10.419	68.863	-148.31	80.262
$\mu=2$	-0.0974	6.879	-46.324	97.670	-51.381
$\mu=3$	0.0216	-1.5248	10.280	-21.289	10.964

Table 17. Tube with internal axial crack. Coefficients for eq.(3.6.2), (n=3).

Since a number of 4 reference loading cases is given before, it is very easy to provide a weight function for this crack problem. Consideration of the loading cases with $n = 0$ and $n = 1$ gives for instance by application of the adjusting method (section 2.5)

$$h = \sqrt{\frac{2}{\pi a}}\left[\frac{\rho}{\sqrt{1-\rho}} + D_0\sqrt{1-\rho} + D_1(1-\rho)^{3/2}\right] \tag{3.6.3}$$

with the coefficients

$$D_0 = -\frac{15}{4}\sqrt{\frac{\pi}{2}}\left(Y_0 - \frac{7}{2\alpha}Y_1\right) - 9 \tag{3.6.4}$$

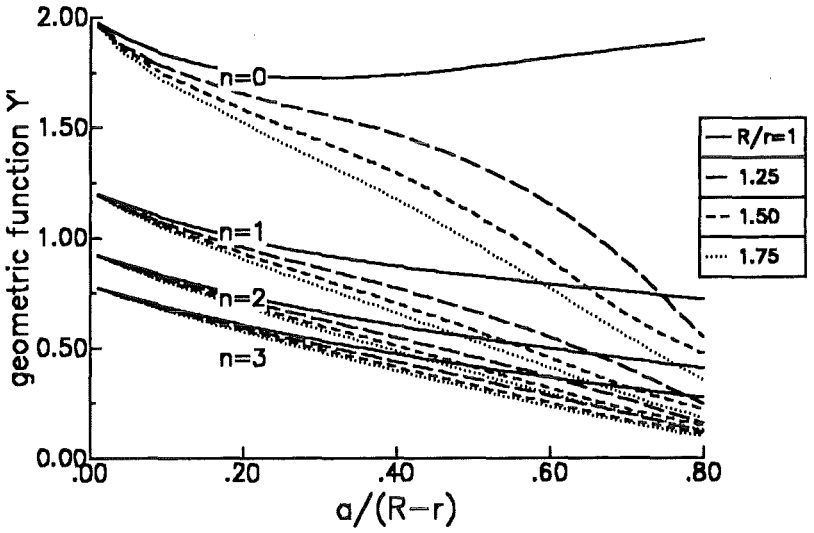

Figure 36. Geometric function for the axial internal crack exposed to power-shaped stress distributions. $Y' = Y(1-\alpha)^{3/2}/\alpha^n$

$$D_1 = \frac{35}{4}\sqrt{\frac{\pi}{2}}\left(Y_0 - \frac{5}{2\alpha}Y_1\right) + \frac{35}{3} \tag{3.6.5}$$

The geometric functions are given by eq.(3.6.2). The accuracy may be increased strongly by use of an additional loading case.

3.6.2 Tube with an external axial crack

Also for the tube with an external axial crack the relations (3.6.1) and (3.6.2) are applicable. In this case the origin of the x-axis is at the outer surface. A fitting procedure similar to that applied to the internal crack yields the coefficients entered in Table 18 to Table 21.

	$A_{\mu 0}$	$A_{\mu 1}$	$A_{\mu 2}$	$A_{\mu 3}$	$A_{\mu 4}$
$\mu=0$	2.156	14.028	-89.22	210.0	-71.963
$\mu=1$	-0.3670	-34.229	206.438	-451.72	147.00
$\mu=2$	0.2622	23.183	-143.86	302.26	-91.835
$\mu=3$	-0.0610	-5.119	32.229	-65.877	18.694

Table 18. Tube with external axial crack. Coefficients for eq.(3.6.2), (n=0).

	$A_{\mu 0}$	$A_{\mu 1}$	$A_{\mu 2}$	$A_{\mu 3}$	$A_{\mu 4}$
$\mu=0$	1.1936	7.3065	-47.627	105.31	-44.803
$\mu=1$	0.0249	-18.337	106.37	-222.57	90.209
$\mu=2$	-0.0095	12.331	-72.862	147.35	-56.315
$\mu=3$	0.0008	-2.715	16.15	-31.827	11.465

Table 19. Tube with external axial crack. Coefficients for eq.(3.6.2), (n = 1).

	$A_{\mu 0}$	$A_{\mu 1}$	$A_{\mu 2}$	$A_{\mu 3}$	$A_{\mu 4}$
$\mu = 0$	0.8571	5.247	-35.34	77.25	-38.68
$\mu = 1$	0.1487	-13.418	77.769	-163.22	79.501
$\mu = 2$	-0.0969	9.035	-53.20	109.13	-51.68
$\mu = 3$	0.0210	-1.996	11.832	-23.871	11.031

Table 20. Tube with external axial crack. Coefficients for eq.(3.6.2), (n = 2).

	$A_{\mu 0}$	$A_{\mu 1}$	$A_{\mu 2}$	$A_{\mu 3}$	$A_{\mu 4}$
$\mu = 0$	0.7208	3.365	-24.151	52.707	-27.074
$\mu = 1$	0.1194	-9.114	52.999	-111.17	55.65
$\mu = 2$	-0.0760	6.108	-36.18	74.36	-36.29
$\mu = 3$	0.0161	-1.345	8.049	-16.31	7.802

Table 21. Tube with external axial crack. Coefficients for eq.(3.6.2), (n = 3).

Also for the external axial crack the weight function is given by eqs.(3.6.3) to (3.6.5).

3.7 Circular disc with a crack

3.7.1 Disc with an edge crack

Circular discs and cylinders are of special interest in case of rotating components. A disc of diameter D with an edge crack of length a is shown in fig.37.

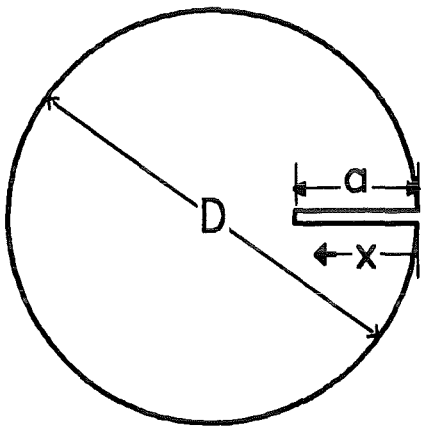

Figure 37. Edge-cracked disc. Geometric data.

The circular disc is one of the rare fracture-mechanical problems for which exact solutions for the reference stress intensity factors are available. Furthermore, the disc is the only finite component, for which an exact solution exists [33]. In case of a homogeneous stress over the crack the geometric function is given by Gregory [33] as

$$Y_0 = \frac{1.988}{(1-\alpha)^{3/2}} \quad , \quad \alpha = a/D \tag{3.7.1}$$

For a quadratic stress distribution,

$$\sigma(x) = \sigma_0\left(1 - \frac{2x}{D}\right)^2 \tag{3.7.2}$$

one obtains from [33] the geometric function plotted in fig.38. These data are compared with results of Rooke and Tweed [45] for $a/D < 0.5$ (extrapolated by Tada [12] up to $a/D = 1$). For more convenient use the results provided by Gregory [33] are fitted as

$$Y_2 = \frac{1.988}{(1-\alpha)^{3/2}}\left(1 - 2.4431\alpha + 3.2427\alpha^2 - 1.8106\alpha^3 + 0.34404\alpha^4\right) \tag{3.7.3}$$

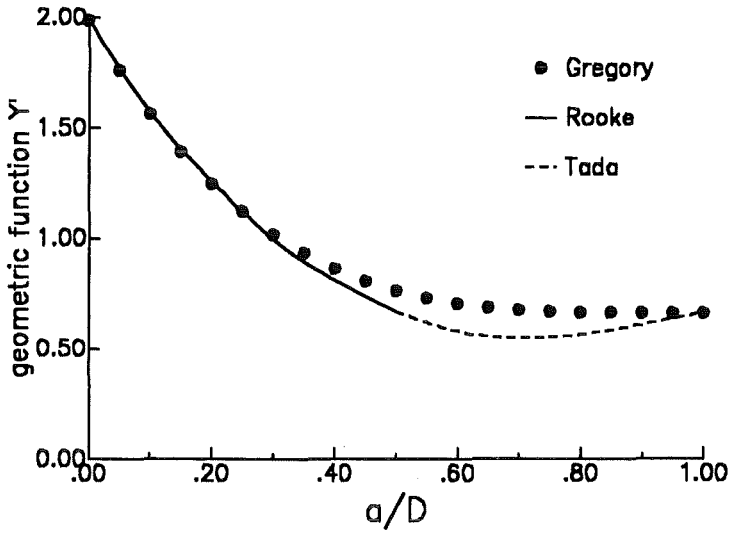

Figure 38. Geometric function for an edge-cracked disc under quadratic stress distribution. Normalised representation $Y' = Y(1-\alpha)^{3/2}$.

with maximum deviations of ±1%. The weight function has been determined using the two reference loading cases and the two geometric conditions given by eqs.(2.5.21) and (2.5.22) in [25], resulting with $\rho = x/a$ in

$$h(x,a) = \sqrt{\frac{2}{\pi a}}\left[\frac{\rho}{\sqrt{1-\rho}} + D_0\sqrt{1-\rho} + D_1(1-\rho)^{3/2} + D_2(1-\rho)^{5/2} + D_3(1-\rho)^{7/2}\right] \quad (3.7.4)$$

with the coefficients $D_0 \ldots D_3$ obtained from the system of linear equations

$$\begin{aligned} D_0 - 3D_1 - 15D_2 - 35D_3 &= 4 \\ D_0 - D_1 + 5D_2 + 35D_3 &= 6 \\ \frac{2}{3}D_0 + \frac{2}{5}D_1 + \frac{2}{7}D_2 + \frac{2}{9}D_3 &= R_1 \\ C^{(0)}D_0 + C^{(1)}D_1 + C^{(2)}D_2 + C^{(3)}D_3 &= R_2 \end{aligned} \quad (3.7.5)$$

with

$$\begin{aligned} C^{(0)} &= \frac{2}{3} - \frac{16}{15}\alpha + \frac{64}{105}\alpha^2 \\ C^{(1)} &= \frac{2}{5} - \frac{16}{35}\alpha + \frac{64}{315}\alpha^2 \\ C^{(2)} &= \frac{2}{7} - \frac{16}{63}\alpha + \frac{64}{693}\alpha^2 \\ C^{(3)} &= \frac{2}{9} - \frac{16}{99}\alpha + \frac{64}{1287}\alpha^2 \end{aligned} \quad (3.7.6)$$

and

$$R_1 = Y_0\sqrt{\pi/2} - \frac{4}{3}$$

$$R_2 = Y_2\sqrt{\pi/2} - \frac{4}{3} + \frac{64}{15}\alpha - \frac{384}{105}\alpha^2 \tag{3.7.7}$$

The weight function resulting from eqs.(3.7.5), (3.7.6) and (3.7.7) is represented in Table 22 [25]

$$h = \sqrt{\frac{2}{\pi a}}\,\frac{g(\rho,\alpha)}{\sqrt{1-\rho}\,(1-\alpha)^{3/2}} \tag{3.7.8}$$

α	$\rho=0$	0.2	0.4	0.6	0.8	0.9	1.0
0.2	2.440	2.058	1.683	1.325	0.996	0.848	0.7155
0.3	2.769	2.265	1.785	1.337	0.932	0.750	0.5857
0.4	3.092	2.466	1.881	1.345	0.868	0.656	0.4648
0.5	3.410	2.661	1.970	1.347	0.804	0.567	0.3536
0.6	3.726	2.850	2.052	1.344	0.740	0.481	0.2530
0.7	4.041	3.033	2.126	1.334	0.674	0.399	0.1643
0.8	4.356	3.211	2.192	1.315	0.606	0.322	0.0894
0.9	4.650	3.373	2.245	1.291	0.541	0.254	0.0316
1.0	4.978	3.562	2.314	1.259	0.445	0.157	0.0000

Table 22. Weight function. Normalised representation $g(\rho,\alpha)$ according to eq.(3.7.8).

If only the two reference solutions are applied, one obtains

$$h(x,a) = \sqrt{\frac{2}{\pi a}}\left[\frac{\rho}{\sqrt{1-\rho}} + D_0\sqrt{1-\rho} + D_1(1-\rho)^{3/2}\right] \tag{3.7.9}$$

with the two coefficients D_0 and D_1

$$D_0 = \frac{6615}{1792\alpha^2 - 2016\alpha}\left[Y_2\sqrt{\pi/2} - \frac{4}{3} + \frac{64}{15}\alpha - \frac{128}{35}\alpha^2 - \right. \tag{3.7.10}$$

$$\left.\left(Y_0\sqrt{\pi/2} - \frac{4}{3}\right)\left(1 - \frac{8}{7}\alpha + \frac{32}{63}\alpha^2\right)\right]$$

and

$$D_1 = \frac{5}{2}\sqrt{\pi/2}\,Y_0 - \frac{10}{3} - \frac{5}{3}D_0 \tag{3.7.11}$$

Taking into consideration also the next term of the expansion, namely

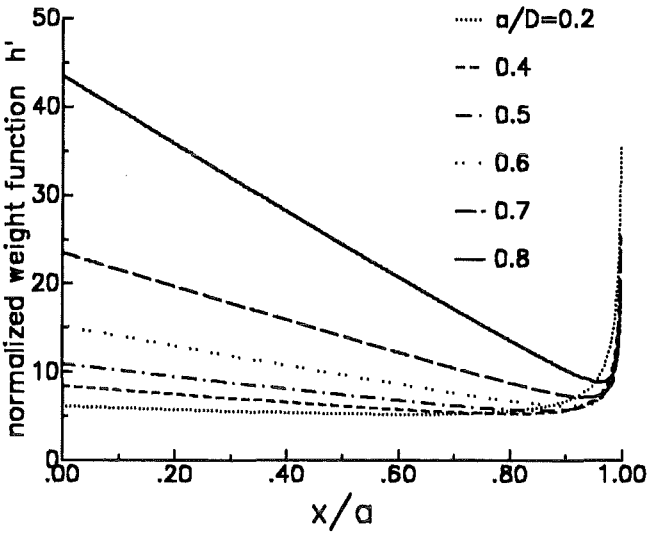

Figure 39. Weight function for the edge-cracked circular disc. Normalised representation $h' = h\sqrt{D}$

$$h(x,a) = \sqrt{\frac{2}{\pi a}}\left[\frac{\rho}{\sqrt{1-\rho}} + D_0\sqrt{1-\rho} + D_1(1-\rho)^{3/2} + D_2(1-\rho)^{5/2}\right] \tag{3.7.12}$$

we obtain with the condition - $h'' = 0$ for $\rho = 0$ -

$$\begin{aligned} D_0 - 3D_1 - 15D_2 &= 4 \\ \frac{2}{3}D_0 + \frac{2}{5}D_1 + \frac{2}{7}D_2 &= Y_0\sqrt{\pi/2} - \frac{4}{3} \\ C^{(0)}D_0 + C^{(1)}D_1 + C^{(2)}D_2 &= Y_2\sqrt{\pi/2} - \left(\frac{4}{3} - \frac{64}{15}\alpha + \frac{384}{105}\alpha^2\right) \end{aligned} \tag{3.7.13}$$

with

$$\begin{aligned} C^{(0)} &= \frac{2}{3} - \frac{16}{15}\alpha + \frac{64}{105}\alpha^2 \\ C^{(1)} &= \frac{2}{5} - \frac{16}{35}\alpha + \frac{64}{315}\alpha^2 \\ C^{(2)} &= \frac{2}{7} - \frac{16}{63}\alpha + \frac{64}{693}\alpha^2 \end{aligned} \tag{3.7.14}$$

The coefficients D_0, D_1, D_2 yield

$$D_0 = \frac{180R_2 - C^{(1)}(525R_1 + 40) + C^{(2)}(105R_1 + 56)}{180C^{(0)} - 360C^{(1)} + 84C^{(2)}}$$

$$D_1 = \frac{-360R_2 + C^{(0)}(525R_1 + 40) + C^{(2)}(35R_1 - 280/3)}{180C^{(0)} - 360C^{(1)} + 84C^{(2)}} \tag{3.7.15}$$

$$D_2 = \frac{84R_2 - C^{(0)}(105R_1 + 56) - C^{(1)}(35R_1 - 280/3)}{180C^{(0)} - 360C^{(1)} + 84C^{(2)}}$$

or fitted to simpler expressions:

$$\begin{aligned} D_0 &\simeq (1.5721 + 2.4109\alpha - 0.8968\alpha^2 - 1.4311\alpha^3)/(1-\alpha)^{3/2} \\ D_1 &\simeq (0.4612 + 0.5972\alpha + 0.7466\alpha^2 + 2.2131\alpha^3)/(1-\alpha)^{3/2} \\ D_2 &\simeq (-0.2537 + 0.4353\alpha - 0.2851\alpha^2 - 0.5853\alpha^3)/(1-\alpha)^{3/2} \end{aligned} \tag{3.7.16}$$

The weight function resulting from eqs.(3.7.12)-(3.7.15) is illustrated in fig.39.

3.7.2 A circular disc with a central crack

For the circular disc with central crack two reference solutions are known. Rooke and Tweed [46], [47] derived stress intensity factors for constant crack-surface loads and quadratically distributed stresses. For $\sigma = const.$ one can fit the geometric function Y_0 as

$$Y_0 = \sqrt{\pi}\ \frac{1 - 0.5\alpha + 1.6873\alpha^2 - 2.671\alpha^3 + 3.2027\alpha^4 - 1.8935\alpha^5}{\sqrt{1-\alpha}} \quad , \quad \alpha = a/R \tag{3.7.17}$$

In case of a stress distribution described by

$$\sigma = \sigma_0 \left(\frac{x}{a}\right)^2 \tag{3.7.18}$$

the geometric function can be approximated as

$$Y_2 = \sqrt{\pi}\ \frac{0.5 - 0.25\alpha + 0.4421\alpha^2 - 1.1091\alpha^3 + 1.5591\alpha^4 - 0.867\alpha^5}{\sqrt{1-\alpha}} \tag{3.7.19}$$

It is evident that with these two solutions for *symmetric* stresses only a *symmetric* weight function can be derived. An appropriate set-up for the symmetric weight function is given by

$$h_{symm} = \frac{2}{\sqrt{\pi a}} \left[\frac{1}{\sqrt{1-\rho^2}} + D_0\sqrt{1-\rho^2} + D_1(1-\rho^2)^{3/2} + \ldots \right] \tag{3.7.20}$$

Because of the symmetry, the weight functions correspond to the crack tips A and B of fig.40. Adjusting the weight function to the two reference load cases, eq.(3.7.17) and (3.7.19), yields the coefficients

$$\begin{aligned} D_0 &= -\frac{4}{\sqrt{\pi}} Y_0 + \frac{24}{\sqrt{\pi}} Y_2 - 8 \\ D_1 &= \frac{8}{\sqrt{\pi}} Y_0 - \frac{32}{\sqrt{\pi}} Y_2 + 8 \end{aligned} \tag{3.7.21}$$

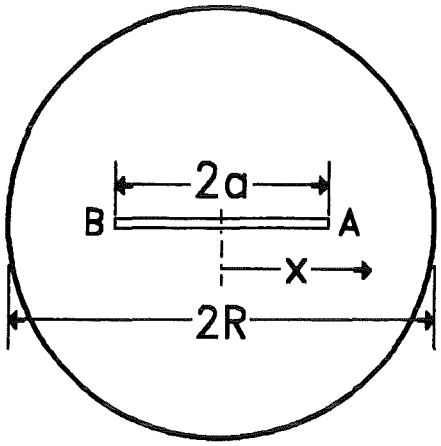

Figure 40. Centrally cracked circular disc. Geometric data.

$$D_0 = \frac{8 - 4\alpha + 3.8612\alpha^2 - 15.9344\alpha^3 + 24.6076\alpha^4 - 13.234\alpha^5}{\sqrt{1-\alpha}} - 8 \qquad (3.7.22)$$

$$D_1 = -\frac{8 - 4\alpha + 0.6488\alpha^2 - 14.1232\alpha^3 + 24.2696\alpha^4 - 12.596\alpha^5}{\sqrt{1-\alpha}} + 8 \qquad (3.7.23)$$

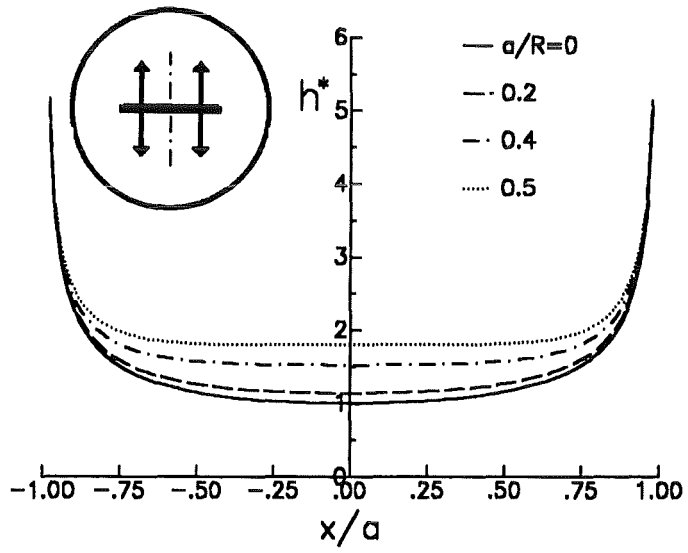

Figure 41. Symmetric weight function for a central crack in the circular disc. Normalized representation ($h^* = h\sqrt{\pi a/2}$).

3.8 Round-CT-specimen

Weight functions are known for the special case of a disc, which is identical with the RCT-specimen if the load application holes are neglected. As a consequence of Saint Venant's theorem, the differences between the disc and the RCT-specimen have to be expected to occur only near the load application holes, i.e. for $x \simeq 0$ (fig.42).
In order to take into account the influence of the real geometry, the weight function of the RCT-specimen will be derived additionally.

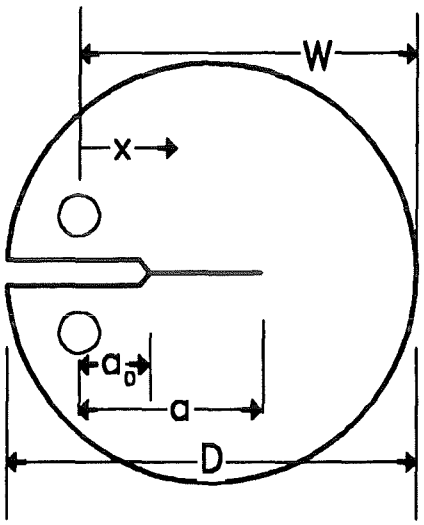

Figure 42. Round-CT-specimen (RCT). Geometric data.

For the specially chosen test specimen (RCT-specimen, see fig.42) Newman [48] determined stress intensity factors and CODs at different locations of the crack surface. The stress intensity factor solution of Newman [48] can be written as

$$K_I = \sigma_0 \sqrt{W}\, F_I \;, \quad \sigma_0 = \frac{P}{Wt} \;, \quad F_I = \frac{(2+\alpha)(0.76 + 4.8\alpha - 11.58\alpha^2 + 11.43\alpha^3 - 4.08\alpha^4)}{(1-\alpha)^{3/2}} \tag{3.8.1}$$

(t = thickness, P = applied load). The results for the RCT-specimen obtained with the procedure described in Section 2 are illustrated in fig.43.
Table 23 shows the weight-function values in a representation which lends itself easily to interpolation by bicubic splines

$$h = \sqrt{\frac{2}{\pi a}}\, \frac{g(x/a, \alpha)}{\sqrt{1 - x/a}\,(1-\alpha)^{3/2}} \tag{3.8.2}$$

Using the data from Table 23, the weight function can be expressed within $\pm 1\%$ accuracy by the approximation formula

$$h = \sqrt{\frac{2}{\pi a}}\, \frac{1}{\sqrt{1 - x/a}\,(1-\alpha)^{3/2}} \left[(1-\alpha)^{3/2} + \sum D_{\nu\mu} (1 - x/a)^{\mu+1} (\alpha)^{\nu} \right] \tag{3.8.3}$$

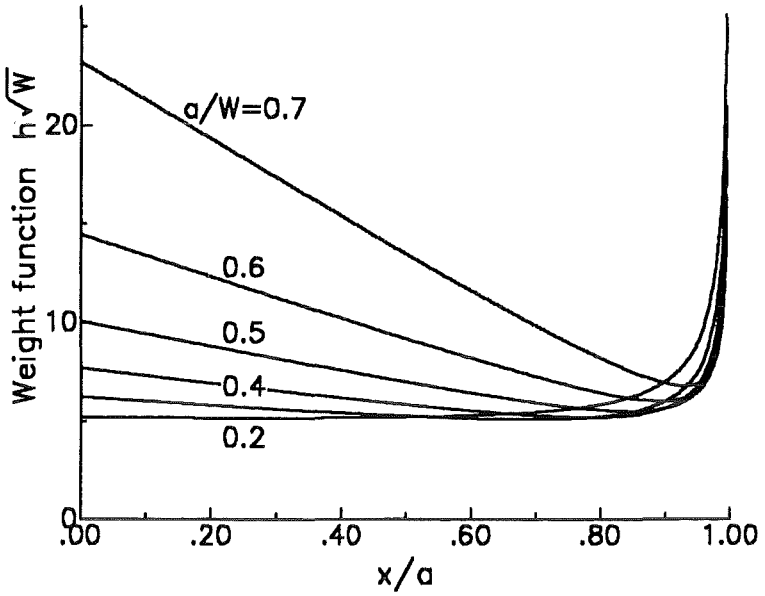

Figure 43. Weight function for the RCT-specimen. Influence of the crack depth.

α	x/a=0.0	0.2	0.4	0.6	0.8	0.9	0.95	1.0
0.2	2.081	1.848	1.603	1.337	1.044	0.885	0.801	0.716
0.25	2.305	1.972	1.642	1.314	0.984	0.818	0.734	0.650
0.3	2.501	2.085	1.686	1.303	0.936	0.759	0.672	0.586
0.35	2.673	2.185	1.725	1.294	0.894	0.705	0.614	0.524
0.4	2.830	2.277	1.761	1.286	0.854	0.654	0.558	0.465
0.45	2.985	2.367	1.797	1.279	0.815	0.604	0.504	0.408
0.5	3.151	2.464	1.837	1.273	0.778	0.557	0.453	0.354
0.55	3.338	2.577	1.886	1.272	0.742	0.510	0.403	0.302
0.60	3.551	2.708	1.943	1.273	0.707	0.465	0.355	0.253
0.7	3.997	2.975	2.055	1.267	0.632	0.376	0.265	0.164
0.8	4.062	2.966	1.995	1.175	0.531	0.283	0.179	0.089

Table 23. Weight function for the Round-CT specimen. Normalised representation g(x/a, α) according to eq.(3.8.3).

ν	μ=0	1	2	3	4
0	2.826	-5.865	0.8007	-0.2584	0.6856
1	-10.948	48.095	-3.839	1.280	-6.734

2	35.278	-143.789	6.684	-5.248	25.188
3	-41.438	196.012	-4.836	11.435	-40.140
4	15.191	-92.787	-0.7274	-7.328	22.047

Table 24. . Coefficients for eq.(3.8.3).

3.9 Stress intensity factors and weight functions for cracks in front of notches

Under externally applied loads, notches are acting as stress concentrators. Therefore, cracks emanating from the notch root are of special interest in general fracture mechanics. Stress intensity factor solutions are available in the literature for externally applied tensile and bending loads [48]-[53]. In many cases the stress in front of a notch is not caused by external forces. Such cases are for example:

- Crack surfaces directly loaded by internal pressure (pipes, vessels),
- cracks influenced by thermal stresses near the notch root,
- cracks in coarse-grained ceramics with crack-surface interaction.

The weight-function method is an appropriate procedure for the computation of related stress intensity factors under such special loadings.

3.9.1 Internal elliptical notches

The stresses in front of internal notches are available only in cases involving simple geometry and mechanics. This is true for elliptical notches in infinite bodies, for which the problem has been solved by Muskelishvili ([1]) and other authors. The stress distribution at an elliptical notch in an infinite body under uniaxial remote tensile stress σ_0 results as ([54],[55])

$$(a-b)^2\frac{\sigma_y}{\sigma_0}=b^2+\frac{a|\kappa|}{\sqrt{\kappa^2-a^2+b^2}}\left[a-2b+\frac{b^2(a-b)}{\kappa^2-a^2+b^2}\right] \tag{3.9.1}$$

$$(a-b)^2\frac{\sigma_x}{\sigma_0}=-a^2+\frac{a|\kappa|}{\sqrt{\kappa^2-a^2+b^2}}\left[a-\frac{b^2(a-b)}{\kappa^2-a^2+b^2}\right] \tag{3.9.2}$$

with $\kappa = x + a$. σ_y is the stress component perpendicular to the half-axis a and σ_x is the component in direction of the half-axis a, (fig.44). The radius of the notch root is given by

$$\rho = b^2/a \tag{3.9.3}$$

The maximum stress at $x = a$ is

$$\sigma_{y,max}/\sigma_0 = 2\sqrt{a/\rho}+1 \tag{3.9.4}$$

A notch in an infinite body is shown in fig.45a. Its length is 2a and the notch radius is ρ. A small one-dimensional crack of length ℓ is placed at the notch root. The infinite body is loaded by a

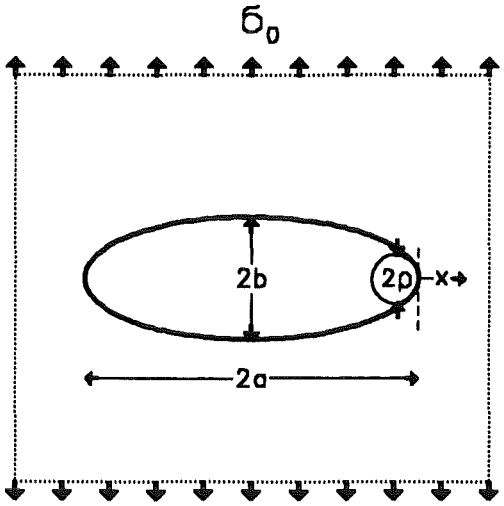

Figure 44. Elliptical notch in an infinite body. Notch under remote tensile stresses σ_0.

tensile stress σ_0. In order to allow analytical calculations to be made, the notch is replaced by a slender ellipse of the same length and the same radius ρ (fig.45b).
The stress intensity factor of the crack/notch-configuration may be written as

$$K_I = \sigma_0\left(1 + 2\sqrt{a/\rho}\,\right) F \sqrt{\pi \ell} \tag{3.9.5}$$

The geometric function F can be concluded from results of Newman [48] obtained with the Boundary Collocation Method. In [48] stress intensity factors for cracks at the root of elliptical notches in an infinite body are given for values $a/\rho = 1/16, 1/4, 1, 4$, and 16. These data were also used in Schijve's [51] analysis.

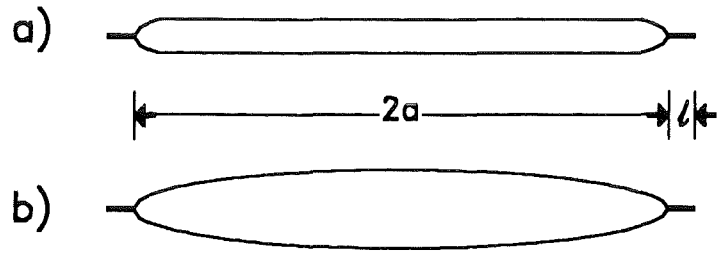

Figure 45. A small crack in front of an internal notch. a) slot-shaped-notch, b) elliptical notch.

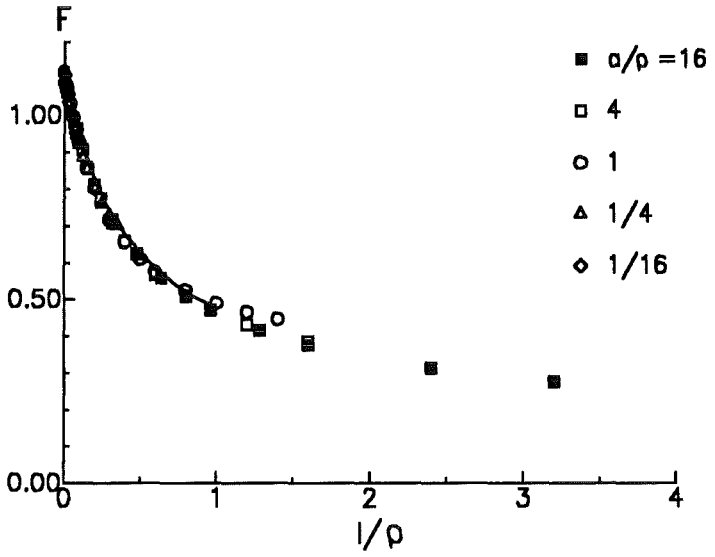

Figure 46. Elliptical notch. Stress intensity factors for small cracks at a notch root (Newman [48]).

The resulting geometric function is plotted in fig.46. It should be noted that for small values of ℓ/ρ the geometric function F is only dependent on ℓ/ρ and nearly independent of the ratio a/ρ. In fig.47 the results of Newman for the narrowest ellipse ($a/\rho = 16$) are compared with results calculated by Nisitani and Isida [58] which were obtained for the same value a/ρ by parabolic interpolation of tabulated data (represented in [14]). The agreement is excellent. The solid line describes the solution for $a/\rho \to \infty$ given in (Nisitani and Isida [58]). There is obviously no significant deviation from the data resulting for $a/\rho = 16$. The additionally drawn dashed curve represents the approximation of Lukas and Klesnil [57] which does not contain a/ρ:

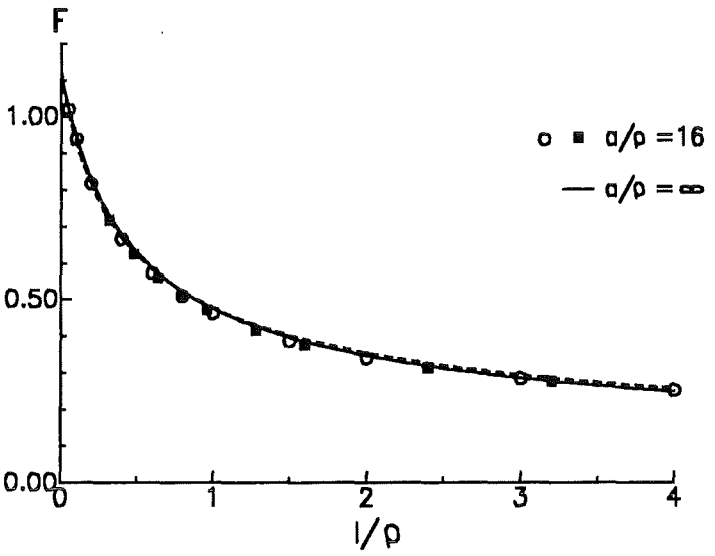

Figure 47. Elliptical notch. Comparison of stress intensity factors for $a/\rho \gg 1$; symbols: $a/\rho = 16$ (squares: Newman [48]; circles: Nisitani and Isida, [58]); curves: solid line $a/\rho \to \infty$, dashed line eq.(3.9.6) (Lukas and Klesnil, [57]).

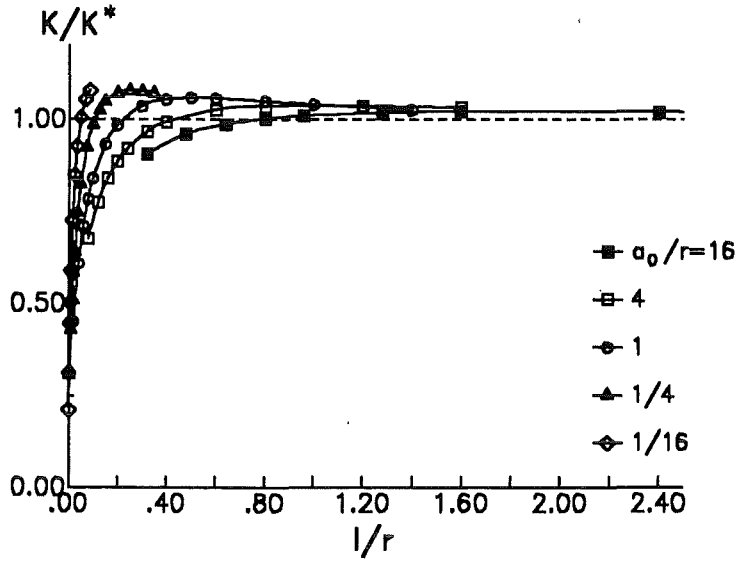

Figure 48. Elliptical notch. Stress intensity factors for small cracks in front of elliptical notches normalised to the "long-crack" solution K^*.

$$F = \frac{1.1215}{\sqrt{1 + 4.5\ell/\rho}} \tag{3.9.6}$$

Their formula is in good agreement with the solution for $a/\rho \to \infty$ of Nisitani and Isida.
If we normalise the stress intensity factors described by eq.(3.9.5) on the stress intensity factors for long cracs $K^* = \sigma_0\sqrt{\pi(a_0 + \ell)}$, we observe the well-known behaviour of an "overshooting" of short-crack stress intensity factors over the long-crack values (fig.48).

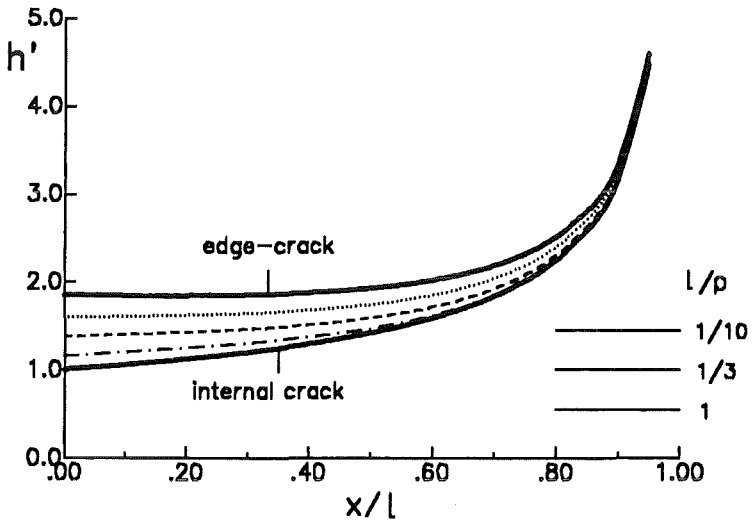

Figure 49. Weight function for an elliptical notch. Normalised weight function for cracks in front of an internal elliptical notch: $h' = h\sqrt{\pi\ell/2}$ for $a/\rho = 16$; solid lines: limit cases for edge-crack in a plate and internal crack in an infinite body.

In order to determine the weight function for the crack/notch-problem the numerical results of Newman [48] and Nisitani and Isida [58] for $a/\rho \leq 1$ were chosen as the reference stress intensity factor and the stress distribution, eq.(3.9.1), as the reference stress σ_r. The weight function data resulting with the procedure described before are shown in fig.49 for the case $a/\rho = 16$ and for several ratios ℓ/ρ. In addition, the two limit cases of an edge-crack in a plate ($\ell/\rho \to 0$) - using the solution derived in [27] - and an internal crack through the thickness of an infinite body ($\ell/\rho \to \infty$) are entered in fig.49. In case of a symmetric crack/notch-configuration (cracks at both sides of the notch) which has been considered in [48] and [58], the well-known formula for the weight function of a symmetrically loaded crack can be rewritten as

$$h_{int\,crack} = \frac{1}{\sqrt{\pi(\ell + a)}} \left(\sqrt{\frac{2a + \ell + x}{\ell - x}} + \sqrt{\frac{\ell - x}{2a + \ell + x}} \right) \tag{3.9.7}$$

ℓ/ρ	$x/\ell = 0$	0.2	0.4	0.6	0.8	0.9	1.0
0.0	1.835	1.630	1.442	1.271	1.122	1.060	1.000
0.1	1.630	1.478	1.324	1.188	1.082	1.038	1.000
0.2	1.506	1.383	1.255	1.144	1.060	1.028	1.000
0.3	1.418	1.319	1.212	1.119	1.048	1.022	1.000
0.4	1.359	1.276	1.187	1.106	1.041	1.020	1.000
0.6	1.294	1.227	1.159	1.090	1.034	1.015	1.000
0.8	1.252	1.200	1.141	1.080	1.029	1.015	1.000
1.0	1.228	1.180	1.128	1.072	1.026	1.013	1.000

Table 25. Normalised weight function. $g(x/\ell, \ell/\rho)$ for $a/\rho = 1$.

ℓ/ρ	$x/\ell = 0$	0.2	0.4	0.6	0.8	0.9	1.0
0.0	1.835	1.630	1.442	1.271	1.122	1.060	1.000
0.1	1.622	1.473	1.319	1.185	1.080	1.037	1.000
0.2	1.492	1.374	1.247	1.137	1.056	1.026	1.000
0.3	1.406	1.304	1.198	1.107	1.042	1.018	1.000
0.4	1.345	1.254	1.165	1.089	1.034	1.014	1.000
0.6	1.270	1.195	1.128	1.069	1.026	1.011	1.000
0.8	1.217	1.165	1.108	1.057	1.020	1.008	1.000
1.0	1.177	1.147	1.094	1.050	1.017	1.007	1.000

Table 26. Normalised weight function. $g(x/\ell, \ell/\rho)$ for $a/\rho = 4$.

ℓ/ρ	$x/\ell = 0$	0.2	0.4	0.6	0.8	0.9	1.0
0.0	1.835	1.630	1.442	1.271	1.122	1.060	1.000
0.1	1.593	1.449	1.302	1.173	1.075	1.034	1.000
0.2	1.470	1.351	1.229	1.125	1.050	1.022	1.000

0.3	1.393	1.290	1.184	1.096	1.035	1.015	1.000
0.4	1.338	1.247	1.153	1.076	1.026	1.010	1.000
0.6	1.259	1.186	1.111	1.051	1.014	1.005	1.000
0.8	1.202	1.147	1.083	1.036	1.008	1.002	1.000
1.0	1.161	1.122	1.065	1.028	1.005	1.000	1.000

Table 27. Normalised weight function. $g(x/\ell, \ell/\rho)$ for $a/\rho = 16$.

In Table 25-Table 27 the weight function is given in the representation

$$h = \sqrt{\frac{2}{\pi \ell}} \frac{g(x/\ell, a/\rho)}{\sqrt{1 - x/\ell}} \tag{3.9.8}$$

which lends itself easily to interpolation. From a practical point of view it is recommended to perform the interpolation with respect to the inverse parameter ρ/a or $\sqrt{\rho/a}$.

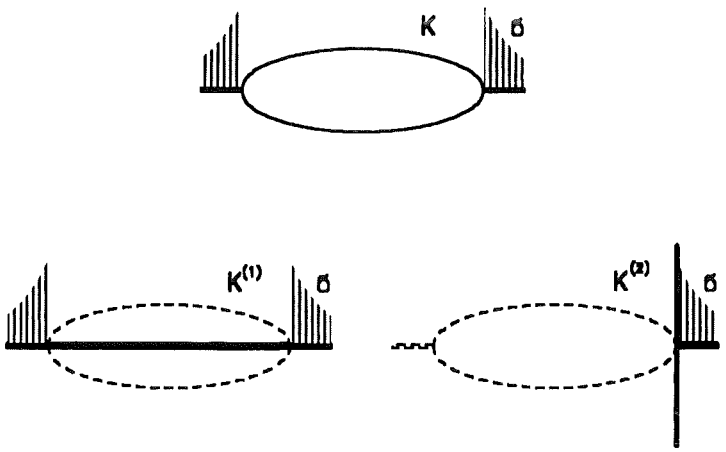

Figure 50. Limit cases. Definition of the limit cases for stress intensity factors for a crack in front of an internal elliptical notch: $K^{(1)} < K < K^{(2)}$.

3.9.1.1 Limit cases for stress intensity factors

Two limit cases for the stress intensity factor of small cracks in front of an elliptical notch can be identified (fig.50). The lower limit is given by an internal crack of total length $2(\ell + a)$ which is loaded by the stress distribution σ (eq.(3.9.1)) over the length ℓ. The limit stress intensity factor $K^{(1)}$ is

$$K^{(1)} = \int_0^{\ell} h_{int\ crack}\, \sigma\, dx \tag{3.9.9}$$

where $h_{int\ crack}$ is given by eq.(3.9.7). For small cracks ($\ell \ll \rho$) the situation of an edge crack is approached which yields the stress intensity factor $K^{(2)}$

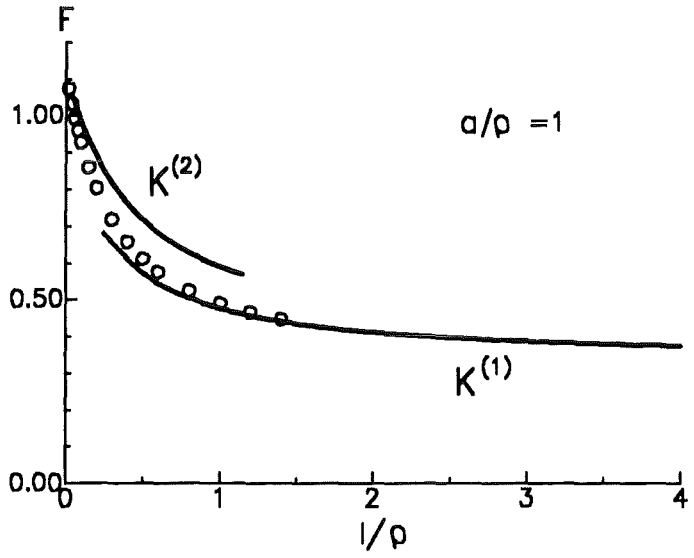

Figure 51. Limit cases. Comparison of limit-case solutions with numerical data of Newman [48] for $a/\rho = 1$

$$K^{(2)} = \int_0^{\ell} h_{edge\ crack}\, \sigma\, dx \tag{3.9.10}$$

with the weight function $h_{edge\ crack}$ for an edge crack in a semi-infinite plate.
Figure 51 shows the limit cases $K^{(1)}$ and $K^{(2)}$ together with Newman's results for $a/\rho = 1$, and in fig.52 an intercomparison is made for $a/\rho = 16$. The agreement between numerical data and the limit case $K^{(1)}$ is very good for $\ell/\rho > 1.5$. Therefore, the limit case $K^{(1)}$ is appropriate to represent

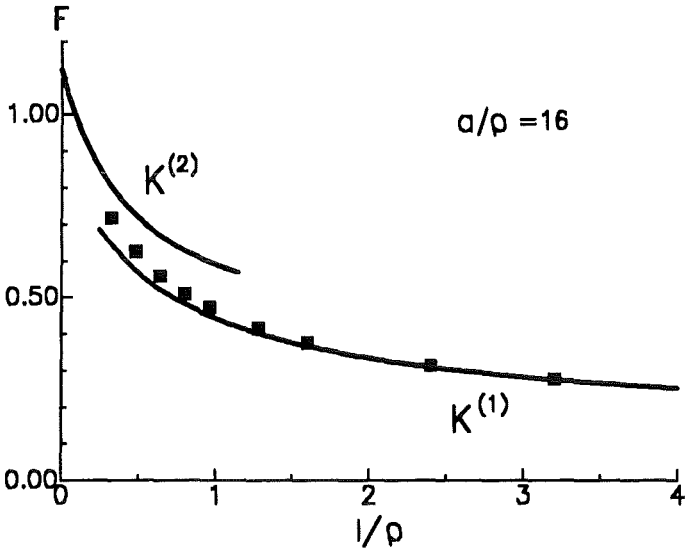

Figure 52. Limit cases. Comparison of limit-case solutions with numerical data of Newman [48] for $a/\rho = 16$

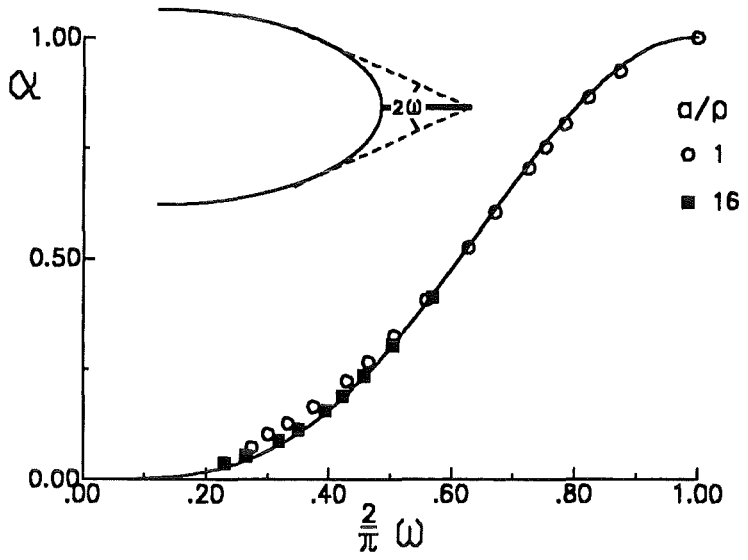

Figure 53. Interpolation of limit cases. Interpolation factor α as a function of the "view angle" ω.

the stress intensity factors for $\ell/\rho > 1.5$. This asymptotic agreement leads to an interpolation formula

$$K = \alpha K^{(2)} + (1-\alpha)K^{(1)} \tag{3.9.11}$$

In order to characterise the notch-crack-configuration, we introduce a "view angle" ω as illustrated in fig.53. The crack-tip "sees" the notch under the total angle 2ω. The angle ω results from simple geometry-related considerations and is given as the solution of the implicit equation

$$\frac{a}{b}\tan\omega\left[\frac{a}{b}\tan\omega - \left(1+\frac{\ell}{a}\right)\sqrt{1+\left(\frac{a}{b}\tan\omega\right)^2}\right]+1=0 \tag{3.9.12}$$

In fig.53 the interpolation factor α is plotted versus ω. The resulting dependency can be approximated by the simple expression

$$\alpha \simeq \sin^{7/2}\omega \tag{3.9.13}$$

which is plotted as solid line in fig.53.

3.9.1.2 Limit cases for the weight function

The comparison of the weight function data of fig.49 with the two limit cases leads to an interpolation factor β defined by

$$h = \beta h^{(2)} + (1-\beta)h^{(1)} \tag{3.9.14}$$

where $h^{(2)}$ is the weight function for an edge crack and $h^{(1)}$ is the value for an internal crack according to eq.(3.9.7). It becomes obvious from fig.49 that - in contrast to the interpolation factor α for stress intensity factors - β must also depend on x/ℓ. If we ignore this fact and substitute α for β, we obtain the predicted weight functions represented in fig.54. The comparison between the

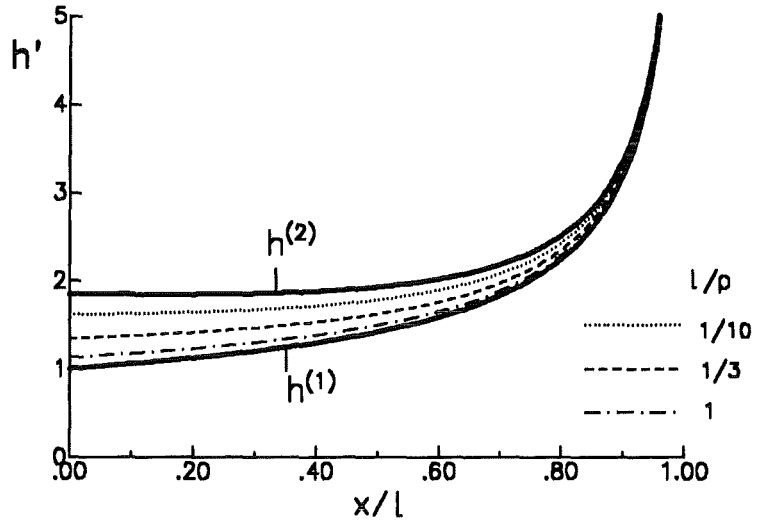

Figure 54. Interpolation of limit cases. Normalised weight function for cracks in front of an internal elliptical notch: $h' = h\sqrt{\pi\ell/2}$ for $a/\rho = 16$; solid lines: limit cases $h^{(1)}$, $h^{(2)}$; broken lines: interpolated with eq.(3.9.14) ($\beta = \alpha$).

weight function of fig.49 and the interpolations of fig.54 shows that the maximum deviations are of about 3%. This accuracy is sufficient in most practical cases.

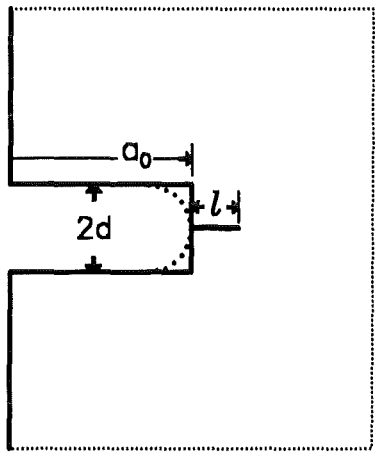

Figure 55. Edge notch. A notch in a specimen with a small crack at the notch tip.

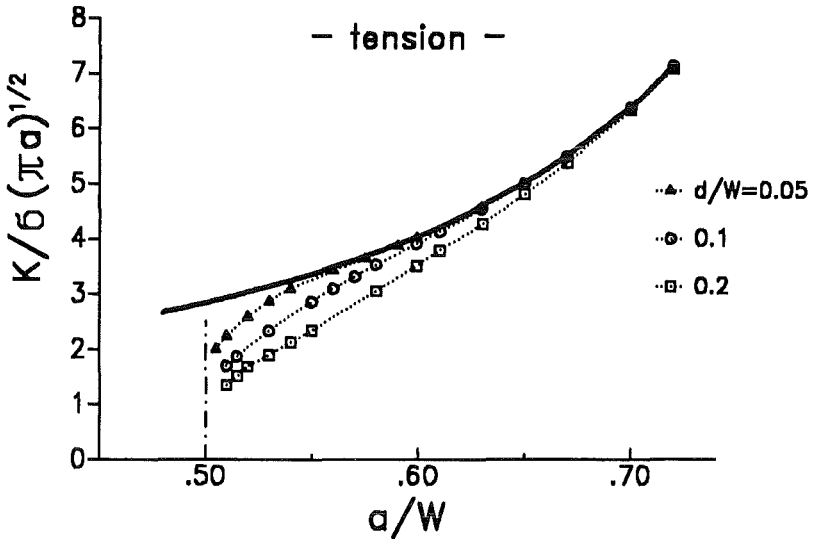

Figure 56. Rectangular edge notch. Stress intensity factor for cracks at the tip of a rectangular notch under tensile load ($a_0/W = 0.5$).

3.9.2 External notches

An external notch in a body is shown in fig.55. Its length is a_0 and the notch width is $2d$. A small one-dimensional crack of length ℓ is placed at the notch root. Such notch-crack configurations are often used in fracture-toughness testing of ceramic materials to approximate naturally sharp cracks. During the saw procedure small cracks are generated at the notch root. The real geometry of a saw-cut can be approximated by the two limit cases of a rectangular notch profile and a circular notch. Notches prepared with thick saw blades tend to adopt a more rectangular shape

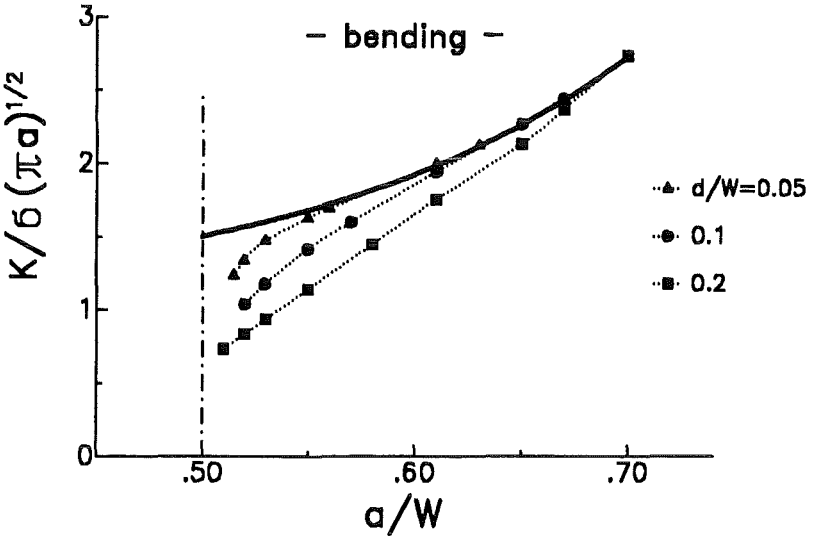

Figure 57. Rectangular edge notch. Stress intensity factor for cracks at the tip of a rectangular notch under bending load ($a_0/W = 0.5$).

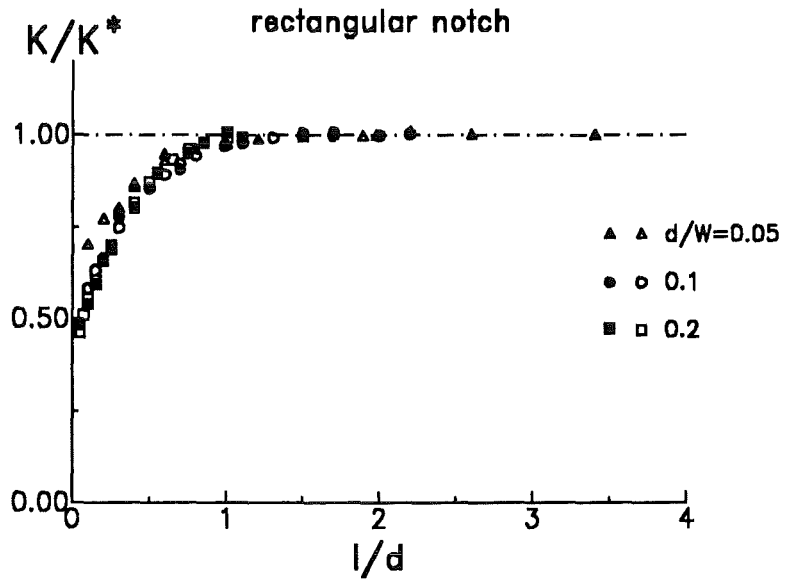

Figure 58. Rectangular edge notch. Normalised stress intensity factors for cracks in front of a rectangular notch under tensile load (open symbols) and bending load (solid symbols) ($a_0/W = 0.5$).

and thin saw blades a more circular shape. The two limit cases will be considered below. Calculations with the BCM were carried out with the geometric data $a_0/W = 0.5$ and $H/W = 1$. Figure 56 is a normalised representation of the resulting stress intensity factors for the rectangular notch under tensile load for different values of the relative total crack length a/W and relative notch width d/W. The solid line is the result for a crack of length $a_0 + \ell$ without notch obtained by application of the same Boundary Collocation procedure. In fig.57 shows the stress intensity factors for the bending-load case. Finally, fig.58 shows the ratio of the stress intensity factor for

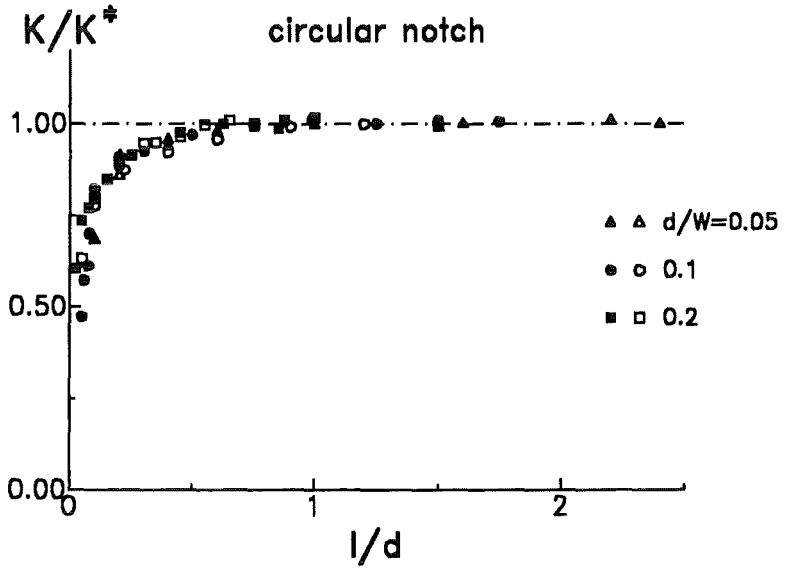

Figure 59. Semi-circular edge notch. Normalised stress intensity factors for cracks in front of a semi-circular notch under tensile load (open symbols) and bending load (solid symbols) ($a_0/W = 0.5$).

the notch/crack- configuration to the stress intensity factor K^* - representing a crack of the same total length under the same load

$$K_I^* = \sigma\sqrt{\pi a}\, F \tag{3.9.15}$$

(F = geometric function) - as a function of the ratio ℓ/d. The ratio of stress intensity factors attains the value $K_I/K^* = 1$ at about $\ell/d = 1$. This is independent of the load case chosen.
The results for the circular notch are plotted in normalised representation in fig.59. The following consequences are obvious:

- The stress intensity factor of the crack/notch-configuration increases monotonically with crack extension.
- The stress intensity factor for the crack of length $a_0 + \ell$ is an upper limit for the crack at the notch root. It is obvious that an "overshooting effect" as observed for cracks in front of internal elliptical notches (fig.48) can hardly be detected for the geometries investigated.
- For cracks with a length greater than the notch radius ($\ell > d$) the crack/notch-configuration can be replaced by a crack of total length $a_0 + \ell$.
- For a semi-circular notch the short-crack solution equals the long-crack solution earlier than for a rectangular notch.

The stress intensity factors for the circular notch (fig.59) can be expressed by

$$K/K^* \simeq \tanh\left(3\sqrt{\ell/d}\right) \tag{3.9.16}$$

for $a_0/W = 0.5$ and $0.05 \leq d/W \leq 0.2$. This dependency is entered in fig.60 as a solid curve.
Similar calculations as shown for $a_0/W = 0.5$ were performed also for $a_0/W = 0.30$ and 0.70. The final results are represented in fig.61. The results obtained for the relatively wide notches investigated by BCM can be fitted as in eq.(3.9.16) by

$$K/K^* = \tanh\left(\gamma\sqrt{\ell/d}\right) \tag{3.9.17}$$

with

$$\gamma \simeq \begin{cases} 3.7 & \text{for} \quad a_0/W = 0.3 \\ 3.0 & \text{for} \quad a_0/W = 0.5 \\ 2.3 & \text{for} \quad a_0/W = 0.7 \end{cases} \tag{3.9.18}$$

i.e. the value of γ decreases with the relative width d/a_0 of the notch. A theoretical lower limit of γ for $d/a_0 \to 0$ is $\gamma = 2.243$ as will be shown below.

3.9.2.1 Stress intensity factors for slender external notches

In case of very small cracks in front of a notch ($\ell/d \to 0$) the stress intensity factor is given by

$$K = \sigma_{max} 1.1215\sqrt{\pi\ell} \tag{3.9.19}$$

where σ_{max} is the maximum stress at the root of the notch. This maximum stress is available only for special notch problems. One of them is the slender notch with $d/a_0 \ll 1$.

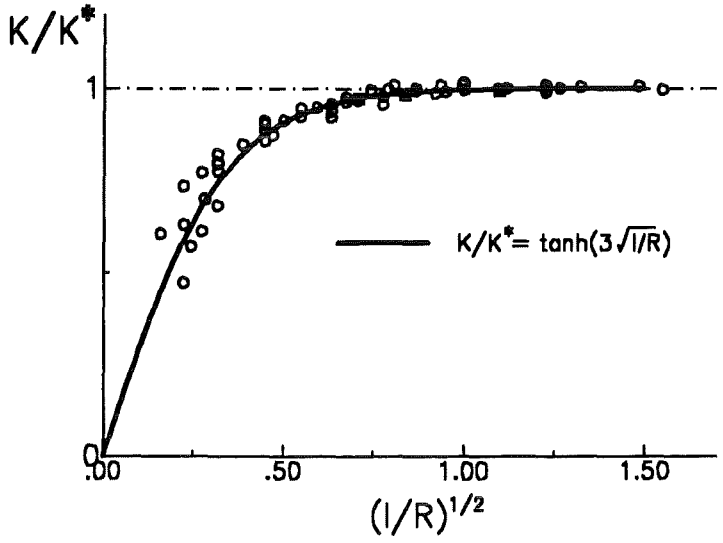

Figure 60. Semi-circular edge notch. Normalised stress intensity factors for cracks in front of a semi-circular notch ($R = d$).

Stresses in front of a slender edge notch A simple means of to determining the stresses in front of a slender notch is given by the procedure of Creager and Paris [61] according to which the stresses in front of a slender notch of length a_0 with radius R can be derived from the stress intensity factor of a crack with the same length. They calculated the stress distribution for arbitrarily loaded notches using the corresponding crack solution $K(a_0)$.

$$\sigma_y\Big|_{y=0} = \frac{K(a_0)}{\sqrt{\pi R z}}\left(1+\frac{1}{z}\right) \quad , \quad z = 1 + 2x/R \tag{3.9.20}$$

This relation describes fairly well the near notch-tip behaviour of slender notches ($R/a \to 0$). Equation (3.9.20) is a good approximation of the stress field for $\ell/d < 1$. Additional terms for a higher order representation (which describes also the far stress field

$$\sigma_y\Big|_{y=0} = \frac{K(a_0)}{\sqrt{\pi R z}}\left(1+\frac{C_1}{z}+\frac{C_2}{z^2}+\frac{1-C_1-C_2}{z^3}\right) \tag{3.9.21}$$

can be obtained from the equilibrium conditions

$$\int_{a_0}^{W} \sigma_y\, dx = \begin{cases} \sigma_0 W & \textit{for tension} \\ 0 & \textit{for bending} \end{cases} \tag{3.9.22}$$

and

$$\int_{a_0}^{W} \sigma_y\left(x-\frac{W}{2}\right) dx = \begin{cases} 0 & \textit{for tension} \\ M_b & \textit{for bending} \end{cases} \tag{3.9.23}$$

where M_b denotes the externally applied bending moment. For $\ell < d$ we can restrict the stress analysis to eq.(3.9.20). The maximum stress ($x = 0$) then results

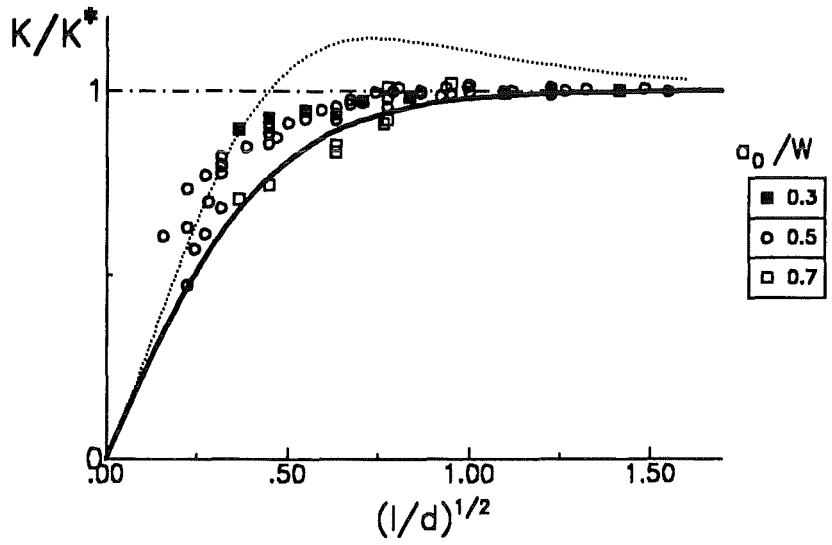

Figure 61. Semi-circular edge notch. Normalised stress intensity factors for cracks in front of a semi-circular notch ($R = d$); solid line: eq.(3.9.27), dotted line: eq.(3.9.29).

$$\sigma_{max} = \frac{2K(a_0)}{\sqrt{\pi R}} \tag{3.9.24}$$

Stress intensity factors: The stress intensity factor for $\ell \ll R$ reads

$$K = 1.1215\sqrt{\ell/R}\, 2K(a_0) \tag{3.9.25}$$

Consequently, we obtain

$$K/K^* = 2.243\sqrt{\ell/R} \tag{3.9.26}$$

It is important that eq.(3.9.26) is independent of the type of the external load and is valid for tension as well as for bending. Taking into consideration the long-crack behaviour ($K/K^* \to 1$ for large ℓ/W) one may assume for the total dependency

$$K/K^* \simeq \tanh\left(2.243\sqrt{\ell/R}\right) \tag{3.9.27}$$

Equation (3.9.27) is additionally plotted as a solid line in fig.61. Since in the special case of slender notches the two limit stress intensity factors are known, namely $K^{(1)}/K^* = 1$ and $K^{(2)}/K^*$, one can check the applicability of the interpolation formula, eq.(3.9.11), for external notches with cylindrical notch roots.
A simple consideration of geometry gives the "view angle"

$$\omega = \arcsin\left(\frac{d}{d+\ell}\right) \tag{3.9.28}$$

The prediction resulting from eqs.(3.9.11) and (3.9.13)

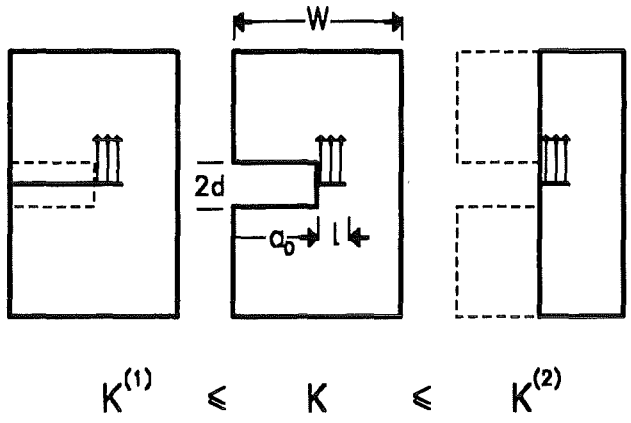

Figure 62. Limit cases for edge notches. Definition of the two limit stress intensity factors $K^{(1)}$ and $K^{(2)}$.

$$\frac{K_\omega}{K^*} = 1 - \frac{1 - 2.243\sqrt{\ell/d}}{(1+\ell/d)^{7/2}} \tag{3.9.29}$$

is plotted in fig.61 as a dotted line. The "overshooting effect" predicted by the interpolation procedure is in reality much less pronounced or completely absent.
In this context, one should keep in mind that the stress distribution given by eq.(3.9.20) is only an approximative one.

3.9.2.2 Limit cases for stress intensity factors of cracks in front of external notches

Similar to the treatment for internal notches, two limit stress intensity factors can be identified also for external notches as illustrated in fig.62. In fig.62 $K^{(1)}$ corresponds to the partially loaded edge-crack of length $a_0 + \ell$, and $K^{(2)}$ is the stress intensity factor of an edge-crack of length ℓ in a body of reduced thickness W' ($W' = W - a_0$). Both limit cases are shown in fig.63 in terms of the geometric function F defined by

$$F = \frac{K}{\sigma\sqrt{\pi\ell}} \tag{3.9.30}$$

For first rough estimations it may be recommended to describe the stress intensity factor by the mean value of the limit-case solutions resulting in deviations less than 10% for $\ell = a - a_0 > 0.02W$.
On the basis of fig.63 an interpolation function α can be introduced for edge notches, too. In order to decide whether or not the interpolation factor α determined for internal notches, eq.(3.9.11), is also appropriate for strongly deviating conditions, BCM-computations were performed for

- external notches with
- rectangular notch roots exposed to
- constant crack surface loading.

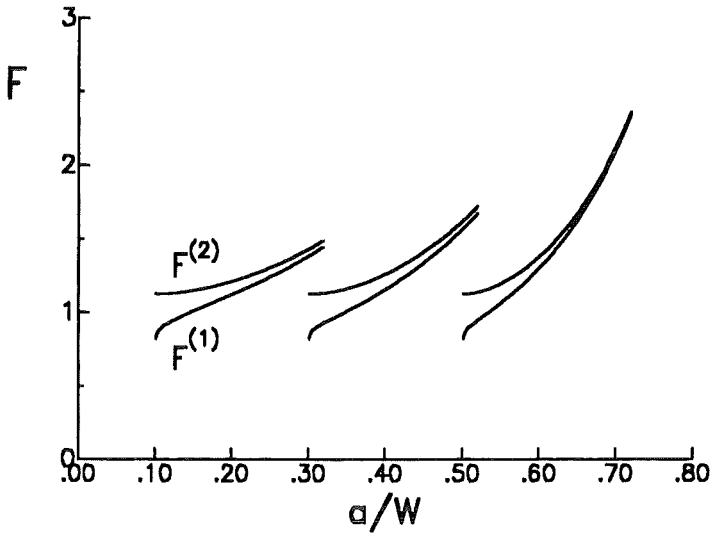

Figure 63. Limit cases for edge notches. Limit stress intensity factors $K^{(1)}$ and $K^{(2)}$ for different notch depths.

Figure 66 shows the geometric function F, defined by eq.(3.9.30), for a rectangular edge notch with $a_0/W=0.5$ and $d/W=0.2$. The circles represent results obtained with the Boundary Collocation Method. The solid lines correspond to the limit cases $K^{(1)}, K^{(2)}$, and the dotted line is calculated with the interpolation factor α according to eqs.(3.9.11) and (3.9.13). For elliptical notches the "view angle" ω was defined by the tangents running from the crack tip to the ellipse of the notch. Since in the present case no ellipse is considered but a rectangular notch, we can introduce two extremal estimates for ω. In fig.64 the angle between the corners of the notch root is the maximum possible value expressed as

$$\omega_{max} = arctan\left(\frac{d}{\ell}\right) \tag{3.9.31}$$

A minimum view angle is defined by the radius $R = d$ of the root of an elliptical notch of width d, and its value is given by

$$\omega_{min} = arcsin\left(\frac{d}{d+\ell}\right) \tag{3.9.32}$$

The effective view angle is limited by

$$\omega_{min} < \omega < \omega_{max} \tag{3.9.33}$$

The results for the limit values ω_{min} and ω_{max} are also entered in fig.65. The agreement between predicted and numerically computed data is sufficient. The deviations between predicted and numerically determined stress intensity factors is less than 2%.

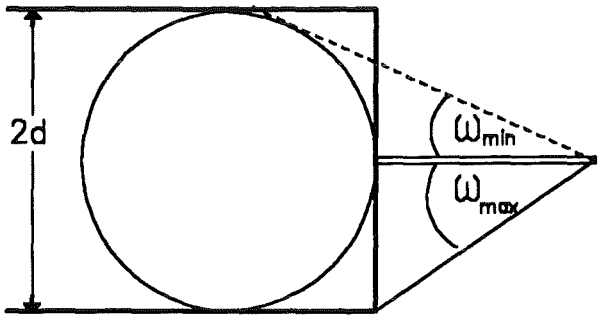

Figure 64. Limit cases. Limit cases for the "view angle" ω and a rectangular edge notch.

3.9.2.3 Weight function for cracks in front of external notches

Limit cases: Similar to the treatment of cracks in front of internal notches the limit cases of the weight functions were also determined for cracks in front of external notches. The lower limit case of the weight function $h^{(1)}$ is identical with that of an edge crack of total length $a = a_0 + \ell$

$$h^{(1)} = h_{edge}\left(\frac{x + a_0}{\ell + a_0}, \frac{\ell + a_0}{W} \right) \tag{3.9.34}$$

The upper limit case corresponds to an edge-crack of length ℓ in a body of reduced width $W' = W - a_0$

$$h^{(2)} = h_{edge}\left(\frac{x}{\ell}, \frac{\ell}{W - a_0} \right) \tag{3.9.35}$$

These two limit cases are plotted in fig.66 for $a_0/W = 0.5$ and $\ell/W = 0.1$ and 0.2. In fig.66 also the interpolated weight functions determined by

$$h = \alpha h^{(2)} + (1 - \alpha) h^{(1)} \quad , \quad \alpha = \sin^{7/2}(\omega) \tag{3.9.36}$$

and ω determined by eq.(3.9.28), are entered.

Weight function for slender notches: In order to be able to check the accuracy of the interpolation formula and of the procedure of determination of the weight function from stress intensity factors described in Section 1.2, the stress distribution in front of the notch root must be known. Also in this analysis the stresses given by eq.(3.9.20) were used.
Numerically obtained weight functions for $\ell/R = 0.25$ and 0.5 are entered as symbols in fig.67. The comparison between the numerical data and the interpolations of the limit cases (broken lines) shows maximum deviations of about 5%. These deviations should not be overrated since the stress distribution applied is only an approximation.

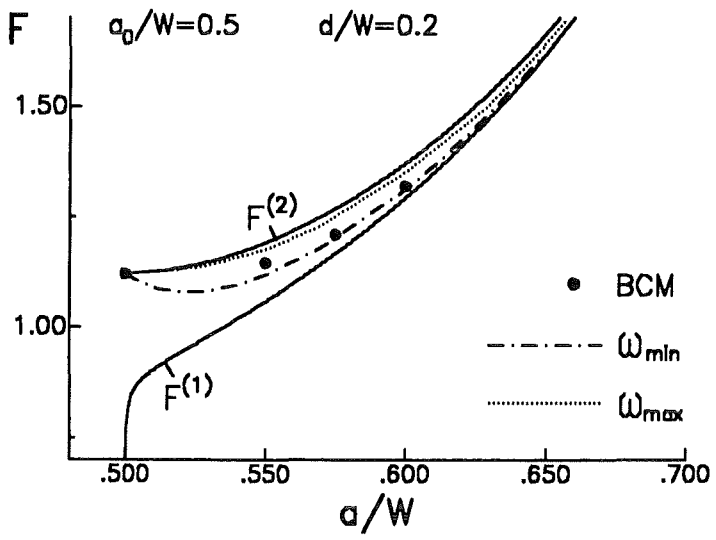

Figure 65. Limit cases. Geometric function for cracks in front of external rectangular notches; symbols: determined with the Boundary Collocation Method, solid lines: limit cases; dotted and dash-dotted lines: interpolation of the limit stress intensity factors using eq.(3.9.13) for two extremal view angles.

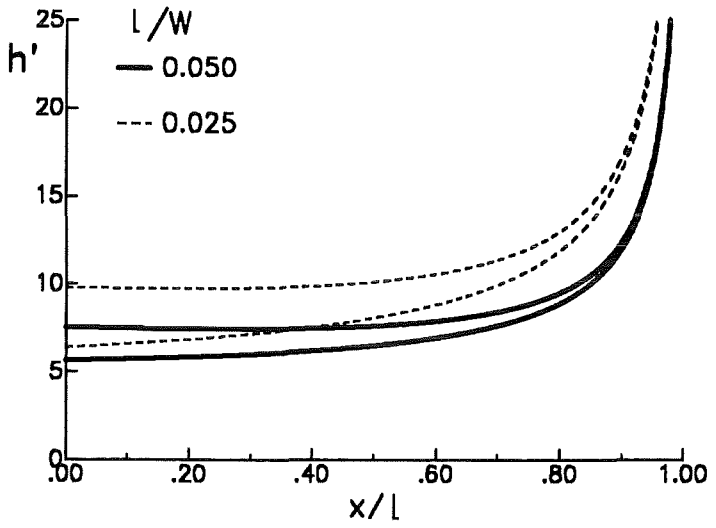

Figure 66. Limit cases. Limit cases of weight functions ($h' = h\sqrt{\pi\ell/2}$) for small cracks in front of an external notch with $a_0/W = 0.5$ (upper curves: $h^{(2)}$, lower curves: $h^{(1)}$).

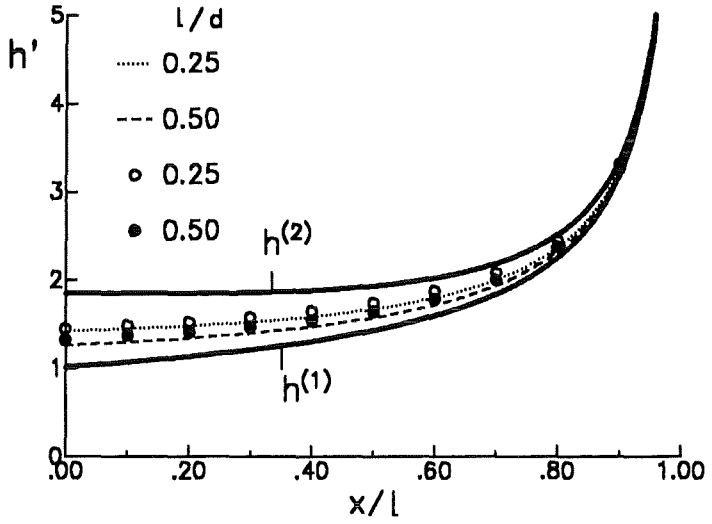

Figure 67. Limit cases. Limit cases, interpolations and numerical weight functions of weight functions for small cracks in front of an external notch ($a_0/W = 0.5$, $\ell/W = 0.0025$).

3.10 Weight function for remote tractions

The weight function for tractions, acting at an arbitrary location of the body, is given by eqs.(2.9.12) to (2.9.15). The cefficients were determined for a rectangular plate. Pure bending was considered as the reference loading case. BCM-computations were made with 180 collocation points at the outer boundary [27]. The geometry was chosen as $L/W=1.5$ and a total number of 90 coefficients A, A^* were used. In order to allow cubic interpolations to be made, the data were normalised according to

$$\tilde{A}_n = A_n (1-\alpha)^{\beta}/\sigma_{bend} \quad , \quad \alpha = a/W \tag{3.10.1}$$

$$\tilde{A^*}_n = A^*_n (1-\alpha)^{\beta}/\sigma_{bend} \tag{3.10.2}$$

The coefficient A_0 can be expressed by the geometric function F

$$A_0 = F\sqrt{\frac{\alpha}{18}}\,\sigma_{bend} \tag{3.10.3}$$

and the geometric function results from the BCM-computations as

$$F = \frac{1.1215 - 2.3652\alpha + 3.5129\alpha^2 - 2.750\alpha^3 + 0.855\alpha^4}{(1-\alpha)^{3/2}} \qquad \alpha \le 1 \tag{3.10.4}$$

An approximation by polynomials

Although the 90-coefficient solution of the stress function - and consequently of stresses, displacements and weight function - is very accurate, an approximative representation with a

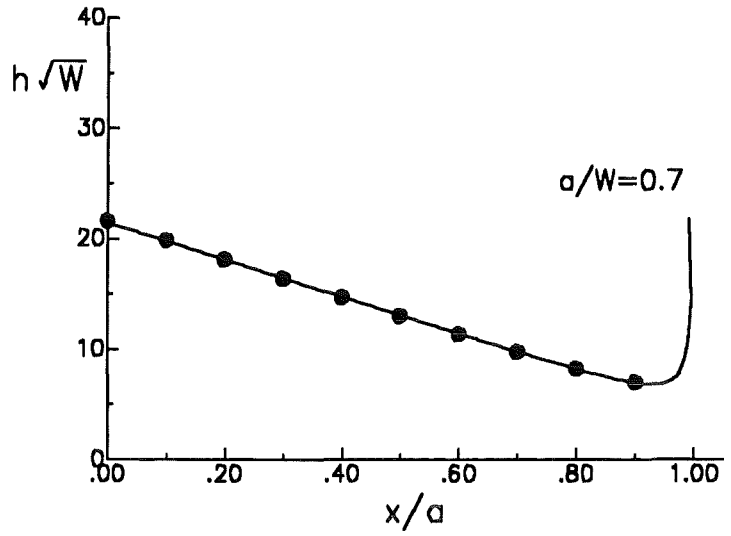

Figure 68. Crack-face weight function. Weight function approximation by a 20-terms polynomial for $\varphi = \pi$ compared with the crack-face weight function given in [27].

strongly reduced number of terms is desirable from the point of view of practical application. A polynomial was derived which describes the stress function in the surroundings of the crack. By a least-squares procedure in the region $0 < x < W$, $0 < y < 0.4\,W$ it was found

$$\Phi_s \simeq \sum_{n=0}^{9} r^{n+3/2} A_n \left[\cos(n+3/2)\varphi - \frac{n+3/2}{n-1/2} \cos(n-1/2)\varphi \right]$$

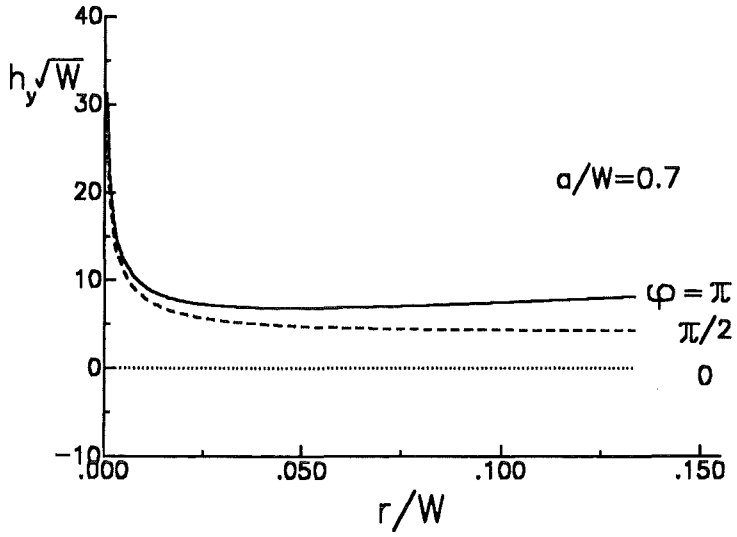

Figure 69. y-component. Weight function h_y for several angles φ.

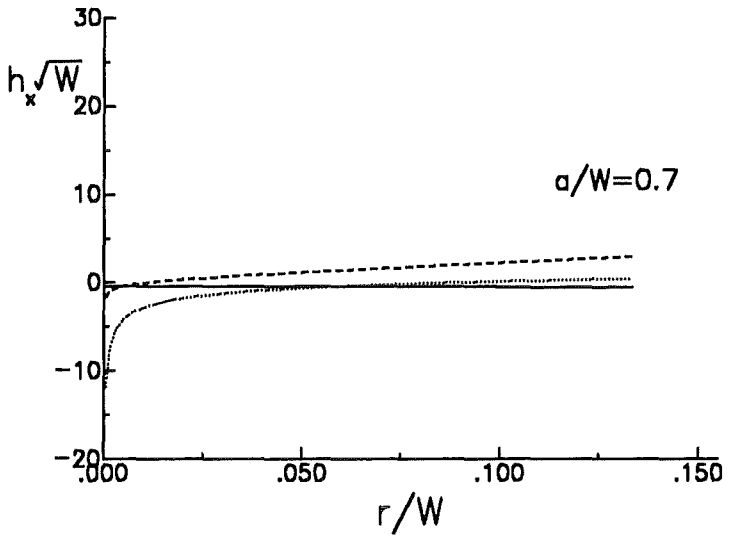

Figure 70. x-component. Weight function h_x for several angles φ (curves as in fig.5).

$$+ \sum_{n=0}^{9} r^{n+2} A_n^* [\cos(n+2)\varphi - \cos n\varphi] \qquad (3.10.5)$$

with the coefficients A_n, A_n^* listed in Table 28 and Table 29. The coefficients are normalised according to eqs.(3.10.1) and (3.10.2). Figure 68 shows the component h_y for a crack of normalised depth $\alpha = 0.6$ along the crack surface, i.e. $\varphi = \pi$ together with the crack face weight function.

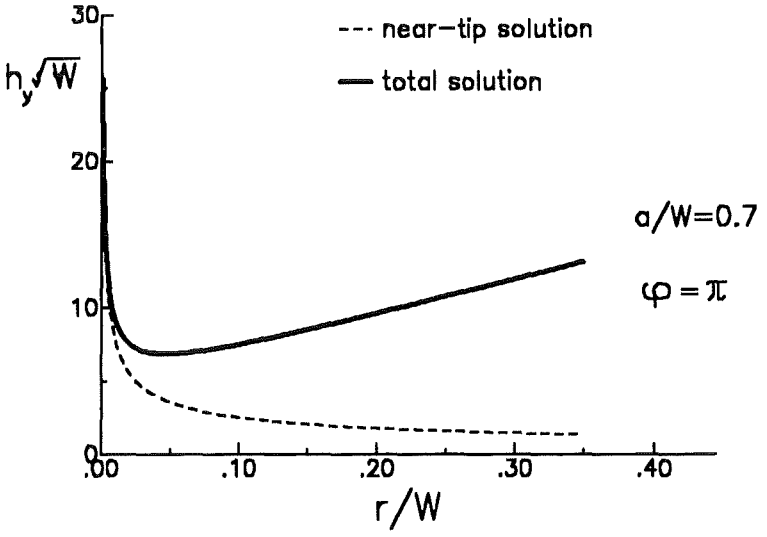

Figure 71. Comparison with the near-tip solution. Weight function h_x compared with the near-tip solution [12],[35].

The agreement is very good. The two components h_y and h_x are plotted in fig.69 and fig.70 along different straight lines, namely $\varphi = 0$, $\pi/2$, and π.

Comparison with the near-tip weight function

From the near-tip displacement field - related to the first term in eq.(2.9.6) - Tada et al. [12] derived a near-tip weight function, which for symmetrical loads reads

$$h_x = \frac{1}{\sqrt{2\pi r}\,(1-\nu)}\left[2\nu - 1 + \sin\left(\frac{\varphi}{2}\right)\sin\left(\frac{3}{2}\varphi\right)\right]\cos\left(\frac{1}{2}\varphi\right) \qquad (3.10.6)$$

$$h_y = \frac{1}{\sqrt{2\pi r}\,(1-\nu)}\left[2 - 2\nu - \cos\left(\frac{\varphi}{2}\right)\cos\left(\frac{3}{2}\varphi\right)\right]\sin\left(\frac{1}{2}\varphi\right) \qquad (3.10.7)$$

A comparison of this limit case with the total weight function is shown in fig.71 for $a/W = 0.7$. In this case the deviations become obvious (>10% for $r/W > 0.006$).

	n=0	1	2	3	4	5	6	7	8	9
α	$\beta = 1.5$	2.5	3.5	3.5	3.5	3.5	3.5	3.5	3.5	3.5
0.25	0.0829	0.0215	0.0533	0.0439	-0.152	0.2830	-0.203	-0.573	4.0130	1.7727
0.30	0.0850	0.0267	0.0448	0.0229	-0.074	0.1661	-0.169	-0.092	1.3618	0.5719
0.40	0.0873	0.0329	0.0320	0.0115	-0.004	0.0422	-0.046	0.1080	0.0102	-0.386
0.50	0.0882	0.0356	0.0245	0.0149	0.0168	0.0289	0.0175	0.0351	-0.027	-0.013
0.60	0.0884	0.0366	0.0209	0.0227	0.0334	0.0474	0.0628	0.0874	0.0912	0.0669
0.65	0.0883	0.0367	0.0200	0.0276	0.0453	0.0718	0.1111	0.1600	0.1854	0.1300
0.70	0.0883	0.0367	0.0196	0.0338	0.0631	0.1147	0.1972	0.2719	0.2514	0.1229
0.75	0.0883	0.0367	0.0195	0.0419	0.0923	0.1910	0.3335	0.4077	0.2831	0.0796
0.80	0.0884	0.0367	0.0197	0.0535	0.1386	0.3058	0.5152	0.5868	0.3903	0.1148
0.85	0.0897	0.0381	0.0208	0.0694	0.1934	0.4198	0.6598	0.6837	0.4087	0.1052
0.90	0.0919	0.0409	0.0206	0.0800	0.2272	0.4622	0.6465	0.5762	0.2837	0.0524

Table 28. . Coefficients $\tilde{B}_n$ for a 20-terms polynomial representation.

	n=0	1	2	3	4	5	6	7	8	9
α	$\beta = 2$	3	4	4	4	4	4	4	4	4
0.25	0.02300	-0.0370	-0.0922	0.09128	0.00272	-0.3372	0.96039	-1.6678	-4.3971	-0.2444
0.30	0.00967	-0.0425	-0.0586	0.05902	-0.0383	-0.0982	0.35271	-0.6572	-1.3918	-0.0750
0.40	-0.0109	-0.0423	-0.0248	0.01192	-0.0262	0.00452	0.00300	-0.1321	0.21273	0.1835
0.50	-0.0248	-0.0361	-0.0147	-0.0061	-0.0194	-0.0134	-0.0210	-0.0061	0.03872	0.0005
0.60	-0.0333	-0.0298	-0.0125	-0.0155	-0.0254	-0.0331	-0.0483	-0.0589	-0.0507	-0.0181
0.65	-0.0359	-0.0275	-0.0126	-0.0197	-0.0336	-0.0529	-0.0823	-0.1087	-0.0989	-0.0306
0.70	-0.0377	-0.0259	-0.0130	-0.0247	-0.0473	-0.0875	-0.1412	-0.1648	-0.1159	-0.0297
0.75	-0.0387	-0.0249	-0.0135	-0.0312	-0.0701	-0.1400	-0.2131	-0.2064	-0.1060	-0.0212

0.80	-0.0395	-0.0248	-0.0143	-0.0406	-0.1013	-0.2005	-0.2823	-0.2515	-0.1207	-0.0214
0.85	-0.0436	-0.0291	-0.0167	-0.0531	-0.1326	-0.2477	-0.3223	-0.2668	-0.1227	-0.0232
0.90	-0.0556	-0.0361	-0.0165	-0.0544	-0.1299	-0.2202	-0.2540	-0.1860	-0.0773	-0.0149

Table 29. . Coefficients B^*_n for a 20-terms polynomial representation.

Whereas an exact solution for the weight function in the near-tip limit exists for finite cracks in finite bodies only numerical solutions are generally available. Most of them are crack-face weight functions which are restricted to $\varphi = 0$. For cracks in finite plates and bars a weight function is

$$h_y = \frac{1}{\sqrt{2\pi r}\,(1-\nu)}\left[2 - 2\nu - \cos\left(\frac{\varphi}{2}\right)\cos\left(\frac{3}{2}\varphi\right)\right]\sin\left(\frac{1}{2}\varphi\right) + g_x(a/W, \varphi, r/W) \quad (3.10.8)$$

$$h_x = \frac{1}{\sqrt{2\pi r}\,(1-\nu)}\left[2\nu - 1 + \sin\left(\frac{\varphi}{2}\right)\sin\left(\frac{3}{2}\varphi\right)\right]\cos\left(\frac{1}{2}\varphi\right) + g_y(a/W, \varphi, r/W) \quad (3.10.9)$$

with the functions g_x, g_y entered in the following tables.

r/W	$\varphi/\pi = 0$	0.2	0.4	0.6	0.8	1.0
0.0001	-0.0944	-0.0966	-0.1004	-0.0993	-0.0893	-0.0722
0.001	-0.1425	-0.1495	-0.1613	-0.1577	-0.1257	-0.0716
0.01	-0.2975	-0.3203	-0.3580	-0.3456	-0.2409	-0.0652
0.1	-0.7812	-0.8900	-1.0805	-1.0702	-0.6800	0.0002

Table 30. Weight function. $g_x(a/W, \varphi, a/W) \cdot \sqrt{W}$ according to eq.(3.10.8) for $a/W = 0.3$, $\nu = 0.2$.

r/W	$\varphi/\pi = 0$	0.2	0.4	0.6	0.8	1.0
0.0001	0.0603	0.0577	0.0534	0.0546	0.0661	0.0858
0.001	0.0051	-0.0030	-0.0167	-0.0128	0.0239	0.0862
0.01	-0.1707	-0.1975	-0.2426	-0.2304	-0.1113	0.0908
0.1	-0.7007	-0.8345	-1.0718	-1.0762	-0.6410	0.1322

Table 31. Weight function. $g_x(a/W, r/W, \varphi) \cdot \sqrt{W}$ according to eq.(3.10.8) for $a/W = 0.4$, $\nu = 0.2$.

r/W	$\varphi/\pi = 0$	0.2	0.4	0.6	0.8	1.0
0.0001	0.1814	0.1783	0.1731	0.1745	0.1883	0.2119
0.001	0.1153	0.1055	0.0891	0.0937	0.1377	0.2124
0.01	-0.0943	-0.1270	-0.1821	-0.1683	-0.0257	0.2173
0.1	-0.7119	-0.8874	-1.1999	-1.2209	-0.6928	0.2591

Table 32. Weight function. $g_x(a/W, \varphi, a/W) \cdot \sqrt{W}$ according to eq.(3.10.8) for $a/W = 0.5$, $\nu = 0.2$.

r/W	$\varphi/\pi=0$	0.2	0.4	0.6	0.8	1.0
0.0001	0.2792	0.2754	0.2688	0.2706	0.2879	0.3174
0.001	0.1966	0.1843	0.1637	0.1695	0.2245	0.3181
0.01	-0.0654	-0.1069	-0.1774	-0.1608	0.0185	0.3247
0.1	-0.8167	-1.0654	-1.5075	-1.5544	-0.8689	0.3778

Table 33. Weight function. $g_x(a/W, \varphi, a/W) \cdot \sqrt{W}$ according to eq.(3.10.8) for $a/W=0.6$, $\nu=0.2$

r/W	$\varphi/\pi=0$	0.2	0.4	0.6	0.8	1.0
0.0001	0.3633	0.3581	0.3494	0.3518	0.3749	0.4143
0.001	0.2527	0.2363	0.2087	0.2165	0.2901	0.4153
0.01	-0.0969	-0.1539	-0.2510	-0.2303	0.0115	0.4256
0.1	-1.0568	-1.4584	-2.1640	-2.2657	-1.2890	0.5024

Table 34. Weight function. $g_x(a/W, \varphi, a/W) \cdot \sqrt{W}$ according to eq.(3.10.8) for $a/W=0.7$, $\nu=0.2$.

r/W	$\varphi/\pi=0$	0.2	0.4	0.6	0.8	1.0
0.0001	0.5621	0.5514	0.5334	0.5385	0.5866	0.6683
0.001	0.3311	0.2970	0.2401	0.2572	0.4116	0.6730
0.01	-0.4012	-0.5299	-0.7510	-0.7133	-0.1879	0.7167
0.1	-2.3063	-3.5897	-5.8873	-6.3491	-3.7863	0.9456

Table 35. Weight function. $g_x(a/W, \varphi, a/W) \cdot \sqrt{W}$ according to eq.(3.10.8) for $a/W=0.85$, $\nu=0.2$.

r/W	$\varphi/\pi=0$	0.2	0.4	0.6	0.8	1.0
0.0001	0.0000	-0.0091	-0.0235	-0.0429	-0.0604	-0.0676
0.001	0.0000	-0.0286	-0.0741	-0.1355	-0.1912	-0.2139
0.01	0.0000	-0.0883	-0.2321	-0.4287	-0.6080	-0.6816
0.1	0.0000	-0.2214	-0.6835	-1.3815	-2.0407	-2.3164

Table 36. Weight function. $g_y(a/W, \varphi, a/W) \cdot \sqrt{W}$ according to eq.(3.10.9) for $a/W=0.4$, $\nu=0.2$.

r/W	$\varphi/\pi=0$	0.2	0.4	0.6	0.8	1.0
0.0001	0.0000	-0.0109	-0.0281	-0.0513	-0.0724	-0.0810
0.001	0.0000	-0.0342	-0.0887	-0.1623	-0.2291	-0.2563
0.01	0.0000	-0.1055	-0.2779	-0.5140	-0.7295	-0.8178
0.1	0.0000	-0.2507	-0.8083	-1.6644	-2.4735	-2.8104

Table 37. Weight function. $g_y(a/W, \varphi, a/W) \cdot \sqrt{W}$ according to eq.(3.10.9) for $a/W=0.5$, $\nu=0.2$.

r/W	$\varphi/\pi=0$	0.2	0.4	0.6	0.8	1.0
0.0001	0.0000	-0.0136	-0.0352	-0.0642	-0.0906	-0.1013
0.001	0.0000	-0.0428	-0.1110	-0.2031	-0.2866	-0.3207

0.01	0.0000	-0.1312	-0.3469	-0.6434	-0.9145	-1.0257
0.1	0.0000	-0.2823	-0.9862	-2.0961	-3.1500	-3.5885

Table 38. Weight function. $g_y(a/W, \varphi, a/W) \cdot \sqrt{W}$ according to eq.(3.10.9) for $a/W = 0.6$, $\nu = 0.2$.

r/W	$\varphi/\pi = 0$	0.2	0.4	0.6	0.8	1.0
0.0001	0.0000	-0.0182	-0.0470	-0.0858	-0.1210	-0.1354
0.001	0.0000	-0.0571	-0.1482	-0.2713	-0.3831	-0.4287
0.01	0.0000	-0.1732	-0.4618	-0.8606	-1.2261	-1.3763
0.1	0.0000	-0.2990	-1.2571	-2.8306	-4.3318	-4.9561

Table 39. Weight function. $g_y(a/W, \varphi, a/W) \cdot \sqrt{W}$ according to eq.(3.10.9) for $a/W = 0.7$, $\nu = 0.2$.

r/W	$\varphi/\pi = 0$	0.2	0.4	0.6	0.8	1.0
0.0001	0.0000	-0.0376	-0.0973	-0.1778	-0.2508	-0.2805
0.001	0.0000	-0.1174	-0.3060	-0.5620	-0.7948	-0.8901
0.01	0.0000	-0.3376	-0.9365	-1.7885	-2.5779	-2.9056
0.1	0.0000	0.3378	-1.9803	-6.1359	-10.0379	-11.6461

Table 40. Weight function. $g_y(a/W, \varphi, a/W) \cdot \sqrt{W}$ according to eq.(3.10.9) for $a/W = 0.85$, $\nu = 0.2$.

r/W	$\varphi/\pi = 0$	0.2	0.4	0.6	0.8	1.0
0.0001	0.0000	-0.0079	-0.0203	-0.0372	-0.0524	-0.0586
0.001	0.0000	-0.0248	-0.0642	-0.1175	-0.1658	-0.1856
0.01	0.0000	-0.0763	-0.2009	-0.3713	-0.5270	-0.5912
0.1	0.0000	-0.1942	-0.5915	-1.1919	-1.7636	-2.0074

Table 41. Weight function. $g_y(a/W, \varphi, a/W) \cdot \sqrt{W}$ according to eq.(3.10.9) for $a/W = 0.3$, $\nu = 0.2$.

3.11 Weight function for internal cracks under remote tractions

The influence of remote tractions is taken into account for edge cracks in finite bodies in section 2.9. Here we consider the internal crack in an infinite body loaded with remote tractions. The most general loading case has been investigated by Isida [71] is illustrated in fig.72a. The stress intensity factor solution is given by

$$K_{I,A} + iK_{II,A} = \frac{1}{2(\kappa+1)\sqrt{\pi a}} \left[(Q - iP) \left\{ \kappa - 1 + \sqrt{r_A/r_B} \left(e^{i(\theta_A - \theta_B)/2} - \kappa e^{-i(\theta_A - \theta_B)/2} \right) \right\} + \right. \quad (3.11.1)$$

$$\left. + \frac{2y(P - iQ)}{\sqrt{r_A r_B}} \left\{ e^{-i(\theta_A + \theta_B)/2} - \frac{r_B}{r_A} e^{-i(3\theta_A - \theta_B)/2} + \frac{a}{r_A} e^{-i(3\theta_A + \theta_B)/2} \right\} \right]$$

where the subscript A refers to crack tip A. The quantity κ is defined as

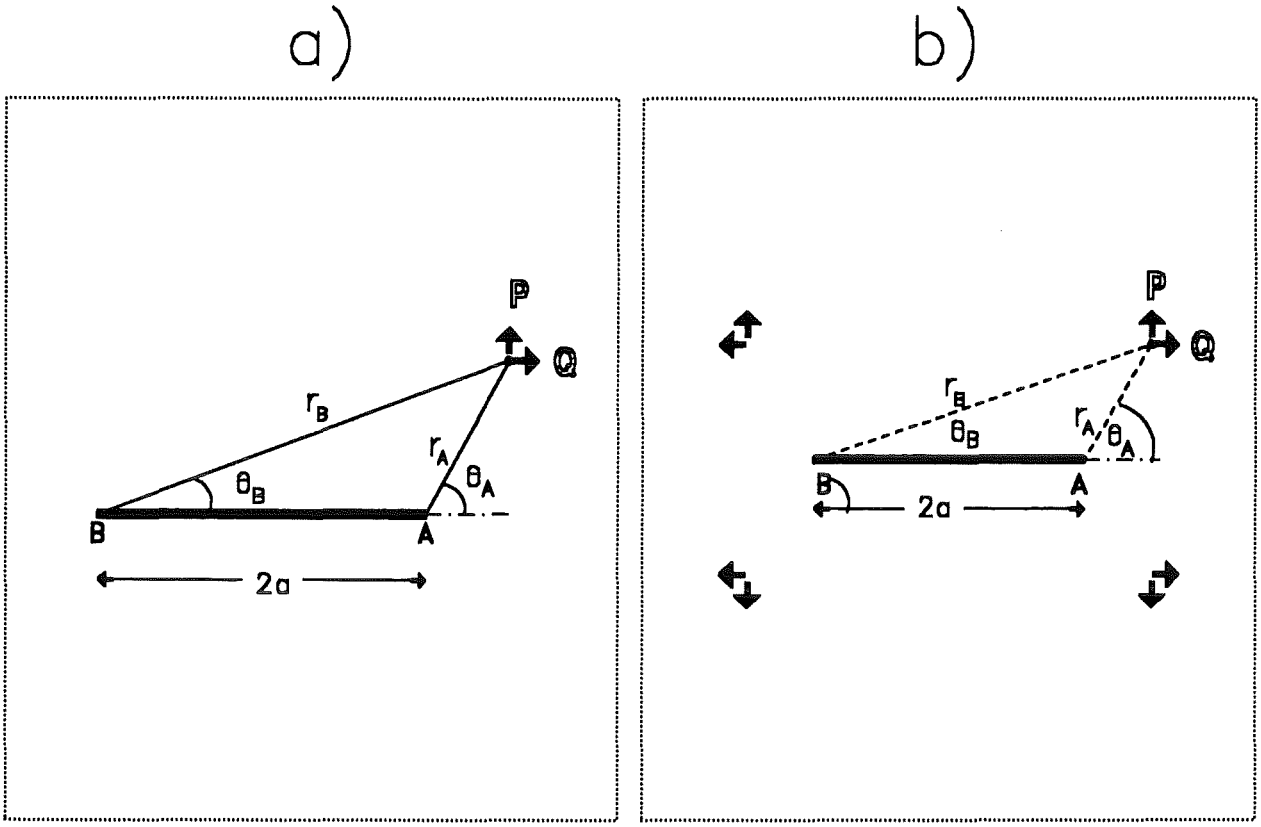

Figure 72. Internal crack. a) Internal crack in an infinite body loaded with remote tractions. b) Internal crack loaded symmetrically with remote tractions.

$$\kappa = \begin{cases} (3-\nu)/(1+\nu) & \text{for plane stress} \\ 3-4\nu & \text{for plane strain} \end{cases} \tag{3.11.2}$$

Based on this general result one can derive the weight function. For the case of symmetric loading (see fig.72b) we obtain the weight function for point A after some complex analysis as

$$\mathbf{h} = (h_x, h_y, 0)^T \tag{3.11.3}$$

with the components

$$h_x = \frac{1}{2\sqrt{\pi a}} \left\{ \frac{\kappa - 1}{\kappa + 1} \left(\sqrt{\frac{r_A}{r_B}} - \sqrt{\frac{r_B}{r_A}} \right) \cos \frac{\theta_A - \theta_B}{2} + \right. \tag{3.11.4}$$

$$\left. + \frac{2}{\kappa + 1} \sqrt{\frac{r_A}{r_B}} \sin \theta_A \left[\frac{r_B}{r_A} \sin \frac{3\theta_A - \theta_B}{2} - \frac{r_A}{r_B} \sin \frac{3\theta_B - \theta_A}{2} - \frac{a}{r_A} \sin \frac{3\theta_A + \theta_B}{2} \right] \right\}$$

$$h_y = \frac{1}{2\sqrt{\pi a}} \left\{ \left(\sqrt{\frac{r_B}{r_A}} + \sqrt{\frac{r_A}{r_B}} \right) \sin \frac{\theta_A - \theta_B}{2} + \right. \tag{3.11.5}$$

$$\left. + \frac{2}{\kappa + 1} \sqrt{\frac{r_A}{r_B}} \sin \theta_A \left[\frac{r_A - a}{r_B} \cos \frac{3\theta_B - \theta_A}{2} - \frac{r_B - a}{r_A} \cos \frac{3\theta_A - \theta_B}{2} \right] \right\}$$

$$h_y = \frac{1}{\sqrt{\pi a}} \left\{ \left(\sqrt{\frac{r_B}{r_A}} + \sqrt{\frac{r_A}{r_B}} \right) \sin \frac{\theta_A - \theta_B}{2} + \right. \tag{3.11.6}$$

$$\left. + \frac{2}{\kappa + 1} \sqrt{\frac{r_A}{r_B}} \sin \theta_A \left[\frac{r_A}{r_B} \cos \frac{3\theta_B - \theta_A}{2} - \frac{r_B}{r_A} \cos \frac{3\theta_A - \theta_B}{2} + \frac{a}{r_B} \cos \frac{3\theta_B + \theta_A}{2} + \frac{a}{r_A} \cos \frac{3\theta_A + \theta_B}{2} \right] \right\}$$

with

$$r_B = \sqrt{r_A^2 + 4a^2 + 4a r_A \cos \theta_A} \tag{3.11.7}$$

and the angle

$$\theta_B = \arccos \left(\frac{2a + r_A \cos \theta_A}{r_B} \right) \tag{3.11.8}$$

4. Mode-II and mixed-mode stress intensity factors and weight functions

4.1 Edge cracked plate under mode II loading

To be able to evaluate fracture-toughness measurements knowledge is required of the stress intensity factor solution applicable to the load case chosen. Besides in mode-I loading which had been studied thoroughly, the interest is growing in mode-II and mixed-mode loadings. Here, the continuous surface crack under constant shear loading τ_0 will be examined as the reference-load case for weight-function applications (s. fig.73)

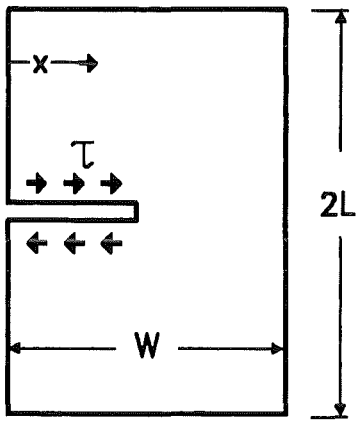

Figure 73. The edge crack in a plate under shear stresses

The geometric functions F_{II} obtained for the edge crack with constant shear stress loading on the crack faces were calculated with the Boundary Collocation Method [27]. For shear loading the geometric function is defined as

$$K_{II} = \tau\sqrt{\pi a}\, F_{II} \qquad (4.1.1)$$

The geometric functions F_{II} determined in [27] can be represented analytically by the relation

$$F_{II} = \frac{1.122 - 0.561a/W - 0.20(a/W)^2 + 0.89115(a/W)^3 - 0.42609(a/W)^4}{\sqrt{1 - a/W}} \tag{4.1.2}$$

Determination of the mode-II weight function The computation of stress intensity factors for cracks loaded by **shear stresses** can be performed using the weight function for mode-II loadings. If the stress distribution $\tau(x)$ acts on the crack surfaces of the one-dimensional crack, the mode-II stress intensity factor is expressed by

$$K_{II} = \tau^* \sqrt{\pi a}\, F = \int_0^a h_{II}(x,a)\tau(x)\, dx \tag{4.1.3}$$

where τ^* is a characteristic stress value of the stress distribution $\tau(x)$. The weight function h_{II} can be calculated by

$$h_{II}(x,a) = \frac{E'}{K_{IIr}} \frac{\partial}{\partial a} u_r(x,a) \tag{4.1.4}$$

from the crack opening displacements determined with the BC-method. Very accurate solutions are available for the limit cases $a/W \to 0$ and $a/W \to 1$ [12]. Together with these limit cases, the values of the weight function for discrete values of a/W and x/a (s. fig.73) have been entered in Table 42 in the normalised representation

$$h = \sqrt{\frac{2}{\pi a}} \frac{g(x/a, a/W)}{\sqrt{1 - x/a}\sqrt{1 - a/W}} \tag{4.1.5}$$

An analytical approximative representation for $a/W \leq 0.9$ can be described by

$$h = \sqrt{\frac{2}{\pi a}} \frac{1}{\sqrt{1 - x/a}\,(1 - a/W)^{1/2}} \left[\left(1 - \frac{a}{W}\right)^{1/2} + \sum A_{\nu\mu} (1 - x/a)^{\nu+1} \left(\frac{a}{W}\right)^{\mu} \right] \tag{4.1.6}$$

The related coefficients $A_{\nu\mu}$ are entered in Table 42.

a/W	x/a = 0.0	0.2	0.4	0.6	0.8	0.9	1.0
0.0	1.834	1.624	1.440	1.273	1.128	1.061	1.000
0.2	1.662	1.488	1.311	1.146	1.007	0.947	0.894
0.4	1.543	1.382	1.209	1.048	0.902	0.834	0.775
0.6	1.556	1.382	1.199	1.009	0.813	0.728	0.632
0.8	1.690	1.502	1.289	1.048	0.778	0.615	0.447
0.9	1.766	1.570	1.356	1.096	0.791	0.573	0.316
1.0	1.834	1.641	1.421	1.160	0.820	0.580	0.000

Table 42. Mode-II weight function. Normalised representation g(x/a,a/W) according to eq.(4.1.5).

	$\mu=0$	1	2	3
$\nu=0$	0.59250	0.08077	-2.93912	6.06686
1	0.15745	-1.83168	11.7816	-14.599
2	0.21108	2.8108	-14.701	15.329
3	-0.12416	-1.6465	6.69787	-6.15696

Table 43. Mode-II weight function. Coefficients of the weight function eq.(4.1.6).

Stress intensity factors for short plates The influence of the height H on the geometric function F_{II} is represented in Table 44. For small values of H/W (H/W≤0.4) and a/W<0.8 a simple relation becomes obvious when the F_{II}-data are plotted versus a/H. A unique relation is obtained which can be described by the simple relation

$$F_{II} \simeq \left[1.684(a/H)^2 + 1.1215^4\right]^{1/4} \tag{4.1.7}$$

H/W	a/W=0.1	0.2	0.3	0.4	0.5	0.7	0.9
0.025	2.369	3.272	3.977	4.582	5.092	6.022	6.826
0.05	1.762	2.373	2.858	3.272	3.644	4.292	4.845
0.1	1.366	1.763	2.090	2.375	2.629	3.075	3.479
0.2	1.172	1.366	1.575	1.763	1.934	2.237	2.772
0.4	1.122	1.174	1.261	1.366	1.474	1.707	2.611
0.5			1.205	1.282	1.371	1.615	
0.6			1.174	1.232	1.309	1.567	
0.75			1.152	1.194	1.262	1.536	

Table 44. Geometric function for the short plate

4.2 Mixed-mode stress intensity factors in 3-point bending

The mode-II fracture toughness of brittle materials as well as considerations of failure under mixed-mode loading are of increasing interest. In [62] and [63] stress intensity factors were determined by the Boundary Collocations Method and by FE-calculations.
The weight-function method can be successfully applied to determine the geometric functions F_I , F_{II} defined by

$$K_I = \sigma_0 F_I \sqrt{\pi a} \quad , \quad K_{II} = \sigma_0 F_{II} \sqrt{\pi a} \quad , \quad \sigma_0 = \frac{3}{2} \frac{PL}{W^2 B} \tag{4.2.1}$$

The symmetrically supported 3-point bending bar, fig.74, was studied by Filon [66] who derived an analytical solution for the stress state. This solution takes into consideration the stress magnification due to the line contacts of the rollers.
The mode-I and mode-II stress intensity factors were calculated by use of the mode-I and mode-II weight functions given in [27]. The results are expressed by the normalised geometric functions $F'_I = F_I(1-\alpha)^{3/2}$ and $F'_{II} = F_{II}(1-\alpha)^{1/2}$ and compiled in Table 45 to Table 50.

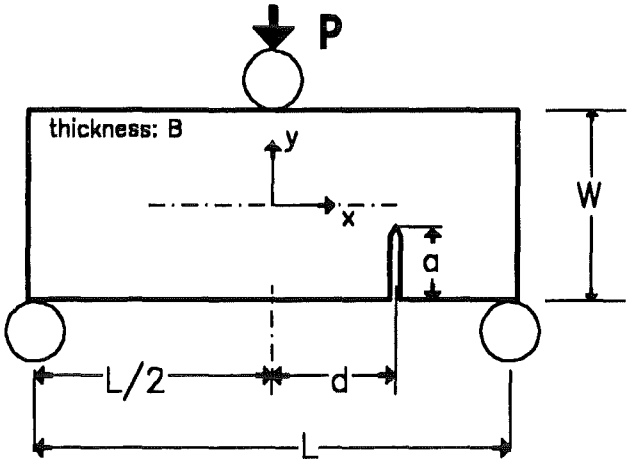

Figure 74. Geometric data of the asymmetrically notched bending bar.

	2d/L=0.	0.2	0.4	0.6	0.7	0.8	0.9
α=0.	1.0426	0.9757	0.8171	0.6462	0.5747	0.5348	0.5692
0.1	0.8067	0.7560	0.6292	0.4663	0.3647	0.2089	-0.1222
0.2	0.6583	0.6145	0.5032	0.3521	0.2564	0.1345	-0.0011
0.3	0.5655	0.5240	0.4210	0.2864	0.2094	0.1274	0.0497
0.4	0.5065	0.4648	0.3664	0.2468	0.1837	0.1206	0.0601
0.5	0.4674	0.4235	0.3276	0.2194	0.1648	0.1106	0.0584
0.6	0.4390	0.3911	0.2972	0.1982	0.1490	0.1005	0.0521
0.7	0.4164	0.3627	0.2719	0.1809	0.1359	0.0911	0.0467
0.8	0.3977	0.3362	0.2510	0.1672	0.1254	0.0837	0.0421

Table 45. Normalised geometric function for mode-I at L/W=2

	2d/L=0.2	0.4	0.6	0.7	0.8	0.9
α=0.1	0.0320	0.0481	0.0529	0.0642	0.1164	0.3687
0.2	0.0557	0.0868	0.1069	0.1359	0.2146	0.3893
0.3	0.0743	0.1167	0.1453	0.1750	0.2315	0.3093
0.4	0.0899	0.1378	0.1649	0.1858	0.2172	0.2522
0.5	0.1041	0.1513	0.1709	0.1825	0.1979	0.2116
0.6	0.1183	0.1585	0.1689	0.1740	0.1802	0.1841
0.7	0.1333	0.1598	0.1628	0.1641	0.1660	0.1662
0.8	0.1462	0.1551	0.1545	0.1546	0.1549	0.1534

Table 46. Normalised geometric function for mode-II at L/W=2

	2d/L=0.2	0.4	0.6	0.7	0.8	0.9
$\alpha=0$	0.9450	0.7187	0.5058	0.4223	0.3596	0.3466
0.1	0.7480	0.5750	0.3998	0.3188	0.2267	0.0397
0.2	0.6179	0.4755	0.3252	0.2496	0.1604	0.0344
0.3	0.5315	0.4067	0.2745	0.2070	0.1331	0.0533
0.4	0.4720	0.3581	0.2398	0.1801	0.1187	0.0571
0.5	0.4280	0.3220	0.2148	0.1615	0.1079	0.0547
0.6	0.3924	0.2935	0.1956	0.1470	0.0986	0.0504
0.7	0.3615	0.2700	0.1799	0.1351	0.0904	0.0458
0.8	0.3348	0.2506	0.1670	0.1253	0.0836	0.0419

Table 47. Normalised geometric function for mode-I at L/W=3

	2d/L=0.2	0.4	0.6	0.7	0.8	0.9
$\alpha=0.1$	0.0328	0.0406	0.0348	0.0324	0.0402	0.1282
0.2	0.0553	0.0696	0.0638	0.0649	0.0871	0.1912
0.3	0.0712	0.0895	0.0856	0.0895	0.1131	0.1779
0.4	0.0827	0.1018	0.0995	0.1036	0.1206	0.1550
0.5	0.0915	0.1081	0.1063	0.1091	0.1189	0.1358
0.6	0.0983	0.1097	0.1080	0.1093	0.1139	0.1208
0.7	0.1028	0.1076	0.1061	0.1065	0.1081	0.1107
0.8	0.1030	0.1030	0.1022	0.1022	0.1025	0.1030

Table 48. Normalised geometric function for mode-II at L/W=3

	2d/L=0.2	0.4	0.6	0.7	0.8	0.9
$\alpha=0$	0.9324	0.6859	0.4640	0.3712	0.2961	0.2648
0.1	0.7450	0.5540	0.3741	0.2938	0.2158	0.0445
0.2	0.6187	0.4625	0.3111	0.2399	0.1651	0.0607
0.3	0.5330	0.3989	0.2673	0.2034	0.1364	0.0597
0.4	0.4729	0.3536	0.2362	0.1785	0.1194	0.0583
0.5	0.4278	0.3196	0.2132	0.1605	0.1075	0.0545
0.6	0.3914	0.2924	0.1949	0.1465	0.0981	0.0502
0.7	0.3604	0.2697	0.1798	0.1349	0.0902	0.0458
0.8	0.3343	0.2505	0.1670	0.1253	0.0836	0.0422

Table 49. Normalised geometric function for mode-I at L/W=4

	2d/L=0.2	0.4	0.6	0.7	0.8	0.9
α=0.1	0.0295	0.0316	0.0272	0.0244	0.0238	0.0567
0.2	0.0497	0.0543	0.0481	0.0454	0.0499	0.1049
0.3	0.0633	0.0693	0.0632	0.0616	0.0692	0.1131
0.4	0.0722	0.0781	0.0730	0.0723	0.0793	0.1062
0.5	0.0777	0.0820	0.0783	0.0779	0.0827	0.0971
0.6	0.0805	0.0824	0.0800	0.0798	0.0822	0.0888
0.7	0.0805	0.0804	0.0792	0.0790	0.0799	0.0823
0.8	0.0778	0.0770	0.0765	0.0764	0.0766	0.0772

Table 50. Normalised geometric function for mode-II at L/W=4

	2d/L=0.2	0.4	0.6	0.7	0.8	0.9
α=0.	0.9014	0.6711	0.4474	0.3363	0.2311	0.1480
0.1	0.7289	0.5432	0.3621	0.2723	0.1864	0.1079
0.2	0.6101	0.4553	0.3035	0.2282	0.1551	0.0825
0.3	0.5279	0.3945	0.2630	0.1976	0.1333	0.0682
0.4	0.4692	0.3511	0.2341	0.1757	0.1180	0.0597
0.5	0.4250	0.3184	0.2123	0.1593	0.1065	0.0537
0.6	0.3895	0.2920	0.1946	0.1460	0.0974	0.0490
0.7	0.3595	0.2696	0.1793	0.1348	0.0899	0.0451
0.8	0.3340	0.2505	0.1670	0.1253	0.0835	0.0418

Table 51. Normalised geometric function for mode-I at L/W=8

	2d/L=0.2	0.4	0.6	0.7	0.8	0.9
α=0.1	0.0161	0.0149	0.0149	0.0146	0.0133	0.0119
0.2	0.0276	0.0259	0.0258	0.0253	0.0236	0.0249
0.3	0.0352	0.0333	0.0332	0.0328	0.0311	0.0345
0.4	0.0395	0.0378	0.0377	0.0373	0.0361	0.0396
0.5	0.0413	0.0400	0.0400	0.0397	0.0388	0.0413
0.6	0.0414	0.0405	0.0405	0.0403	0.0398	0.0411
0.7	0.0403	0.0398	0.0398	0.0397	0.0395	0.0399
0.8	0.0385	0.0384	0.0384	0.0383	0.0382	0.0383

Table 52. Normalised geometric function for mode-II at L/W=8

4.3 The asymmetric 4-point bending test

For the determination of the fracture toughness K_{IIc} with edge-notched (or precracked) beams asymmetric bending arrangements (fig.75) are recommended.
Otsuka et al [65] have compiled values of the geometric functions F_I and F_{II} defined by

$$K_I = \frac{P}{Wt}\left(1-\frac{d}{L}\right)\sqrt{\pi a}\,F_I \quad , \quad K_{II} = \frac{P}{Wt}\left(1-\frac{d}{L}\right)\sqrt{\pi a}\,F_{II} \tag{4.3.1}$$

for L/W=2.5 and d = W/2, obtained by FE-calculations.
The application of the weight functions given in Sections 3.1.1 and 4.1 and use of Filon's [66] analytical solution for the stress state yield the stress intensity factors [67] (expressed by the geometric functions) listed in Table 53 and Table 54 for L/W=5 and various a/W- and d/W-values.

	d/W=0.25	0.300	0.375	0.500	0.625
α=0.1	0.3746	0.3428	0.3318	0.3450	0.3599
0.2	0.7881	0.7180	0.6719	0.6633	0.6741
0.3	1.0374	0.9933	0.9560	0.9399	0.9431
0.4	1.1858	1.1819	1.1753	1.1702	1.1695
0.5	1.3120	1.3380	1.3579	1.3661	1.3641
0.6	1.4674	1.5079	1.5387	1.5507	1.5472
0.7	1.6948	1.7318	1.7553	1.7600	1.7547
0.8	2.053	2.0687	2.073	2.0684	2.0635
0.9	2.7563	2.7545	2.7505	2.7467	2.7452

Table 53. Geometric function for mode-II

	d/W=0.25	0.300	0.375	0.500	0.625
α=0.1	0.2615	0.3695	0.4241	0.3841	0.2918
0.2	-0.0038	0.1129	0.2110	0.2448	0.2060
0.3	-0.0307	0.0447	0.1184	0.1580	0.1410
0.4	0.0024	0.0483	0.0904	0.1098	0.09534
0.5	0.0407	0.0672	0.0842	0.0806	0.06268
0.6	0.0716	0.0808	0.0771	0.0566	0.03706
0.7	0.0855	0.0769	0.0581	0.03198	0.0164
0.8	0.0641	0.0460	0.0271	0.0106	0.00359
0.9	-0.0048	-0.0002	0.0077	0.01406	0.0138

Table 54. Geometric function for mode-I

As can be seen from Table 53 and Table 54 the geometric function F_{II} in the range $0.375 \leq d/W \leq 625$. is approximately independent of the value of d/W. An analytical approximation can be given by

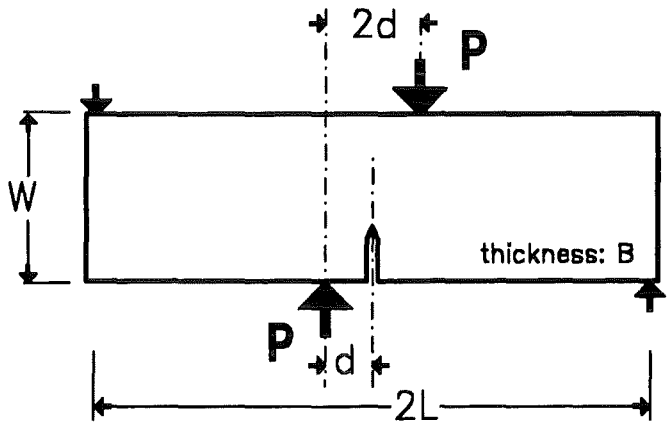

Figure 75. Geometric data of the asymmetrically notched bending bar

$$F_{II} = 3.9204\alpha - 5.1295\alpha^2 + 14.4566\alpha^3 - 26.2916\alpha^4 + 17.073\alpha^5 \quad , \quad \alpha = a/W \tag{4.3.2}$$

4.4 Geometric functions for oblique edge-cracks

Bending specimens with edge cracks or narrow saw cuts are often used to determine the fracture toughness of ceramic materials. Whilst cracks orthogonal to the specimens surface are applied in the determination of K_{Ic}, oblique edge-cracks are appropriate for mixed-mode fracture. Figure 76 illustrates the geometric data of a specimen loaded by a tensile stress σ and a bending moment M, respectively. Several investigations described in the literature deal with oblique edge-cracks (see [72]). Freese [73] solved the tensile case with a mapping technique for $0 \leq \omega \leq 90°$ and $0.1 \leq a/W \leq 0.7$. Wilson [75] applied the Boundary Collocation Method (BCM) and Aliabadi et al. [76] applied the Boundary Element Analysis (BEM) to pure tension and pure bending for $\omega = 0/22.5/45°$ and $0.3 \leq a/W \leq 0.6$. Since the results of Wilson and Aliabadi agree excellently within about 1-2% deviation, the results of Freese and Wilson are intercompared in fig.77 only in terms of the geometric function defined by

$$K_I = \sigma F_I \sqrt{\pi a} \quad , \quad K_{II} = \sigma F_{II} \sqrt{\pi a} \tag{4.4.1}$$

Whilst the agreement between the two solutions is sufficient for F_I, Freese's solution for F_{II} deviates significantly from the others for $\omega = 22.5°$, as can be seen from fig.78. In figs.79 and 80 the geometric functions from the literature are plotted as a function of the angle ω. The literature results are entered as symbols whilst the curves give the fitted dependency.
In order to allow interpolations to be made for arbitrary angles ω in the range $0 \leq \omega \leq 90°$Table 55 and Table 56 provide a field of data for F_I and F_{II} under tension loading. Bicubic splines are recommended for the interpolations.
The mode-II geometric function for tension can be approximated by

$$F_{II} = A \sin\left[\omega(1 - \frac{\pi}{2}B) + \omega^2 B\right] \tag{4.4.2}$$

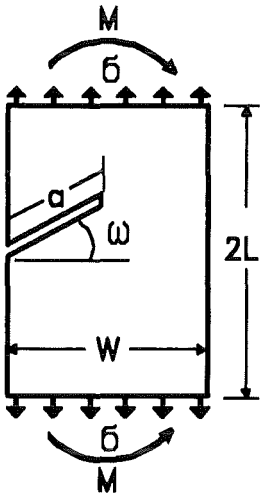

Figure 76. The oblique edge-crack under tension and bending loads.

$$A = 0.3515 + 0.2851a/W + 0.1723(a/W)^2 + 1.212(a/W)^3 \tag{4.4.3}$$

$$B = 0.04362 - 0.0883a/W - 0.8302(a/W)^2 + 0.19617(a/W)^3 \tag{4.4.4}$$

Only a few data are available for oblique cracks in bending. Wilson [75] and Aliabadi et al. [76] considered the angles $\omega = 22.5$ and 45° and Sha and Yang [77] investigated the case $\omega = 22.5°$.

Extension of the data base to bending with approximate weight functions

In order to extend this data base averaged weight functions were applied. A very simple procedure results from application of the direct adjustment of the weight function to the reference loading stress intensity factor ([25]) for which the tensile data can be used.

If η denotes the depth coordinate perpendicular to the free edge, $\eta = x \cos \omega$, the bending stress σ_b is given by

$$\sigma_b = \sigma_0\left(1 - 2\frac{x}{W}\cos\omega\right) \tag{4.4.5}$$

where σ_0 is the outer fibre bending stress. The normal and shear stresses (σ_n, τ) in the plane of the crack are

$$\begin{aligned} \sigma_n(x) &= \sigma(x)\cos^2\omega \\ \tau(x) &= \sigma(x)\cos\omega\ \sin\omega \end{aligned} \tag{4.4.6}$$

The stress intensity factors are then given as

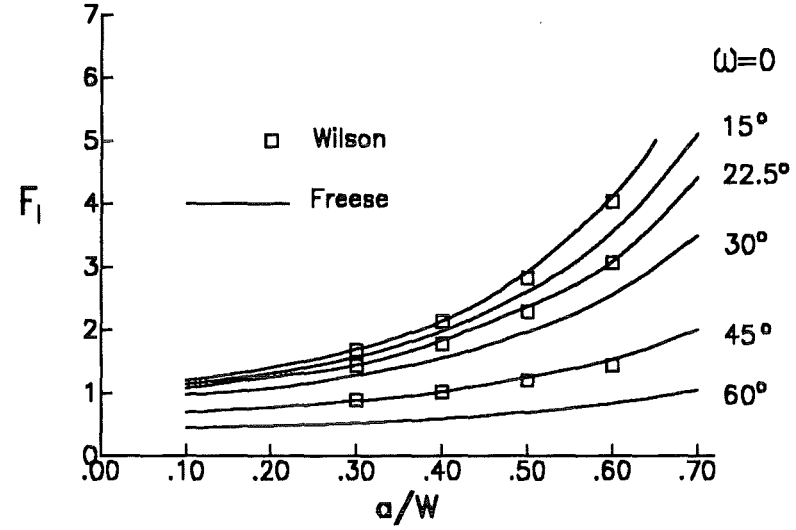

Figure 77. Geometric function (mode-I) for tension. F_I given by Freese [73] and Wilson [75].

$$K_I = \int_0^a \sigma_n(x)\, h_{I1}(x,a)\, dx + \int_0^a \tau(x)\, h_{I2}(x,a)\, dx$$

$$K_{II} = \int_0^a \sigma_y(x)\, h_{II1}(x,a)\, dx + \int_0^a \tau(x)\, h_{II2}(x,a)\, dx \qquad (4.4.7)$$

For a rough estimate we neglect the components h_{I2} and h_{II1} (as done in [72])

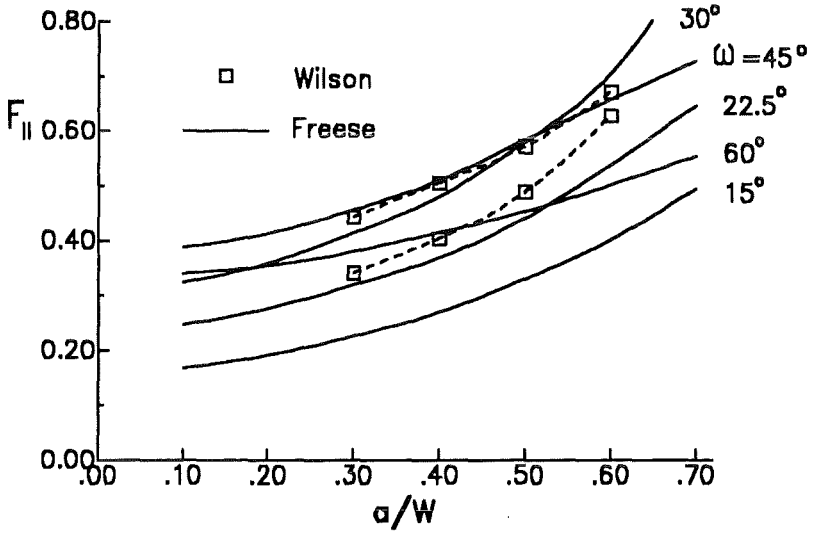

Figure 78. Geometric function (mode-II) for tension. F_{II} given by Freese [73] and Wilson [75].

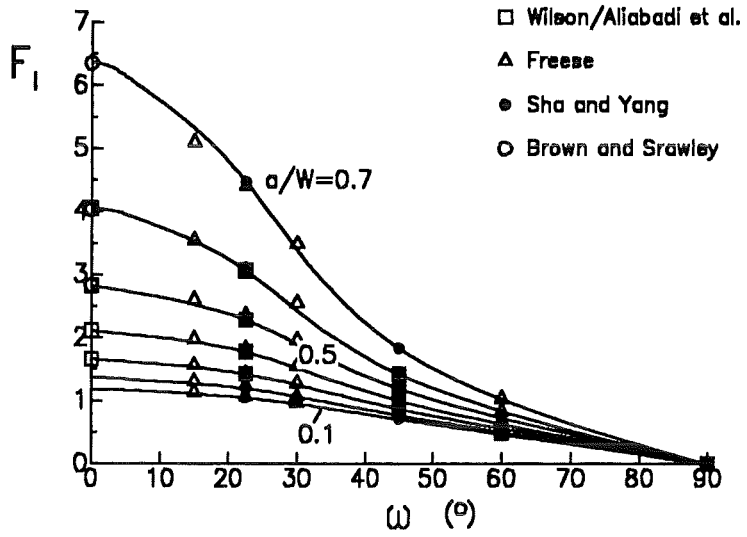

Figure 79. Geometric function (mode-I) for tension. F_I as a function of the angle ω from the literature (symbols, [73][75][76] [77],[36]) and continuous representation (lines) after application of a fit-procedure.

$$K_I \simeq \int_0^a \sigma_n(x)\, h_I(x,a)\, dx \quad , \quad K_{II} \simeq \int_0^a \tau(x)\, h_{II}(x,a)\, dx \tag{4.4.8}$$

(setting $h_{I1} = h_I$ and $h_{II2} = h_{II}$). For the weight functions we use set-ups with one unknown parameter

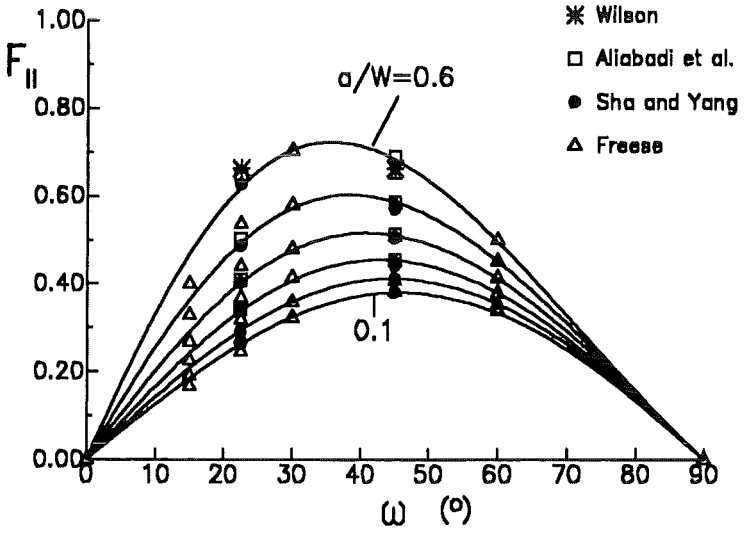

Figure 80. Geometric function (mode-II) for tension. F_{II} as a function of the angle ω from the literature (symbols) and approximative representation by eq.(4.4.2) (lines).

$$h_I = \sqrt{\frac{2}{\pi a}}\left(\frac{1}{\sqrt{1-x/a}} + A\sqrt{1-x/a}\right)$$
$$h_{II} = \sqrt{\frac{2}{\pi a}}\left(\frac{1}{\sqrt{1-x/a}} + B\sqrt{1-x/a}\right) \qquad (4.4.9)$$

Introducing into eqs.(4.4.8) these set-ups and the stress distribution for pure tension yields the geometric functions in terms of eq.(4.4.1) as

$$F_{I,t} = \frac{\sqrt{2}}{\pi}\left(2 + \frac{2}{3}A\right)\cos^2\omega$$
$$F_{II,t} = \frac{\sqrt{2}}{\pi}\left(2 + \frac{2}{3}B\right)\cos\omega\ \sin\omega \qquad (4.4.10)$$

(subscript t for tension) and therefrom the unknown parameters as

$$A = \frac{3\pi}{\sqrt{8}\ \cos^2\omega}F_{I,t} - 3$$
$$B = \frac{3\pi}{\sqrt{8}\ \cos\omega\ \sin\omega}F_{II,t} - 3 \qquad (4.4.11)$$

With these coefficients the stress intensity factors for the bending case can be determined using eqs.(4.4.5) to (4.4.9) and (4.4.11), and it results

$$F_{I,b} = F_{I,t}\left(1 - \frac{4}{5}\frac{a}{W}\cos\omega\right) - \frac{16}{15}\frac{\sqrt{2}}{\pi}\frac{a}{W}\cos^3\omega$$
$$F_{II,b} = F_{II,t}\left(1 - \frac{4}{5}\frac{a}{W}\cos\omega\right) - \frac{16}{15}\frac{\sqrt{2}}{\pi}\frac{a}{W}\cos^2\omega\ \sin\omega \qquad (4.4.12)$$

(subscript b for bending). The geometric functions for bending computed from the tensile data are shown as solid lines together with literature data in figs.81 and 82. These approximative solutions are suitable to compute the general shape of the F_I, F_{II} vs. ω curves and to allow the literature data for $\omega = 0$, 22.5 and 45° to be interpolated.

ω(°)	a/W=0.1	0.2	0.3	0.4	0.5	0.6	0.7
0	1.18	1.370	1.66	2.11	2.83	4.03	6.35
15	1.12	1.29	1.55	1.94	2.53	3.50	5.25
22.5	1.06	1.21	1.45	1.78	2.28	3.03	4.45
30	0.97	1.18	1.26	1.53	1.91	2.45	3.41
45	0.72	0.79	0.88	1.00	1.19	1.44	1.82
60	0.48	0.52	0.58	0.63	0.74	0.85	1.04
90	0.	0.	0.	0.	0.	0.	0.

Table 55. Geometric function for the edge-cracked plate under tension. Influence of the crack length L and the angle ω on F_I.

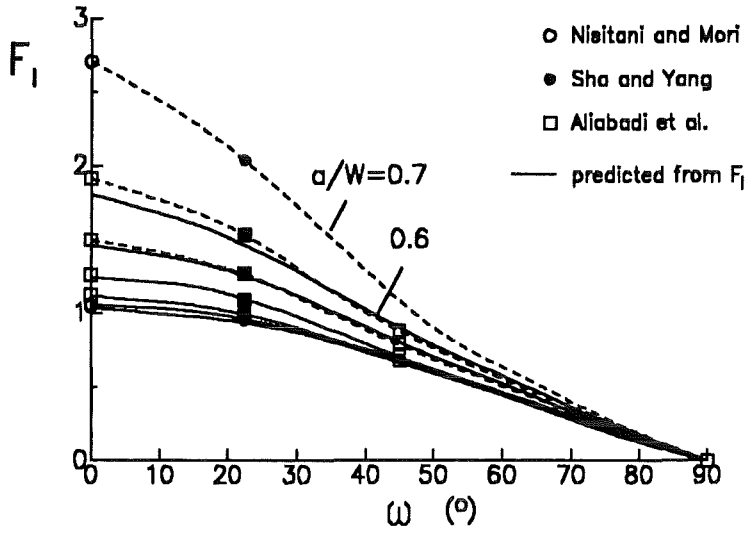

Figure 81. Geometric function (mode-I) for bending. F_{II} as a function of the angle ω; symbols: data from the literature; solid curves eq.(4.4.12), dashed curves: interpolation of literature results in conformity with the general trend, obtained from (4.4.12).

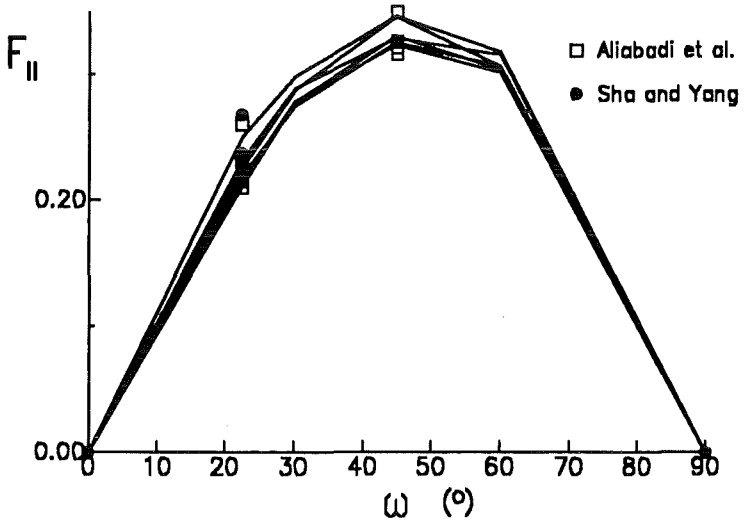

Figure 82. Geometric function (mode-II) for bending. F_{II} for bending as a function of the angle ω (lines: (4.4.12), symbols: data from the literature).

$\omega(°)$	a/W=0.1	0.2	0.3	0.4	0.5	0.6
0	0.	0.	0.	0.	0.	0.
22.5	0.26	0.285	0.335	0.400	0.490	0.620
30	0.33	0.365	0.420	0.480	0.580	0.695
45	0.385	0.410	0.450	0.510	0.577	0.680
60	0.330	0.355	0.380	0.415	0.460	0.500
90	0.	0.	0.	0.	0.	0.

Table 56. Geometric function for the edge-cracked plate under tension. Influence of the crack length L and the angle ω on F_{II}.

In case of $F_{I,b}$ the agreement between the approximated geometric functions and the literature data is good for $a/W \leq 0.5$. For larger cracks deviations become obvious which are caused by the use of the two-terms weight functions. In case of $F_{II,b}$ the agreement with the literature data is sufficient up to $a/W = 0.6$. Extended data-sets resulting from the literature data as well as from the data generated with the weight function method are entered in Table 57 and Table 58.

$\omega(°)$	a/W=0.1	0.2	0.3	0.4	0.5	0.6	0.7
0	1.049	1.058	1.126	1.26	1.495	1.915	2.71
15	0.980	1.02	1.058	1.185	1.365	1.698	2.30
22.5	0.935	0.96	0.985	1.090	1.26	1.53	2.04
30	0.874	0.883	0.91	0.985	1.12	1.32	1.74
45	0.699	0.68	0.695	0.710	0.794	0.89	1.09
60	0.450	0.446	0.451	0.467	0.510	0.56	0.64
90	0.	0.	0.	0.	0.	0.	0.

Table 57. Geometric function for the edge-cracked plate in bending. Influence of the crack length L and the angle ω on F_I.

$\omega(°)$	a/W=0.1	0.2	0.3	0.4	0.5	0.6
0	0.	0.	0.	0.	0.	0.
22.5	0.23	0.216	0.215	0.220	0.235	0.265
30	0.286	0.278	0.274	0.275	0.286	0.302
45	0.344	0.329	0.316	0.321	0.326	0.349
60	0.306	0.304	0.302	0.306	0.315	0.318
90	0.	0.	0.	0.	0.	0.

Table 58. Geometric function for the edge-cracked plate in bending. Influence of the crack length L and the angle ω on F_{II}.

5. Subinterface cracks

5.1 Weight functions for edge cracks

Edge cracks parallel to an interface between dissimilar elastic materials, fig.83, show mixed-mode stress intensity factors even under pure normal stress or pure shear loading. If the crack faces are loaded with the normal stress σ_y, the stress intensity factors read

$$K_I^{(\sigma)} = \int_0^a h_I^{(\sigma)}(x,a)\, \sigma_y(x)\, dx \quad , \quad K_{II}^{(\sigma)} = \int_0^a h_{II}^{(\sigma)}(x,a)\, \sigma_y(x)\, dx \tag{5.1.1}$$

and define the weight functions $h_I^{(\sigma)}$, $h_{II}^{(\sigma)}$. For shear stresses τ acting at the crack faces one can write

$$K_I^{(\tau)} = \int_0^a h_I^{(\tau)}(x,a)\, \tau(x)\, dx \quad , \quad K_{II}^{(\tau)} = \int_0^a h_{II}^{(\tau)}(x,a)\, \tau(x)\, dx \tag{5.1.2}$$

defining the weight functions $h_I^{(\tau)}$, $h_{II}^{(\tau)}$. Under combined crack-face loading the stress intensity factors from eqs.(5.1.1) and (5.1.2) can be superimposed which results in

$$K_I = \int_0^a \left(h_I^{(\sigma)}(x,a)\, \sigma_y(x) + h_I^{(\tau)}(x,a)\, \tau(x) \right) dx \tag{5.1.3}$$

$$K_{II} = \int_0^a \left(h_{II}^{(\sigma)}(x,a)\, \sigma_{(y)}(x) + h_{II}^{(\tau)}(x,a)\, \tau(x) \right) dx \tag{5.1.4}$$

The weight functions can be obtained from the stress intensity factors and the displacements of the crack borders in x- and y-direction of a specific load - the reference load [7]. In case of homogeneous materials the mode-I weight function is related only to the displacements v normal to the crack face and the mode-II weight function to the displacements u in the crack face line. For cracks near the interface we have to expect also an interrelation to exist between the displacements which may be written in a general form

$$h_I^{(\tau)} = m_1 \frac{\partial u^{(\tau)}}{\partial a} + m_2 \frac{\partial u^{(\sigma)}}{\partial a} \tag{5.1.5}$$

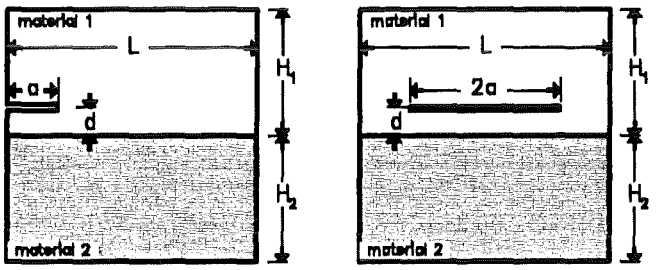

Figure 83. External subinterface crack. Geometric data; left: edge crack, right: internal crack.

$$h_I^{(\sigma)} = m_3 \frac{\partial v^{(\tau)}}{\partial a} + m_4 \frac{\partial v^{(\sigma)}}{\partial a} \tag{5.1.6}$$

$$h_{II}^{(\tau)} = m_5 \frac{\partial u^{(\sigma)}}{\partial a} + m_6 \frac{\partial u^{(\tau)}}{\partial a} \tag{5.1.7}$$

$$h_{II}^{(\sigma)} = m_7 \frac{\partial v^{(\sigma)}}{\partial a} + m_8 \frac{\partial v^{(\tau)}}{\partial a} \tag{5.1.8}$$

where the coefficients $m_1,\ldots,m_8$ will depend on the ratio of the Young's moduli E_2/E_1 and Poisson ratios ν_1, ν_2 as well as on the geometric data and the applied load. The indices (τ) and (σ) describe the loadings which are responsible for the crack opening displacements.

5.1.1 Set-ups for the weight functions

For this type of mixed-mode problem the direct adjusting method described in [25] is an appropriate tool to generate analytical expressions for the four weight function components. Therefore, we will use the following set-ups

$$h_I^{(\sigma)} = \sqrt{\frac{2}{\pi a}} \sum_{\nu=0}^{\infty} D_{I,\nu}^{(\sigma)} (1 - x/a)^{\nu - 1/2} \tag{5.1.9}$$

$$h_{II}^{(\sigma)} = \sqrt{\frac{2}{\pi a}} \sum_{\nu=0}^{\infty} D_{II,\nu}^{(\sigma)} (1 - x/a)^{\nu - 1/2} \tag{5.1.10}$$

$$h_I^{(\tau)} = \sqrt{\frac{2}{\pi a}} \sum_{\nu=0}^{\infty} D_{I,\nu}^{(\tau)} (1 - x/a)^{\nu - 1/2} \tag{5.1.11}$$

$$h_{II}^{(\tau)} = \sqrt{\frac{2}{\pi a}} \sum_{\nu=0}^{\infty} D_{II,\nu}^{(\tau)} (1 - x/a)^{\nu - 1/2} \tag{5.1.12}$$

with

$$D_{I,0}^{(\sigma)} = D_{II,0}^{(\tau)} = 1 \quad , \quad D_{I,0}^{(\tau)} = D_{II,0}^{(\sigma)} = 0 \tag{5.1.13}$$

Let us assume the loading cases for constant pressure $\sigma = \text{const}$ and constant shear $\tau = \text{const}$. directly on the crack faces to be known. Then a sufficient number of conditions is known to compute all coefficients for the approximated representation. Here we will restrict ourself on a two-terms weight function of the form

$$h_I^{(\sigma)} = \sqrt{\frac{2}{\pi a}} \left(\frac{1}{\sqrt{1 - x/a}} + D_{I,1}^{(\sigma)} \sqrt{1 - x/a} + D_{I,2}^{(\sigma)} (1 - x/a)^{3/2} \right) \tag{5.1.14}$$

$$h_{II}^{(\sigma)} = \sqrt{\frac{2}{\pi a}} \left(D_{II,1}^{(\sigma)} \sqrt{1 - x/a} + D_{II,2}^{(\sigma)} (1 - x/a)^{3/2} \right) \tag{5.1.15}$$

$$h_I^{(\tau)} = \sqrt{\frac{2}{\pi a}} \left(D_{I,1}^{(\tau)} \sqrt{1 - x/a} + D_{I,2}^{(\tau)} (1 - x/a)^{3/2} \right) \tag{5.1.16}$$

$$h_{II}^{(\tau)} = \sqrt{\frac{2}{\pi a}} \left(\frac{1}{\sqrt{1 - x/a}} + D_{II,1}^{(\tau)} \sqrt{1 - x/a} + D_{II,2}^{(\tau)} (1 - x/a)^{3/2} \right) \tag{5.1.17}$$

In [19] and [31] it has been shown that the second derivative of the displacements must vanish for the two reference loading cases ($\sigma_y = const.$, $\tau = const.$). This may be repeated here for the case of the displacements v normally to the crack surface. It has been shown in [25] that

$$\begin{aligned} \frac{\partial^2 v}{\partial x^2} &= \frac{2 + \nu}{E} \frac{\partial \tau}{\partial x} - \frac{1 - \nu^2}{E} \frac{\partial \sigma_x}{\partial y} \\ \frac{\partial^3 v}{\partial x^3} &= \frac{2 + \nu}{E} \frac{\partial^2 \tau}{\partial x^2} + \frac{1 - \nu^2}{E} \frac{\partial^2 \tau}{\partial y^2} \end{aligned} \tag{5.1.18}$$

In the chosen reference cases: $\sigma_y = const$ and $\tau = const$ along the crack faces we obtain for free surface conditions along the line $x = 0$

$$\frac{\partial \tau}{\partial x} = 0 \quad , \quad \frac{\partial^2 \tau}{\partial x^2} = 0 \quad \forall \quad x < a \tag{5.1.19}$$

$$\frac{\partial \sigma_x}{\partial y} = 0 \quad , \quad \frac{\partial^2 \tau}{\partial y^2} = 0 \quad \text{for } x = 0, \quad \forall y \tag{5.1.20}$$

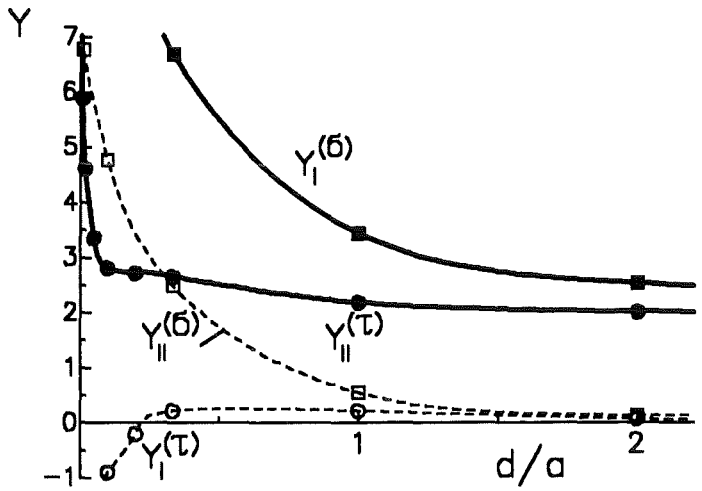

Figure 84. Geometric function for edge cracks. Geometric data: $a/L \leq 0.1$, $H_1 = H_2 = 2L$, material data: $E_1/E_2 = 100$, $\nu_1 = 0.2$, $\nu_2 = 0.4$.

and consequently

$$\frac{\partial^2 v}{\partial x^2} = 0 \quad , \quad \frac{\partial^3 v}{\partial x^3} = 0 \quad \text{for } x = 0 \tag{5.1.21}$$

The same can be shown for the displacements u in x-direction. Introducing this into eqs.(5.1.5) to (5.1.8) leads to

$$\frac{\partial^2 h_I^{(\sigma)}}{\partial x^2} = \frac{\partial^2 h_{II}^{(\sigma)}}{\partial x^2} = \frac{\partial^2 h_I^{(\tau)}}{\partial x^2} = \frac{\partial^2 h_{II}^{(\tau)}}{\partial x^2} = 0 \qquad \text{for} \quad x = 0 \tag{5.1.22}$$

Equation (5.1.22) leads to four relations between the coefficients D_ν:

$$\sum D_\nu (\nu - 1/2)(\nu - 3/2) = 0 \tag{5.1.23}$$

If the reference stress distributions $\sigma_y(x)$ and $\tau(x)$ are constant, eqs.(5.1.1) and (5.1.2) lead to four additional equations:

$$\sum D_\nu \frac{2}{2+\nu} = Y\sqrt{\pi/2} \tag{5.1.24}$$

where the geometric functions Y are defined as

$$\begin{aligned} K_I^{(\sigma)} &= \sigma_y \sqrt{a}\, Y_I^{(\sigma)} \quad , \quad K_{II}^{(\sigma)} = \sigma_y \sqrt{a}\, Y_{II}^{(\sigma)} \\ K_I^{(\tau)} &= \tau \sqrt{a}\, Y_I^{(\tau)} \quad , \quad K_{II}^{(\tau)} = \tau \sqrt{a}\, Y_{II}^{(\tau)} \end{aligned} \tag{5.1.25}$$

From the eqs.(5.1.23) and (5.1.24) the coefficients are obtained as

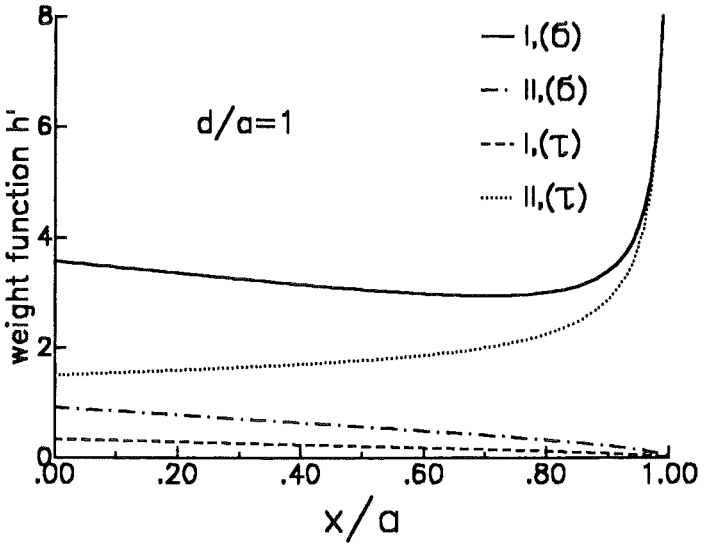

Figure 85. Weight function for edge cracks. Geometric data: $a/L \leq 0.1$, $H_1 = H_2 = 2L$, $E_1/E_2 = 100$, $\nu_1 = 0.2$, $\nu_2 = 0.4$; $d/a = 1$, weight function normalised: $h' = h\sqrt{a}$.

$$
\begin{aligned}
D_{I,1}^{(\sigma)} &= \frac{5}{4}\sqrt{\frac{\pi}{2}}\,Y_I^{(\sigma)} - 2 \quad , \quad D_{I,2}^{(\sigma)} = \frac{5}{12}\sqrt{\frac{\pi}{2}}\,Y_I^{(\sigma)} - \frac{5}{3} \\
D_{II,1}^{(\sigma)} &= \frac{5}{4}\sqrt{\frac{\pi}{2}}\,Y_{II}^{(\sigma)} \quad , \quad D_{II,2}^{(\sigma)} = \frac{5}{12}\sqrt{\frac{\pi}{2}}\,Y_{II}^{(\sigma)} \\
D_{I,1}^{(\tau)} &= \frac{5}{4}\sqrt{\frac{\pi}{2}}\,Y_I^{(\tau)} \quad , \quad D_{I,2}^{(\tau)} = \frac{5}{12}\sqrt{\frac{\pi}{2}}\,Y_I^{(\tau)} \\
D_{II,1}^{(\tau)} &= \frac{5}{4}\sqrt{\frac{\pi}{2}}\,Y_{II}^{(\tau)} - 2 \quad , \quad D_{II,2}^{(\tau)} = \frac{5}{12}\sqrt{\frac{\pi}{2}}\,Y_{II}^{(\tau)} - \frac{5}{3}
\end{aligned}
\tag{5.1.26}
$$

5.1.2 Example of application

Finite Element computations were used to determine the weight functions for edge cracks near an interface. The data were obtained for a Young's modulus ratio $E_1/E_2 = 100$ and $\nu_1 = 0.2$, $\nu_2 = 0.4$. The crack was located in material 1. The resulting geometric functions are plotted in fig.84 as a function of the distance from the interface normalised on the crack length. As could be expected from Saint Venant's principle the influence of the different material 1 on the stress intensity factors can be neglected for $d/a > 3$. For constant pressure at the crack faces the mode-I stress intensity factor K_I tends against the value of the homogeneous material and K_{II} vanishes. In case of constant shear stresses at the crack the the mode-II stress intensity factor K_{II} approaches the value of the homogeneous material and K_I vanishes.
The resulting weight functions are plotted in fig.85 for a crack with $d/a = 1$. Note that the results in fig.84 and fig.85 are for a semi-infinite plate or for a finite plate with $a/L \leq 0.1$.

d/a	$Y_I^{(\sigma)}$	$Y_{II}^{(\sigma)}$	$Y_I^{(\tau)}$	$Y_{II}^{(\tau)}$
0.0025	10.71	7.290	-4.514	8.6845
0.010	10.93	6.786	-2.838	5.891

0.100	9.952	4.769	-0.898	2.811
0.333	6.682	2.491	0.2165	2.65
1.000	3.437	0.5514	0.2195	2.185
2.000	2.536	0.1384	0.0769	2.0116
3.000	2.273	0.052	0.031	1.986
10.00	2.004	0.002	0.0013	1.974

Table 59. Geometric function for subinterface edge-cracks. Geometric data: $a/L \leq 0.1$, $H_1 = H_2 = 2L$, $E_1/E_2 = 100$, $\nu_1 = 0.2$, $\nu_2 = 0.4$.

5.2 Weight functions for internal cracks

The geometry of an internal subinterface crack is illustrated in fig.83. The representation of the stress intensity factors by the weight functions are the same as in case of the subinterface edge crack. In the special case of a *symmetrically* loaded crack we use the set-ups

$$h_I^{(\sigma)} = \frac{2}{\sqrt{\pi a}} \left(\frac{1}{\sqrt{1-(x/a)^2}} + D_I^{(\sigma)} \sqrt{1-(x/a)^2} \right) \tag{5.2.1}$$

$$h_{II}^{(\sigma)} = \frac{2}{\sqrt{\pi a}} D_{II}^{(\sigma)} \sqrt{1-(x/a)^2} \tag{5.2.2}$$

$$h_I^{(\tau)} = \frac{2}{\sqrt{\pi a}} D_I^{(\tau)} \sqrt{1-(x/a)^2} \tag{5.2.3}$$

$$h_{II}^{(\tau)} = \frac{2}{\sqrt{\pi a}} \left(\frac{1}{\sqrt{1-(x/a)^2}} + D_{II}^{(\tau)} \sqrt{1-(x/a)^2} \right) \tag{5.2.4}$$

Here only one energy condition is necessary since the set-up fulfills all symmetry conditions a priori. We obtain the coefficients

$$D_I^{(\sigma)} = \frac{2}{\sqrt{\pi}} Y_I^{(\sigma)} - 2 \quad , \quad D_{II}^{(\sigma)} = \frac{2}{\sqrt{\pi}} Y_{II}^{(\sigma)} \tag{5.2.5}$$

$$D_I^{(\tau)} = \frac{2}{\sqrt{\pi}} Y_I^{(\tau)} \quad , \quad D_{II}^{(\tau)} = \frac{2}{\sqrt{\pi}} Y_{II}^{(\tau)} - 2 \tag{5.2.6}$$

6. Special problems

6.1 Thermal-shock problems

6.1.1 Weight functions for strips with periodical edge cracks

In thermal-shock experiments often an array of periodical cracks is observed [78]. Weight functions for such crack arrangements are necessary for the computation of stress intensity factors under nonhomogeneous thermal stresses. The geometry of endless strips with an infinite number of equidistant edge cracks at one side is shown in fig.86 as well as for cracks at both sides.

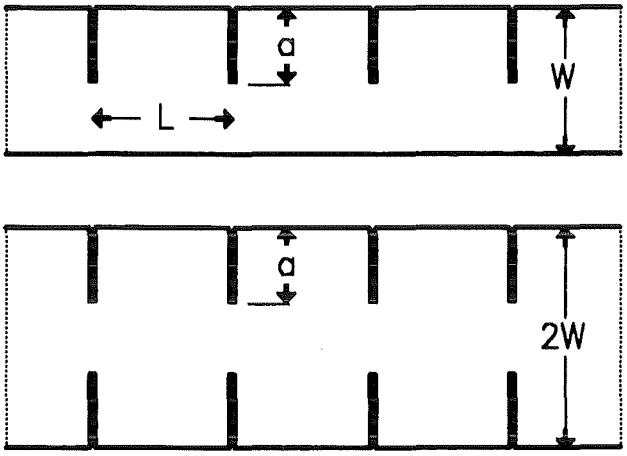

Figure 86. Arrays of edge cracks. Geometrical data.

The stress intensity factors for pure tension load were computed by Isida and Tsuru [79] with the Boundary Collocation Method. Applying the weight function procedure described in section 2 and using the conditions of self-consistency and disappearing second derivative of crack opening displacements at the crack mouth we obtain the weight function according to eq.(2.5.2)

$$h = \sqrt{\frac{2}{\pi a}}\left(\frac{1}{\sqrt{1-\rho}} + B_0\sqrt{1-\rho} + B_1(1-\rho)^{3/2} + B_2(1-\rho)^{5/2}\right) \quad \rho = x/a \qquad (6.1.1)$$

with the coefficients listed in Table 60 for the case of cracks at one side and in Table 61 for cracks at both sides.

L/W		$a/W=0$	0.1	0.2	0.3	0.4	0.5	0.6	0.7
0.50	B_1	0.4498	-0.2665	-0.7658	-0.8416	-0.8860	-0.6393	0.0057	1.0751
	B_2	0.7001	0.8273	0.6791	0.4678	0.5825	0.3613	-0.3651	-1.4542
	B_3	-0.3100	-0.3832	-0.3869	-0.3497	-0.3756	-0.3149	-0.1266	0.1625
0.75	B_1	0.4498	0.0781	-0.3124	-0.4226	-0.3203	-0.0305	0.6241	1.3978
	B_2	0.7001	0.7536	0.7895	0.4915	0.2220	-0.0984	-0.7271	-1.0760
	B_3	-0.3100	-0.3455	-0.3787	-0.3265	-0.2658	-0.1824	-0.0130	0.1084
1.00	B_1	0.4498	0.2444	0.0035	-0.0983	0.0291	0.3209	0.9107	1.8269
	B_2	0.7001	0.7255	0.7407	0.5686	0.2426	-0.0626	-0.5682	-1.1437
	B_3	-0.3100	-0.3288	-0.3479	-0.3203	-0.2466	-0.1661	-0.0257	0.1505
1.50	B_1	0.4498	0.3700	0.3372	0.3192	0.4778	0.7812	1.3410	2.3871
	B_2	0.7001	0.7075	0.7213	0.7442	0.4854	0.2221	-0.2238	-0.9941
	B_3	-0.3100	-0.3168	-0.3218	-0.3276	-0.2652	-0.1923	-0.0658	0.1580
2.00	B_1	0.4498	0.4228	0.5048	0.5969	0.7560	1.1493	1.6665	2.1878
	B_2	0.7001	0.6991	0.6972	0.7915	0.7519	0.4058	0.1750	0.3309
	B_3	-0.3100	-0.3116	-0.3058	-0.3185	-0.3000	-0.2045	-0.1239	-0.1203
2.50	B_1	0.4498	0.4759	0.6144	0.8159	1.0107	1.3983	1.8675	2.2013
	B_2	0.7001	0.6901	0.6333	0.7034	0.8709	0.7243	0.6929	1.1397
	B_3	-0.3100	-0.3063	-0.2857	-0.2863	-0.3068	-0.2516	-0.2141	-0.2812
3.00	B_1	0.4498	0.4941	0.6832	0.9495	1.2331	1.6311	2.0157	2.2706
	B_2	0.7001	0.6860	0.6123	0.7213	0.9187	0.9843	1.2258	1.7463
	B_3	-0.3100	-0.3043	-0.2769	-0.2810	-0.3015	-0.2881	-0.3108	-0.3979
3.50	B_1	0.4498	0.5353	0.7319	1.1121	1.4249	1.7739	2.1588	2.3557
	B_2	0.7001	0.6815	0.5798	0.5320	0.9756	1.3467	1.6784	2.2564
	B_3	-0.3100	-0.3006	-0.2672	-0.2323	-0.3001	-0.3511	-0.3918	-0.4942

Table 60. Strip with crack array. Coefficients for the weight function eq.(6.1.1) for strips with edge cracks at one side.

L/W		$a/W=0$	0.1	0.2	0.3	0.4	0.5	0.6	0.7
0.50	B_1	0.4498	-0.2628	-0.7624	-0.8371	-0.8855	-0.6351	-0.0062	1.0091
	B_2	0.7001	0.8263	0.6721	0.4587	0.5815	0.3527	-0.3413	-1.3418
	B_3	-0.3100	-0.3828	-0.3853	-0.3476	-0.3753	-0.3129	-0.1322	0.1356
0.75	B_1	0.4498	0.0666	-0.2906	-0.4018	-0.4354	-0.0776	0.5521	0.9531
	B_2	0.7001	0.7507	0.6810	0.5082	0.5171	-0.0042	-0.6156	-0.3809
	B_3	-0.3100	-0.3457	-0.3556	-0.3284	-0.3324	-0.2043	-0.0401	-0.0603

1.00	B_1	0.4498	0.2446	0.0021	-0.1050	-0.0025	0.2521	0.7219	1.4138
	B_2	0.7001	0.7250	0.7307	0.5689	0.2798	0.0103	-0.3462	-0.7062
	B_3	-0.3100	-0.3287	-0.3460	-0.3208	-0.2561	-0.1853	-0.0826	0.0355
1.50	B_1	0.4498	0.3299	0.2633	0.0352	0.4983	0.7066	0.5574	1.9769
	B_2	0.7001	0.7100	0.6942	1.0207	-0.1192	0.0473	0.7992	-1.1974
	B_3	-0.3100	-0.3200	-0.3213	-0.4018	-0.1429	-0.1623	-0.3227	0.1713
2.00	B_1	0.4498	0.3573	0.3491	0.3586	0.4306	0.6407	1.0219	1.6240
	B_2	0.7001	0.7070	0.7103	0.7692	0.7223	0.5159	0.1812	-0.2455
	B_3	-0.3100	-0.3176	-0.3188	-0.3299	-0.3158	-0.2605	-0.1681	-0.0426
2.50	B_1	0.4498	0.3866	0.3719	0.4028	0.5106	0.6817	1.0086	1.5520
	B_2	0.7001	0.7067	0.7361	0.7002	0.6077	0.5181	0.2921	-0.0691
	B_3	-0.3100	-0.3156	-0.3224	-0.3132	-0.2875	-0.2582	-0.1912	-0.0827

Table 61. Strip with crack array. Coefficients for the weight function eq.(6.1.1) for strips with edge cracks at both sides.

6.1.2 Stress intensity factors for axial edge cracks in thermally shocked cylinders

The procedure of predicting failure under thermal fatigue conditions includes the following steps:

1. First, the temperatures in the whole component have to be calculated as a function of thermal material properties and thermal boundary conditions.
2. Then the stress distribution has to be calculated as a function of the thermo-mechanical material parameters (thermal expansion coefficient α, Young's modulus E, Poisson ratio μ).
3. The stress intensity factors for the cracks have to be calculated for the given thermal stress distribution.

In this section axial edge cracks are considered (see fig.87).

Calculation of temperatures and stresses in a thermally shocked cylinder The temperature distribution in a circular cylinder with an initial temperature T_0, cooled by transfer into a cooling medium of temperature $T=0$, is given by

$$T = T_0 \frac{2h}{\lambda R} \sum_{n=1}^{\infty} \frac{\exp(-\alpha_n^2 \kappa t)}{\alpha_n^2 + h^2/\lambda^2} \frac{J_0(\alpha_n \rho)}{J_0(\alpha_n R)} \tag{6.1.2}$$

where R is the radius of the cylinder, ρ is the radial coordinate, and κ is defined by the thermal conductivity λ, the specific heat capacity C_p, and the density d as

$$\kappa = \frac{\lambda}{C_p d} \tag{6.1.3}$$

The α_n values are roots of

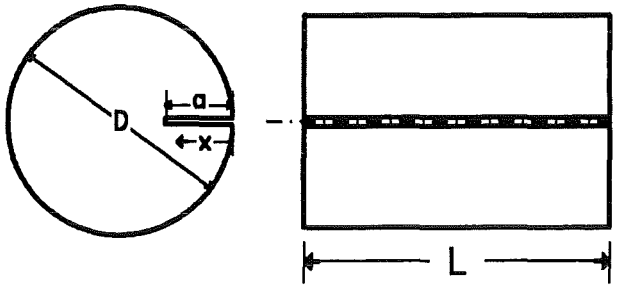

Figure 87. Edge-cracked cylinder. Geometrical data.

$$\alpha_n J_1(R\alpha_n) - \frac{h}{\lambda} J_0(R\alpha_n) = 0 \tag{6.1.4}$$

with the heat transfer coefficient h and the Bessel functions J_0, J_1 of the first kind. The thermal stresses result as

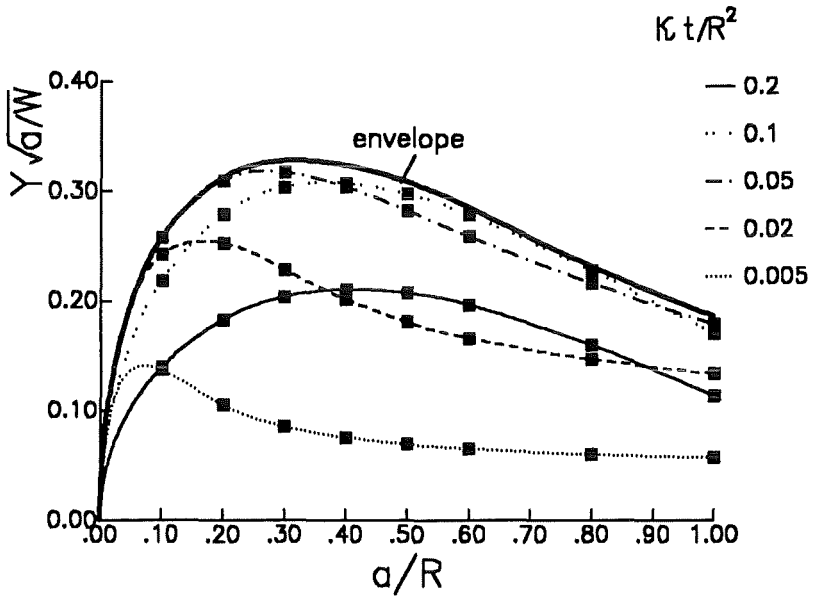

Figure 88. Stress intensity factors in thermally shocked cylinders. Stress intensity factors with envelope for a Biot-number $B = 10$.

$$\sigma_\rho = T_0 \frac{2\alpha E h}{\lambda R(1-\nu)} \sum_{n=1}^{\infty} \frac{\exp(-\alpha_n^2 \kappa t)}{(\alpha_n^2 + h^2/\lambda^2) J_0(\alpha_n R)} \left[\frac{J_1(\alpha_n R)}{\alpha_n R} - \frac{J_1(\alpha_n \rho)}{\alpha_n \rho} \right] \tag{6.1.5}$$

$$\sigma_z = T_0 \frac{2\alpha E h}{\lambda R(1-\nu)} \sum_{n=1}^{\infty} \frac{\exp(-\alpha_n^2 \kappa t)}{(\alpha_n^2 + h^2/\lambda^2) J_0(\alpha_n R)} \left[\frac{2J_1(\alpha_n R)}{\alpha_n R} - J_0(\alpha_n \rho) \right] \tag{6.1.6}$$

$$\sigma_\varphi = T_0 \frac{2\alpha E h}{\lambda R(1-\nu)} \sum_{n=1}^{\infty} \frac{\exp(-\alpha_n^2 \kappa t)}{(\alpha_n^2 + h^2/\lambda^2) J_0(\alpha_n R)} \left[\frac{J_1(\alpha_n R)}{\alpha_n R} + \frac{J_1(\alpha_n \rho)}{\alpha_n \rho} - J_0(\alpha_n \rho) \right] \tag{6.1.7}$$

The highest tensile stresses occur at the cylinder surface. Intercomparison of eqs.(6.1.5) to (6.1.7) makes obvious that for the cylinder surface ($\rho = R$) the circumferential and axial stresses are identical and produce an equibiaxial stress state. The radial stress component vanishes at the free surface. In the center of the specimen the radial and circumferential stresses are identical. The axial stress is twice the circumferential stress.

Stress intensity factors For edge cracks the stress component σ_φ is responsible for the stress intensity factor. Using eq.(6.1.7) and the weight function for the edge-notched circular disc one can calculate the stress intensity factors. This was done for differently chosen Biot numbers B. The results are given in the representation

$$K = \frac{\alpha E T_0}{1-\nu} Y(B, \kappa t/R^2) \sqrt{a} \quad , \quad B = \frac{hR}{\lambda} \tag{6.1.8}$$

with the geometric function Y entered in the following tables

$\kappa t/R^2$	$a/R=0$	0.1	0.2	0.3	0.4	0.5	0.6	0.8	1.0
0.02	0.0256	0.0181	0.0128	0.0093	0.0071	0.0057	0.0048	0.0037	0.0030
0.05	0.0352	0.0286	0.0231	0.0187	0.0152	0.0125	0.0104	0.0077	0.0058
0.10	0.0419	0.0362	0.0311	0.0266	0.0227	0.0193	0.0164	0.0117	0.0082
0.20	0.0456	0.0406	0.0359	0.0316	0.0275	0.0238	0.0204	0.0145	0.0097
0.50	0.0443	0.0397	0.0354	0.0313	0.0274	0.0238	0.0205	0.0146	0.0096
1.00	0.0402	0.0360	0.0321	0.0284	0.0249	0.0216	0.0186	0.0132	0.0087
2.00	0.0331	0.0297	0.0264	0.0234	0.0205	0.0178	0.0153	0.0109	0.0072
5.00	0.0184	0.0165	0.0147	0.0130	0.0114	0.0099	0.0085	0.0061	0.0040
10.0	0.0069	0.0062	0.0055	0.0049	0.0043	0.0037	0.0032	0.0023	0.0015

Table 62. Stress intensity factors for axially edge-cracked cylinders. Geometric function Y according to eq.(6.1.8), Biot-number $B = 0.1$.

$\kappa t/R^2$	$a/R=0$	0.05	0.1	0.2	0.3	0.4	0.5	0.6	0.8	1.0
0.005	0.1350	0.0942	0.0654	0.0351	0.0234	0.0179	0.0147	0.0126	0.0101	0.0086
0.01	0.1781	0.1396	0.1084	0.0669	0.0453	0.0341	0.0278	0.0237	0.0187	0.0157
0.02	0.2275	0.1932	0.1631	0.1157	0.0840	0.0640	0.0514	0.0432	0.0334	0.0273
0.10	0.3155	0.2957	0.2764	0.2399	0.2067	0.1770	0.1510	0.1284	0.0919	0.0638
0.20	0.2948	0.2803	0.2659	0.2378	0.2108	0.1851	0.1609	0.1383	0.0981	0.0648
0.50	0.1881	0.1795	0.1709	0.1539	0.1373	0.1213	0.1059	0.0912	0.0646	0.0422
1.00	0.0855	0.0816	0.0777	0.0700	0.0625	0.0552	0.0481	0.0415	0.0294	0.0192
2.00	0.0177	0.0169	0.0160	0.0145	0.0129	0.0114	0.0099	0.0086	0.0061	0.0040

Table 63. Stress intensity factors for axially edge-cracked cylinders. Geometric function Y according to eq.(6.1.8), Biot-number $B = 1.0$.

$\kappa t/R^2$	$a/R=0$	0.05	0.1	0.2	0.3	0.4	0.5	0.6	0.8	1.0
0.005	0.8423	0.6104	0.4333	0.2358	0.1567	0.1197	0.0983	0.0842	0.0671	0.0572
0.01	0.9519	0.7739	0.6177	0.3916	0.2661	0.2001	0.1625	0.1383	0.1088	0.0913
0.02	1.0043	0.8827	0.7661	0.5648	0.4171	0.3188	0.2557	0.2143	0.1643	0.1337
0.05	0.9347	0.8750	0.8137	0.6917	0.5786	0.4803	0.3991	0.3341	0.2418	0.1787
0.10	0.7522	0.7224	0.6907	0.6235	0.5541	0.4857	0.4204	0.3598	0.2548	0.1699
0.20	0.4708	0.4568	0.4415	0.4080	0.3714	0.3327	0.2932	0.2538	0.1788	0.1136
0.50	0.1133	0.1101	0.1066	0.0988	0.0902	0.0811	0.0716	0.0621	0.0437	0.0276
1.00	0.0105	0.0102	0.0099	0.0092	0.0084	0.0075	0.0067	0.0058	0.0041	0.0026

Table 64. Stress intensity factors for axially edge-cracked cylinders. Geometric function Y according to eq.(6.1.8), Biot-number $B = 10$.

$\kappa t/R^2$	$a/R=0$	0.05	0.1	0.2	0.3	0.4	0.5	0.6	0.8	1.0
0.0005	1.4622	0.5283	0.2562	0.1300	0.0892	0.0691	0.0572	0.0494	0.0399	0.0348
0.001	1.5476	0.7759	0.4056	0.2008	0.1374	0.1063	0.0878	0.0757	0.0610	0.0529
0.002	1.5873	1.0097	0.6150	0.3030	0.2054	0.1583	0.1305	0.1123	0.0901	0.0777
0.005	1.5663	1.2180	0.9074	0.5097	0.3374	0.2569	0.2105	0.1803	0.1432	0.1218
0.01	1.4907	1.2726	1.0568	0.7017	0.4818	0.3611	0.2921	0.2480	0.1943	0.1621
0.02	1.3573	1.2316	1.0997	0.8463	0.6399	0.4924	0.3943	0.3291	0.2504	0.2019
0.05	1.0785	1.0270	0.9705	0.8486	0.7256	0.6116	0.5124	0.4300	0.3083	0.2230
0.10	0.7842	0.7610	0.7347	0.6751	0.6090	0.5400	0.4712	0.4050	0.2856	0.1863
0.20	0.4390	0.4287	0.4170	0.3895	0.3577	0.3227	0.2857	0.2479	0.1743	0.1093
0.50	0.0800	0.0782	0.0761	0.0712	0.0655	0.0592	0.0525	0.0546	0.0320	0.0200

Table 65. Stress intensity factors for axially edge-cracked cylinders. Geometric function Y according to eq.(6.1.8), Biot-number $B = 100$.

The development of stress intensity factors during a thermal shock is plotted in fig.88.

7. References

[1] N.I. Muskhelishvili, "Some basic problems of mathematical theory of elasticity", Noordhoff, Holland, 1953.

[2] O.L. Bowie, J. Math. and Phys., **35**(1956),60ff.

[3] H. Neuber, "Kerbspannungslehre", Springer-Verlag, Berlin, 1958.

[4] J.P. Benthem, W.T. Koiter, Asymptotic approximations to crack problems, in: Mechanics of Fracture I, ed. G.C. Sih, Noordhoff International Publ., Leyden, 1973, 131-178.

[5] I.N. Sneddon, M. Lowengrub, "Crack problems in the classical theory of elasticity", Wiley, New York, 1969.

[6] H. Bueckner, A novel principle for the computation of stress intensity factors, ZAMM **50**(1970),529-546.

[7] J. R. Rice, Int. J. Solids Structures **8**(1972)751-758

[8] W.K. Wilson, Finite element methods for elastic bodies containing cracks, in: Mechanics of Fracture I, ed. G.C. Sih, Noordhoff International Publ., Leyden, 1973, 484-515.

[9] B. Gross, J.E. Srawley, W.F. Brown, NASA, Technical Note, D-2395, 1965.

[10] B. Gross, J.E. Srawley, NASA, Technical Note, D-2603, 1965.

[11] G.C. Sih "Handbook of stress-intensity factors", Institute of Fracture and Solid Mechanics, Lehigh University, Bethlehem, Pennsylvania, 1973.

[12] H. Tada, P.C. Paris, G.R. Irwin "The stress analysis of cracks handbook", Del Research Corporation (1986).

[13] D.P. Rooke, D.J. Cartwright, Her Majesty's Stationary Office, London 1974.

[14] Y.Murakami et al, Stress intensity factors handbook, Pergamon Press 1986.

[15] T. Fett, M. Caspers, D. Munz, H. Stamm, Int. J. Fract. **43**(1990),195-211.

[16] E. Betti, Il nuovo Cimento, Ser.2, **7** and **8** (1872).

[17] H.J. Petroski, J.D. Achenbach, Engng. Fract. Mech. **10**(1978)257-66

[18] G.R. Irwin, Analysis of stresses and strains near the end of a crack transversing a plate, Trans. Amer. Soc. Mech. Engnrs., J. Appl. Mechanics **24**(1957),361.

[19] T. Fett, C. Mattheck, D. Munz, Engng. Fract. Mech. **27**(1987)697-715.

[20] T. Fett, Conditions for the determination of approximative COD-fields, Engng. Fract. Mech. **39**(1991),905-914.

[21] J.C. Newman. Int. J. Fract. **17**(1981) 567-578.

[22] X.R. Wu, Int. J. Fract. **48**(1991) 179-192.

[23] T. Fett, A weight function for the RCT-specimen, Int. J. Fract. **63**(1993) R81-R85.

[24] T. Fett, D. Munz, The weight function method for calculation of stress intensity factors, (in German), Proceedings of the "DVM-Arbeitskreis BRUCHVORGÄNGE", Berlin 26/27 March 1991, 249-258.

[25] T. Fett, Direct determination of weight functions from reference loading cases and geometrical conditions, Engng. Fract. Mech. **42**(1992),435-444.

[26] J.E. Srawley, B. Gross, Side-cracked plates subject to combined direct and bending forces, ASTM STP 601, Philadelphia, 1976.

[27] T. Fett, "Stress intensity factors and weight functions for the edge cracked plate calculated by the Boundary Collocation Method", KfK-Report 4791, Kernforschungszentrum Karlsruhe, 1990.

[28] T.L. Sham, The determination of the elastic T-term using higher order weight functions, Int. J. Fract. **48**(1991),81-102.
[29] P.S. Leevers, J.C. Radon, Inherent stress biaxiality in various fracture specimen geometries, Int. J. Fract. **19**(1982),311-325.
[30] A.P. Kfouri, Some evaloations of the elastic T-term using Eshelby's method, Int. J. Fract. **30**(1986),301-315.
[31] T. Fett, Approximative stress intensity factors for mode-II loading, Theor. and Appl. Fract. Mech. **12**(1990)213-223.
[32] T. Fett, Consideration on set-up and boundary conditions for the determination of mode-I and mode-II crack opening displacements, Engng. Fract. Mech. **46**(1993) 655-662.
[33] R.D. Gregory, The spinning circular disc with a radial edge crack; an exact solution, Int. J. of Fracture **41**(1989),39-50.
[34] L.A. Wigglesworth, Mathematica **4**(1957),76-96.
[35] R.M. McMeeking, A.G. Evans, Mechanics of transformation toughening in brittle materials, J. Amer. Ceram. Soc. **65**(1982)242-46.
[36] W.F. Brown, J.E. Srawley, Plane strain crack toughness testing of high strength metallic materials, ASTM STP 410, 1966.
[37] H. Nisitani, K. Mori, Tech. Reports of the Kyushu Univ. Vol 58 (1985),751-755 (zitiert in [14])
[38] J.E. Srawley, B. Gross, Side-cracked plates subject to combined direct and bending forces, ASTM STP 601, 1976, 559-579.
[39] T. Fett, H. Stamm, G. Walz, Weight function for finite strip with double-edge notches, Theor. and Appl. Fract. Mech. **10**(1988) 227-230.
[40] M. Isida, stress intensity factors for the tension of an eccentrically cracked strip, Trans. ASME, J. of Appl. Mech., **33**(1965),674.
[41] F. Erdogan, Theoretical and experimental study of fracture in pipelines containing circumferential flaws, U.S. Department of Transportation, DOT-RSPA-DMA, 50/83/3, September 1982.
[42] C. Mattheck, P. Morawietz, D. Munz, H. Stamm, Comparison of different methods for the determination of stress intensity factors of cracks in pipes with stress gradients, J. Press. and Vessels **106**(1984),209-213.
[43] R. Labbens, A. Pellesier-Tanon, J. Heliot, Practical method for calculating stress intensity factors through weight functions, ASTM STP 590, 1976, 368-384.
[44] C.P. Andrasic, A.P. Parker, Dimensionless stress intensity factors for cracked thick cylinders under polynomial crack face loadings, Engng. Fract. Mech. **19**(1984),187-193.
[45] D.P. Rooke, J. Tweed, The stress intensity factors of an edge crack in a finite rotation disc, Int. Journal of Engineering Science, **11**(1973),279-283.
[46] D.P. Rooke, J. Tweed, The stress intensity factors of a radial crack in a finite rotation disc, Int. Journal of Engineering Science, **10**(1972),709-714.
[47] J. Tweed, S.C. Das, D.P. Rooke, The stress intensity factors of a radial crack in a finite elastic disc, Int. Journal of Engineering Science, **10**(1972),325-335.
[48] J.C. Newman, An improved method of collocation for the stress analysis of cracked plates with various shaped boundaries, NASA TN D-6376 (1971).
[49] Y. Murakami, A method of stress intensity factor calculation for the crack emanating from an arbitrarily shaped hole or the crack in the vicinity of an arbitrarily shaped hole, Trans. Jap. Soc. Mech. Engrs. **44**(1978),423-32.
[50] H. Nisitani, M. Isida, Simple procedure for calculating K_I of a notch with a crack of arbitrary size and its application to non-propagating fatigue crack, Proc. Joint JSME-SESA (1982)150.
[51] J. Schijve, The stress intensity factor of small cracks at notches, Fatigue of Engng. Mater. and Struct. **5**(1982)77-90.
[52] D. Kujawski, Stress intensity factors for small cracks at notches, Fat. Fract. Engng. Mater. Struct. **14**(1991)953-65.
[53] G. Glinka, A. Newport, Universal features of elastic notch-tip stress fields, Int. J. Fatigue **9**(1987)143-150.
[54] J. Schijve, Stress gradients around notches, Report LR-297, University of Technology, Delft, 1980.

[55] D. Maugis, Stresses and displacements around cracks and elliptical cavities: Exact solutions, Engng. Fract. Mech. **43**(1992)217-255.
[56] T. Fett, Stress intensity factors and weight functions for cracks in front of notches, KfK-Report 5254.
[57] P. Lukas, M. Klesnil, Fatigue limit of notched bodies, Mater. Sci. Engng. **34**(1978)61-66.
[58] H. Nisitani, Solutions of notched problems by body force method, in: Mechanics of Fracture (ed. by G.C. Sih), Vol.5 (1978), pp.1-68, Noordhoff, Leyden.
[59] M.L. Williams, J. Appl. Mech. **24**(1957)109-114.
[60] T. Fett, The stress intensity factor for small cracks at the root of a notch, Int. J. Fract. **54**(1992)R57-R64.
[61] M. Creager, P.C. Paris, Elastic field equations for blunt cracks with reference to stress corrosion cracking, Int. J. Fract. **3** 247-52 (1967).
[62] W.K. Jen, H.C. Lin, K. Hua, in: Fracture 1977, Vol.4, D.M.R. Taplin (ed.), Pergamon Press, Oxford (1977)123-33.
[63] H. Gao, S. Chang, Acta Metallurgica Sinica, **12**(1981)1-15.
[64] T. Fett, Mixed-mode stress intensity factors for three-point bending bars, Int. J. Fract. **48**(1991)R67-R74.
[65] A. Otsuka, T. Tohgo, T. Kiba, S. Yamada, "Mode-II fatigue crack growth characteristics and mechanism in aluminium alloy 7N01-T4 weldments under mode-II loading", Advances in Fracture Research,Proc. ICF 6, 3 ,Pergamon,(1984),pp.1671-1678.
[66] L.N.G. Filon, On an approximate solution for the bending of a beam of rectangular cross-section under any system of load, with special reference to points of concentrated or discontinuous loading, Phil. Trans., A, 201(1903),63-155.
[67] T. Fett, Stress intensity factors for edge crack subjected to mixed mode four-point bending, Theor. and Appl. Fract. Mech. **15**(1991)99-104.
[68] T. Fett, An analysis of the three-point bending bar by use of the weight function method, Engng. Fract. Mech. **40**(1991)683-686.
[69] I.N. Sneddon, Proc. of the Royal Soc., London, A 187(1946),229.
[70] T. Fett, Crack opening displacement of a penny-shaped crack in an infinite body loaded by internal pressure over a circular area, Int. J. Fract. **20**(1982),R135-R138.
[71] M. Isida, Data on crack tip stress intensity factors, J. Japan Soc. Mech. Engnrs. **75**(1972),1127-1135.
[72] T. Fett, Mixed-mode stress intensity factors for the oblique edge-crack in rectangular specimens, Int. J. Fract. **61**(1993),R3-R10.
[73] C.E. Freese, (quoted in [2] and [14]).
[74] O.L. Bowie, Solutions of plane crack problems by mapping technique, in: Mechanics of Fracture (Ed. G.C. Sih), Vol.1(1973),pp.1-55, Noordhoff International Publishing, Leyden.
[75] W.K. Wilson, Research Report 69-1E7-FMECH-R1, Westinghouse Research Laboratories, Pittsburgh (1969).
[76] M.H. Aliabadi, D.P. Rooke, D.J. Cartwright, Mixed-mode Bueckner weight functions using boundary element analysis, Int. J. Fract. **34**(1987),131-147.
[77] G.T. Sha, C.T. Yang, Weight function calculations for mixed-mode fracture problems with the virtual crack extension technique, Eng. Fract. Mech. **21**(1985),1119-1149.
[78] H.A. Bahr, H. Bahlke, M. Kuna, H. Liesk, Theor. Appl. Fract. Mech. **8**(1983)355-359.
[79] M. Isida, H. Tsuru, Tension of finite plate with multiple and periodical cracks, Trans. Japan Soc. Mech. Engrs., **49**(1983),641-645.
[80] F.I. Baratta, Stress intensity factor estimates for a peripherally cracked spherical void and a hemispherical surface pit, J. Amer. Ceram. Soc. **61**(1978)490-493.
[81] F.I. Baratta, Refinement of stress intensity factor estimates for a peripherally cracked spherical void and a hemispherical surface pit, J. Amer. Ceram. Soc. **64**(1981)C3-C4.
[82] D.J. Green, Stress intensity factor estimates for annular crack at spherical voids, J. Amer. Ceram. Soc. **63**(1981)138-141.
[83] G.G. Trantina, M. Barishpolsky, Elastic-plastic analysis of small defects - voids and inclusions -, Engng. Fract. Mech. **20**(1984)1-10.